UNIVERSITY OF SOUTHAMPTON

FACULTY OF PHYSICAL SCIENCES AND ENGINEERING

Physics

Precision measurement constraints on the 4-Site model & the effect of interference in searches for new physics

by

Diego Becciolini

Thesis for the degree of Doctor of Philosophy

May 2013

The LHC will not determine which Physics Model is Right,
only which Physics Model is Left.

—

inspired by a quote borrowed from Christos Leonidopoulos, originally on the Trigger

UNIVERSITY OF SOUTHAMPTON

ABSTRACT

FACULTY OF PHYSICAL SCIENCES AND ENGINEERING
Physics

Doctor of Philosophy

PRECISION MEASUREMENT CONSTRAINTS ON THE 4-SITE MODEL
&
THE EFFECT OF INTERFERENCE IN SEARCHES FOR NEW PHYSICS

by Diego Becciolini

This work is divided in two parts.

The first part presents a careful computation of Electroweak Precision Tests constraints on the 4-Site model, and the resulting limits on fermion couplings. The new heavy W and Z bosons present in this model can couple significantly to Standard Model fermions.

Previous computations of these quantities were performed using an approximation that is here shown to have a more restricted validity domain as what was originally thought.

The second part of the discussion is about searches of extra W and Z bosons as predicted in some extensions of the Standard Model (such as the 4-Site model) in the Drell-Yan channels.

The interference between the new physics and the Standard Model is commonly neglected in the interpretation of experimental searches. The importance of this effect is investigated in detail. The quantitative error in exclusion bounds due to neglecting the interference may be small, but important qualitative features are missed when using this approximation.

It is important to be aware of the effect of interference in order to make sure wrong statements and bad conclusions are avoided, and to guarantee that analyses do stay within the domain of validity of the approximations they rely on.

Contents

List of Figures

List of Tables

Declaration of Authorship

I, Diego Becciolini , declare that the thesis entitled *Precision measurement constraints on the 4-Site model & the effect of interference in searches for new physics* and the work presented in the thesis are both my own, and have been generated by me as the result of my own original research. I confirm that:

- this work was done wholly or mainly while in candidature for a research degree at this University;
- where any part of this thesis has previously been submitted for a degree or any other qualification at this University or any other institution, this has been clearly stated;
- where I have consulted the published work of others, this is always clearly attributed;
- where I have quoted from the work of others, the source is always given. With the exception of such quotations, this thesis is entirely my own work;
- I have acknowledged all main sources of help;
- where the thesis is based on work done by myself jointly with others, I have made clear exactly what was done by others and what I have contributed myself;
- parts of this work have been published as: [1], [2], and [3]

Signed:.....

Date:.....

Acknowledgements

First, I would like to thank my supervisors, Elena Accomando and Claire Shepherd-Themistocleous, for following me during these three years.

I owe an eternal debt of gratitude to Stefano Moretti for accompanying me in the last steps of this project: this thesis would not exist if it were not for him.

Many heartfelt thanks go to Jeff Forshaw and Doug Ross, my examiners, for their understanding and flexibility.

I am also very grateful to Francesco Sannino for his patience and support in this difficult transition period.

A big shout-out to my dear PhD colleagues with whom it was a pleasure to share an office: Matt Brown, James Callaghan, James Lyon, Luca Marzola, Ken Mimasu, Ben Samways, Patrik Svantesson.

Much appreciation to my new colleagues, in particular Marc Gillioz and Marco Nardecchia with whom helpful discussions have been held.

Lots of love to all the member of the Southampton University Symphony Orchestra and to their conductor, Robin Browning, for making me feel at home.

I don't know how I will ever repay Robert-Jan Koopmans and Beckie Carey for making their home mine for a short but important period of time.

Last, I feel particularly lucky for all the love and support I have received from my sister and my parents.

Thank you, reader.

Thank you Wolfram, too [4].

Nomenclature

GeV	Giga electron Volts
TeV	Tera electron Volts
VEV	Vacuum Expectation Value
SM	Standard Model
BSM	Beyond the Standard Model
SSM	Sequential Standard Model
LHC	Large Hadron Collider
LEP	Large Electron Positron collider
EWSB	Electroweak Symmetry Breaking
EWPT	Electroweak Precision Tests
QED	Quantum Electrodynamics
QCD	Quantum Chromodynamics
CoM	Centre of Mass
(N)LO	(Next-to-)Leading Order
PDF	Parton Distribution Function
NWA	Narrow Width Approximation
DOF	Degrees Of Freedom
CL	Confidence Level

Chapter 1

Introduction

1.1 Approximations

Physics is, in a certain sense, the art of controlling approximations. It really is the science of applying the mathematics language to describe natural phenomena, but in order to do so, approximations are unavoidable. Apart from the most simplistic ones and from some very particular cases, mathematical riddles do not admit exact analytical solutions. It is therefore natural that physicists make daily use of various approximations.

Approximations are only as good as the control one has on them: it is indispensable to have a sense of the validity domain of the approximations used. First, because it can allow an estimation of the error made in the process; second, because without such understanding, there is a risk of drifting outside of the approximation's validity range without noticing it.

The validation of results and of approximations comes from repeated checks for consistency and the general effort in improving common methods and computations.

The present discussion aims to shed some light on two different approximations that have been used, one in the context of computing Electroweak Precision Test constraints on the so-called 4-Site model, the other in experimental searches for new physics in the Drell-Yan channels.

Although previous and current results do not critically depend on these approximations, it will hopefully be made clear that it is nevertheless important to have a better awareness of the errors associated with these approximations: some qualitative features can be missed when neglecting certain contributions.

The discussion is focused on topics in particle physics, more specifically relevant to investigating what new phenomena might be discovered soon at the Large Hadron Collider (LHC).

1.2 What lies just beyond the Standard Model

The Standard Model of particles (SM) is the current theoretical construction that describes everything known about the behaviour of nature at the shortest distances — or highest energies — that have been probed. It includes the electroweak and strong interactions but not gravitation. Thus, in no way can it be regarded as a Theory of Everything, and one can expect it to predict phenomena at best up to the energy-scale of gravity, the Planck scale. However, there are many reasons to believe it should actually break down at a much lower energy, and that there are "new" — yet unobserved — phenomena to be discovered.

The highest energies reached in particle experiments are close to the electroweak scale, around 10^2-$10^3\,\mathrm{GeV}$, while the Planck scale is of order $10^{19}\,\mathrm{GeV}$. No direct observations have yet led to an understanding of nature between these two energy scales. Even indirect hints are scarce in particle phenomenology: the Standard Model is extremely successful at representing all the experimental data, and there are no significant deviations from the predictions. As will be discussed further, this severely constrains any extension of the theoretical picture. Measurements so far might not be able to tell what is out there, but do quite well determine what is not.

Experimentally, the strongest indications that the description is incomplete come from cosmological observations: none of the known particles seems to be able to play the role of dark matter, and the Standard Model alone struggles with the correct prediction of the baryon asymmetry in the universe.

All other arguments for new physics have theoretical grounds. Most motivations are related to the fairly large number of free parameters in the Standard Model (about 25, including neutrino masses) and/or the fact that some of them are separated by many orders of magnitude. Can the different gauge interactions be unified into a single symmetry group? How come neutrinos are so light? Why is the top quark the only fermion with a mass close to the electroweak scale? Is there a reason for the existence of three generations of fermions? These are some of the most common questions to which Beyond the Standard Model (BSM) scenarios try to bring answers. Additional symmetries are enforced in attempts to link certain parameters; dynamical mechanisms at higher scales are invoked in order to explain size differences. Many ideas are being explored: grand unification, see-saw mechanisms, discrete family symmetries.

There is another important reason to be unsatisfied with the Standard Model, though, which is directly linked to the large gap between the electroweak and Planck scales; it is usually referred to as *the hierarchy problem*. The issue arises in the Higgs sector, which takes care of the electroweak symmetry breaking. In the Standard Model, if one considers it to be an effective field theory, the quantum corrections to the mass of the Higgs boson are the most sensitive to the scale of new physics: they are indeed quadratic, not just logarithmic, in this energy-scale. It used to be considered that, most naturally, the Higgs

boson mass should be at the electroweak scale, not higher than a few hundred GeV; it is now an experimental fact, since a resonance of $125\,\mathrm{GeV}$ which seems to have the right properties has been recently spotted [5, 6]. So if the Standard Model were to be valid up to the Planck scale, the Higgs mass-squared would receive corrections of order $\left(10^{19}\,\mathrm{GeV}\right)^2$ that cancel out the bare parameter almost exactly, but not quite, to leave just the required physical mass-squared of $\left(10^{2}\,\mathrm{GeV}\right)^2$: in other words, the Lagrangian parameter would have to be tuned so that its relative difference with the correction is about 10^{-34}.

Arguably, the most popular idea to eliminate this severe *fine tuning* is supersymmetry: the problematic quadratic corrections are cancelled by contributions from extra particles with different spin properties. It is not the only one, however, as the Planck constant could appear to be so large due to the presence of additional compact spatial dimensions. Finally, the electroweak symmetry breaking mechanism could also be a low-energy manifestation of some hidden strong dynamics (which goes by the name of *technicolour*), very much the same way Quantum Chromodynamics (QCD) appears only as hadrons below a certain scale.

What these scenarios have in common is that, if they are to reduce this fine tuning all the while preserving established Standard Model predictions, their characteristic scale cannot be much larger than the electroweak scale, a few TeV at most. Thus, besides testing the existence of a light Higgs particle (a goal which has now been achieved), the strong expectation that new physics should show up just beyond the current frontier of human knowledge has been the main motivation for building a discovery machine such as the LHC.

Suspecting that the current model should prove inadequate at energies within direct experimental reach is not enough: searches need to be directed in order to deliver their full potential. This is where phenomenology plays a role, identifying possible signals of new physics that should be looked for.

Part I

Electroweak precision measurement constraints on the 4-Site model

Chapter 2

The 4-Site model

2.1 Playing with the Higgs

2.1.1 What if there had not been a light Higgs boson?

Until recently, as no light Higgs-like resonance had yet been observed, one legitimate question was: since the hierarchy problem appears because of the presence of a light scalar in the Standard Model, why not remove the latter completely (*i.e.* at least push it up, above a new physics scale of a few TeV)?

The most naive answer to that question would be to think that it is enough, as the hierarchy problem indeed goes away. However, the Higgs resonance plays another important role: it unitarises the scattering of the W/Z bosons in the high-energy limit. Without the contribution of the Higgs, perturbative unitarity is lost around the TeV scale [7]. The Standard Model on its own cannot resolve this issue without the Higgs resonance, therefore if it were not there, new physics definitely would have to show up at the TeV scale. In other words, not having discovered a light Higgs boson would have reinforced the case for new (strong) dynamics within reach of the LHC.

Another — more subtle — problem arises when the light Higgs is removed. The electroweak sector receives quantum corrections which are very important for the agreement between the Standard Model predictions and experiments, and they depend on the mass of the Higgs boson. From that point of view, one finds that a light Higgs with a similar mass to the W/Z bosons is most favoured, and that a mass above a few hundred GeV already is strongly disfavoured.

The breakdown of perturbative unitarity can nevertheless be delayed and the agreement with electroweak precision tests (EWPT) restored, provided that other ingredients are added to the Standard Model. The 4-Site model is one such framework that would have helped lessen the disagreement with the EWPT had a light scalar not been observed.

Of course, it has now been established that there is a resonance at $125\,\mathrm{GeV}$ with the right properties to be the Standard Model Higgs boson or at least an object similar enough to play its role. The motivation for introducing the particular extension of the Standard Model presented here is therefore somewhat weakened. The general idea behind it, on the other hand, is still not ruled out. In fact, one can add back a light scalar resonance to the minimal model and accommodate for the latest discovery [8]. Motivating its presence rather than its absence in the context of dynamical electroweak symmetry breaking is a little more complicated, however there is no reason, a priori, why it would be impossible. In this discussion, the consequences of such a modification will not be fully explored, as the work had been done prior to this finding. Nevertheless, it should not matter much for the points presented here, and the general results are still valid.

2.1.2 Chiral symmetry of the Higgs sector

A quantum field theory is essentially determined by its symmetries [9]. Any extension of the Standard Model, therefore, cannot have less symmetries, or it will not reproduce the known phenomenology; its symmetry group has to contain the Standard Model one.

As mentioned before, the hierarchy problem can be addressed by extending the Lorentz group. For instance, one or more dimensions can be added to the known 4; these should either be large enough [10], or the hidden space should be appropriately curved [11]. The only other non-trivial way of extending the Lorentz symmetry is supersymmetry [12, 13].

Alternatively, one can choose to leave Lorentz symmetry be and modify the gauge group of the Standard Model instead. It is the electroweak sector that is at the heart of the problem or, more precisely, the *breaking* of the associated symmetry. In order to tackle the hierarchy problem, any extension thus has to be somehow connected to the electroweak symmetry breaking (EWSB) mechanism. So one should first understand what symmetries are involved and what ingredients are needed.

The electroweak gauge bosons are the massive W/Z and the massless photon. The W/Z can gain a mass in a way that is consistent with gauge symmetry, via the Brout-Englert-Higgs mechanism [14, 15], if the electroweak group spontaneously breaks down to electromagnetism,

$$SU(2)_L \times U(1)_Y \longrightarrow U(1)_{EM}. \tag{2.1}$$

The would-be Nambu-Goldstone bosons of the breaking are not describing massless particles if the broken symmetry is local. Instead, they can be gauged away and do not have a physical meaning on their own; they provide the necessary degrees of freedom for the now massive gauge bosons to acquire a longitudinal polarisation.

It is important to stress that only these Goldstone modes are strictly necessary for the symmetry breaking. The fourth component in the Standard Model Higgs fields, which corresponds to the light Higgs particle, does not, *per se*, play a role in the EWSB.

One simple way to make this point more explicit and to show more clearly the possible link with strong dynamics is to rewrite the Higgs field as a 2×2 matrix [16],

$$H \equiv \begin{pmatrix} \phi_+ \\ \phi_0 \end{pmatrix} \longrightarrow \Sigma \equiv \frac{1}{\sqrt{2}f} \begin{pmatrix} \phi_0^* & \phi_+ \\ -\phi_+^* & \phi_0 \end{pmatrix}. \tag{2.2}$$

Σ has been made dimensionless by factoring out a dimensionful parameter f. Since

$$\Sigma\Sigma^\dagger = \frac{|H|^2}{2f^2}\, \mathbb{1}, \tag{2.3}$$

the Higgs Lagrangian is simply

$$\mathcal{L}_{\text{Higgs}} = f^2\, \mathrm{Tr}\left(\partial_\mu \Sigma\, \partial^\mu \Sigma^\dagger\right) - f^2\, \frac{m_H^2}{2} \left(\frac{1}{2}\mathrm{Tr}\left(\Sigma\Sigma^\dagger\right) - 1\right)^2, \tag{2.4}$$

where $\mathrm{Tr}\,(.)$ denotes the trace. The potential is minimised when $\mathrm{Tr}\left(\Sigma\Sigma^\dagger\right) = 2$ or $|H|^2 = 2f^2$, which means $\Sigma\Sigma^\dagger = \mathbb{1}$. Conventionally, the vacuum expectation value (VEV) is chosen to be along the ϕ_0 direction,

$$\langle\phi_0\rangle = \sqrt{2}f,\ \langle\phi_+\rangle = 0 \quad \Rightarrow \quad \langle\Sigma\rangle = \mathbb{1}. \tag{2.5}$$

There are three massless Goldstone modes (leaving $|H|^2$, thus the potential, invariant) and one "radial" mode (changing $|H|^2$) of mass m_H.

Written in this fashion, the Higgs sector is manifestly symmetric under global $SU(2)_L \times SU(2)_R$ transformations, with Σ transforming in the bi-fundamental representation

$$\Sigma \longrightarrow U_L\, \Sigma\, U_R^\dagger. \tag{2.6}$$

The VEV of Σ (2.5) is only invariant under transformations for which $U_L = U_R$, thus it spontaneously breaks the chiral symmetry to its vector subgroup, the *custodial* symmetry,

$$SU(2)_L \times SU(2)_R \longrightarrow SU(2)_V. \tag{2.7}$$

This is where a direct link with strong dynamics can be made. In QCD also there is a spontaneously broken chiral (flavour) symmetry. The Goldstone bosons of the breaking are the pi mesons; since the symmetry is explicitly broken by quark masses, the pions are not massless, but anyhow significantly lighter than the other mesons.

The main difference is that, unlike in the electroweak sector, no QCD resonance has been observed that could be associated with the "radial" mode. In fact, one obtains exactly

the Lagrangian of chiral perturbation theory to lowest order [17] when the radial mode is removed, which is hardly surprising. This is done by taking the limit $m_H \to \infty$; the potential in (2.4) then blows up unless $\Sigma\Sigma^\dagger = \mathbb{1}$. One can picture this as making the "mexican hat" infinitely deep. So the Σ matrix is now constrained to be unitary, the potential vanishes, and one obtains a non-linear sigma model, where the Higgs VEV plays the role of the pion decay constant.

The point made in the previous section about the loss of perturbative unitarity when the Higgs resonance is removed appears here as a breakdown of the effective sigma model description at a scale parametrically larger than f,

$$\Lambda \sim 4\pi f \sim \mathcal{O}\left(\mathrm{TeV}\right). \tag{2.8}$$

Once again, had a light Higgs resonance not been observed, the Higgs sector would look exactly like low-energy QCD, and it would have been a strong evidence that the EWSB were triggered dynamically rather than by a fundamental scalar. The converse is not true, though, and the exact nature of the EWSB mechanism is still unknown. This ambiguity about the fundamental or composite nature of the scalar that breaks the electroweak symmetry has always been clear (*cf.* the concluding remark in Higgs' original paper [15]), and a good understanding of what lies beyond the Standard Model will be necessary to resolve it.

Before moving on to the next section, the interaction of the Higgs field with the gauge sector should be specified. The Standard Model electroweak interactions are obtained by gauging $SU(2)_L$ (which is indeed the Standard Model $SU(2)_L$; the gauge coupling is denoted g and the gauge bosons L^a_μ) and the third direction of $SU(2)_R$ (which corresponds to hypercharge, whose gauge boson is $\mathcal{Y}_\mu$ with gauge coupling g'). The covariant derivative acts on Σ as follows:

$$D_\mu\Sigma = \partial_\mu\Sigma - \imath g L^a_\mu \frac{\tau^a}{2}\Sigma + \imath g' \mathcal{Y}_\mu \, \Sigma\frac{\tau^3}{2}, \tag{2.9}$$

where τ^a are the standard Pauli matrices. As expected, the non-zero VEV of the Σ field (2.5) yields a mass term for the gauge bosons (and the would-be pions are eaten away)

$$\mathcal{L}_{\text{Higgs}} \supset \frac{f^2}{2}\left((gL^1_\mu)^2 + (gL^2_\mu)^2 + (gL^3_\mu - g'\mathcal{Y}_\mu)^2\right). \tag{2.10}$$

2.2 Extending the gauge sector

2.2.1 Hidden local symmetries

In QCD, on top of the pions, there are also vector mesons, namely the rho. They can be included in the pion description in an elegant way as gauge bosons of an extra *hidden local*

symmetry [18]. If the Higgs sector were a manifestation of some strong dynamics at a higher scale, there could well be an analogue of these rho mesons, that would appear as heavier copies of the Standard Model W and Z bosons [16].

The principle is the following: the Σ field is split in $K+1$ factors

$$\Sigma = \Sigma^1 \Sigma^2 \cdots \Sigma^{K+1}, \tag{2.11}$$

each transforming as

$$\Sigma^k \longrightarrow U_{k-1}\, \Sigma^k\, U_k^\dagger \tag{2.12}$$

with $U_0 \equiv U_L$ and $U_{K+1} \equiv U_R$, so that the overall product still transforms the same way (2.6). The other transformations are here simply chosen to be $SU(2)$ as well, so now the symmetry group is

$$SU(2)_L \times (SU(2))^K \times SU(2)_R. \tag{2.13}$$

Each of these sigma fields can have their own decay constant f_k and they each parametrise the Goldstone bosons associated to the breaking of the corresponding $SU(2) \times SU(2)$ to its vector subgroup. The global symmetry is then gauged (and, as before, only the third direction of $SU(2)_{K+1} \equiv SU(2)_R$ is gauged). The full Lagrangian reads

$$\mathcal{L} = \sum_{k=1}^{K+1} f_k^2 \,\mathrm{Tr}\left(\left(D_\mu \Sigma^k\right) \left(D^\mu \Sigma^k\right)^\dagger \right) - \sum_{k=0}^{K+1} \frac{1}{2} \mathrm{Tr}\left(\left(F_{\mu\nu}^k\right)^2 \right), \tag{2.14}$$

where the covariant derivative is

$$D_\mu \Sigma^k = \partial_\mu \Sigma^k - \imath g_{k-1}\, V_\mu^{k-1} \Sigma^k + \imath g_k\, \Sigma^k V_\mu^k, \tag{2.15}$$

the field strength is

$$F_{\mu\nu}^k = \partial_\mu V_\nu^k - \partial_\nu V_\mu^k - \imath g_k \left[V_\mu^k, V_\nu^k \right], \tag{2.16}$$

and the gauge bosons are

$$V_\mu^k \equiv \left(V_\mu^k\right)^a \frac{\tau^a}{2}. \tag{2.17}$$

This kind of setup is commonly represented by a *moose* (or quiver) diagram pictured in Figure 2.1 [19]. The circles represent the gauge groups and the lines the sigma fields that connect them. Since there are in total K+2 $SU(2)$ factors, this setup is conventionally called *(K+2)-Site model*.

Compared to the Standard Model, there are now K more sigma fields, but also K more gauge fields: the additional Goldstone modes get eaten by the new gauge bosons which

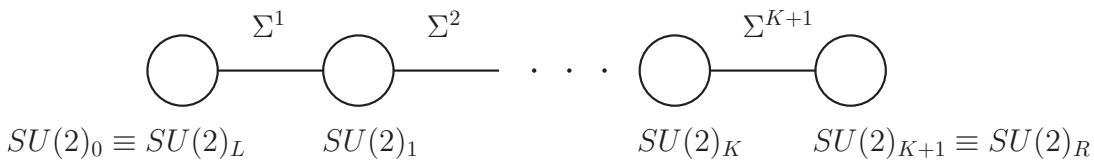

Figure 2.1: Linear moose diagram representing the (K+2)-Site model.

acquire mass. In such a model, one therefore has a tower of heavier copies of W/Z bosons on top of the Standard Model ones; note that there still is only one massless photon (since only one direction of $SU(2)_R$ is gauged).

The scale of the overall breaking (2.7) should be roughly the same as before, f, as it sets what the electroweak scale is. This allows to say something about the individual f_k. Gauging away all the Goldstone modes except one triplet $\Pi \equiv \pi^a \frac{\tau^a}{2}$ that parametrises the breaking (2.7), *i.e.* it is related to Σ

$$\Sigma = \exp\left(\imath \frac{\Pi}{f}\right), \tag{2.18}$$

the other sigma fields can be put in the form

$$\Sigma^k = \exp\left(\imath\, \alpha_k \frac{\Pi}{f}\right) \tag{2.19}$$

with

$$\sum_{k=1}^{K+1} \alpha_k = 1 \tag{2.20}$$

so that the product of the Σ^k is indeed Σ (2.11). The coefficients α_k can be determined by requiring a canonically normalised kinetic term for Π, which is the condition

$$\sum_{k=1}^{K+1} \frac{f_k^2\, \alpha_k^2}{f^2} = 1. \tag{2.21}$$

Since the f_k are independent, combining these last two equations leads to

$$\alpha_k = \frac{f^2}{f_k^2} \tag{2.22}$$

and

$$\frac{1}{f^2} = \sum_{k=1}^{K+1} \frac{1}{f_k^2} \tag{2.23}$$

This result shows that, for a given f, the individual decay constants f_k will be larger than the overall breaking scale. Choosing all the f_k to be the same, for instance, gives $f_k \sim$

$f\sqrt{K+1}$. The individual sigma models break down at $\Lambda \sim 4\pi f_k$, thus one could naively expect the effective description to be valid up to arbitrary high scales by making K sufficiently large. The argument does not hold, though, as there will be a collective effect between the pions; although the violation of unitarity can indeed be somewhat delayed compared to the case $K = 0$, the cutoff saturates in the large K limit [20].

The limit $K \to \infty$ actually correspond to constructing an extra compactified dimension [21]. The sigma fields give rise to the fifth component of a now five-dimensional gauge field, and the tower of resonances is a collection of Kaluza-Klein excitations. In this picture, the loss of perturbative unitarity corresponds to the fact that the gauge coupling now has negative mass-dimension, and thus the theory is non-renormalisable [22].

The corollary of the effective description breaking down at a not much higher scale than in the case with no added hidden local symmetries is that only the first few resonances do have a direct physical meaning. So one might ask if, from a phenomenological point of view, it would be enough to just include the few resonances below the cutoff and if the description then still captures the essence of the full five-dimensional model. It is the case indeed, and K does not need to be very large for the description to exhibit generic features of extra dimensions [23].

The discussion started with strong interactions but ended up with extra-dimensional theories. This is no accident: since Maldacena formulated his conjecture almost 15 years ago [24], the understanding of the subtle link between strong dynamics and extra dimensions has been increasing steadily. In that sense, the (K+2)-Site model can be viewed either as an effective low-energy description of a technicolour sector or as approximating a fifth dimension.

2.2.2 Unitary gauge, mass matrix, and the photon

As before the introduction of hidden local symmetries, the unitary gauge, in which all the Goldstone modes — or pions — are gauged away, corresponds to setting all the sigma fields to the identity matrix, $\Sigma^k \to \mathbb{1}$. One gets mass terms for the gauge bosons similar to (2.10):

$$\mathcal{L} \supset \sum_{k=1}^{K+1} \frac{f_k^2}{2} \left(g_{k-1} (V_\mu^{k-1})^a - g_k (V_\mu^k)^a \right)^2. \tag{2.24}$$

In the basis $\{(V_\mu^0)^a \equiv L_\mu^a, (V_\mu^1)^a, \ldots, (V_\mu^K)^a, \left[(V_\mu^{K+1})^3 \equiv \mathcal{Y}_\mu\right]\}$, the mass matrix is thus

$$M_Z^2 = \begin{pmatrix} g_0^2 f_1^2 & -g_0 g_1 f_1^2 & & & \\ -g_0 g_1 f_1^2 & g_1^2(f_1^2+f_2^2) & -g_1 g_2 f_2^2 & & \\ & -g_1 g_2 f_2^2 & g_2^2(f_2^2+f_3^2) & \ddots & \\ & & \ddots & \ddots & -g_K g_{K+1} f_{K+1}^2 \\ & & & -g_K g_{K+1} f_{K+1}^2 & g_{K+1}^2 f_{K+1}^2 \end{pmatrix}. \tag{2.25}$$

The charged bosons mass matrix M_W^2 is the same except that the last row and column are removed ($\mathcal{Y}_\mu$ is only there for $a = 3$, *i.e.* in the neutral sector).

In terms of mass eigenstates, the pure gauge bosons are

$$(V_\mu^k)^{1,2} = \sum_{i=0}^{K} w_i^k (W_\mu^i)^{1,2}, \quad (V_\mu^k)^3 = \gamma^k A_\mu + \sum_{i=0}^{K} z_i^k Z_\mu^i, \tag{2.26}$$

where A_μ is the zero-mode of the neutral sector, the photon, and there are K+1 massive charged W and neutral Z bosons.

It is easy to see from (2.24) that the neutral mass matrix has indeed a zero-mode: if $\gamma^k \propto \frac{1}{g_k}$, the photon A_μ cancels out completely from the mass term. This does not work in the charged sector, though, since the last link is not entirely gauged (which is a required feature, as massless W bosons would be problematic).

The photon coefficients are determined by requiring proper normalisation, which ensures a canonical kinetic term:

$$\sum_{k=0}^{K+1} (\gamma^k)^2 = 1, \tag{2.27}$$

but looking at the gauge interactions between the photon and the W bosons is more instructive. Forgetting about the details of the Lorentz and $SU(2)$ structures of the interaction — which are the same as in the Standard Model — for simplicity of notation, defining the constant $e \equiv g_k \gamma^k$, and by orthonormality of the w_i^k, the trilinear photon interaction from (2.14) is

$$\left(\sum_{k=0}^{K} g_k \gamma^k w_i^k w_j^k\right) A\, W^i\, W^j = e\, A\, W^i\, W^i. \tag{2.28}$$

In other words, e is the fundamental electric charge, and the electromagnetic interaction does not mix the different mass eigenstates. Looking at the quartic interaction leads to the same conclusion.

Replacing the relation between the electric charge and the γ^k coefficients back into (2.27), one obtains the following equation, relating the gauge couplings to the electric charge:

$$\frac{1}{e^2} = \sum_{k=0}^{K+1} \frac{1}{g_k^2}. \tag{2.29}$$

2.3 Adding the fermions

2.3.1 Delocalisation

In this minimal bottom-up approach, only the hierarchy problem is addressed and taken as a hint to what kind of new physics could be around the corner. All the issues associated with fermion masses are set aside: it is assumed that whatever plays the role of the Higgs field gives the fermions their masses in exactly the same way as in the Standard Model. No additional heavy fermions are introduced either.

Only the way the fermions couple to the modified electroweak gauge sector needs to be specified. The starting point is to assume matter couples to the "external" gauge bosons (the ones corresponding to the first and last links in the moose diagram) the same way it couples to $SU(2)_L \times U(1)_Y$ in the Standard Model; hence the naming convention $SU(2)_0 \equiv SU(2)_L$ and $SU(2)_{K+1} \equiv SU(2)_R$. An economical way to write this is as follows:

$$\begin{aligned}\mathcal{L}^{\text{SM}}_{\text{fermions}} = \psi_L^\dagger \imath \bar{\sigma}^\mu \left(\partial_\mu - \imath g L_\mu^a \frac{\tau^a}{2} - \imath g' \mathcal{Y}_\mu \frac{(B-L)}{2}\right) \psi_L \\ + \psi_R^\dagger \imath \sigma^\mu \left(\partial_\mu - \imath g' \mathcal{Y}_\mu \frac{\tau^3 + (B-L)}{2}\right) \psi_R,\end{aligned} \tag{2.30}$$

where $\sigma^\mu = (\mathbb{1}, \vec{\sigma})$ and $\bar{\sigma}^\mu = (\mathbb{1}, -\vec{\sigma})$ are the generalised Pauli matrices acting in the spinor space. B and L are respectively the baryon and lepton numbers (the context should be clear enough to distinguish between the different L), and the chiral fermions are combined in doublets

$$\psi_{L,R} \equiv \begin{pmatrix} u_{L,R} \\ d_{L,R} \end{pmatrix} \ (B = \frac{1}{3} \text{ and } L = 0), \quad \begin{pmatrix} \nu_{L,(R)} \\ e_{L,R} \end{pmatrix} \ (B = 0 \text{ and } L = 1). \tag{2.31}$$

It has to be stressed from the beginning that, since the mixing in the mass eigenstates is not the same as in the Standard Model, the couplings to the physical W/Z bosons will be different; so different, as a matter of fact, that a good agreement with EWPT is not possible in general (as will be shown in Section 4.3.1). This constraint can be bypassed with a simple modification, though, which counters the effect of the mixing on the couplings: left-handed

fermions are allowed to interact with the "hidden" sites via the sigma fields [25]. Defining

$$\chi_L^k \equiv (\Sigma^k)^\dagger (\Sigma^{k-1})^\dagger \cdots (\Sigma^1)^\dagger \psi_L, \qquad k = 1, \ldots, K, \tag{2.32}$$

one sees immediately, from (2.12), that it has the right transformation property to interact with the gauge bosons of $SU(2)_k$, and one can add terms like

$$b_k \, (\chi_L^k)^\dagger \imath \bar{\sigma}^\mu \left(\partial_\mu - \imath g_k (V_\mu^k)^a \, \frac{\tau^a}{2} - \imath g' \mathcal{Y}_\mu \, \frac{(B-L)}{2} \right) \chi_L. \tag{2.33}$$

In the unitary gauge, all Σ^k are sent to the identity and thus $\chi_L^k \to \psi_L$. For ψ_L to have a canonically normalised kinetic term, it needs to be rescaled

$$\psi_L \longrightarrow \frac{1}{\sqrt{\sum_{k=0}^K b_k}} \, \psi_L, \tag{2.34}$$

where $b_0 \equiv 1$.

Finally, adding the extra pieces (2.33) to (2.30) and performing the above rescaling, the fermion Lagrangian, in the unitary gauge, is

$$\begin{aligned} \mathcal{L}_{\text{fermions}} = \psi_L^\dagger \imath \bar{\sigma}^\mu & \left(\partial_\mu - \imath \frac{1}{\sum_{l=0}^K b_l} \sum_{k=0}^K \left[b_k \, g_k \, (V_\mu^k)^a \right] \frac{\tau^a}{2} - \imath g' \mathcal{Y}_\mu \, \frac{(B-L)}{2} \right) \psi_L \\ & + \psi_R^\dagger \imath \sigma^\mu \left(\partial_\mu - \imath g' \mathcal{Y}_\mu \, \frac{\tau^3 + (B-L)}{2} \right) \psi_R. \end{aligned} \tag{2.35}$$

This can be seen, in the extra-dimensional picture, as allowing the fermions to propagate in the bulk; they are not localised on the external brane any more, and the b_k parameters correspond to the wave-function along the fifth dimension.

As for the interaction with the other gauge bosons, it is easy to check that the photon couples to fermions exactly the way it is supposed to, thanks to preserving the custodial symmetry; replacing in (2.26) with $\gamma^k \equiv \frac{e}{g_k}$ one finds indeed that electric charge of both left- and right-handed fermions is, in units of e,

$$Q = \frac{\tau^3 + (B-L)}{2}. \tag{2.36}$$

2.3.2 Physical fermion couplings

Physical couplings of the fermions to the massive vector bosons are obtained by replacing the gauge eigenstates in (2.35) with (2.26). Since the components w_i^k and z_i^k are only defined up to an overall sign for each i, the overall sign of the fermion couplings to each given mass eigenstate is completely arbitrary, and indeed would not appear in any measurable

quantity. Once a sign has been fixed, however, the corresponding trilinear and quartic gauge couplings are set as well, and the relative sign here does have a physical meaning.

2.3.2.a Neutral couplings

It is straightforward to read the tree-level couplings of left- and right-handed fermions to the i-th Z boson ($i = 0$ would be the Standard Model one) from (2.35):

$$\begin{aligned} a_L^i &= g' z_i^{K+1} Q + \left(\frac{1}{\sum_{l=0}^K b_l} \sum_{k=0}^K \left[b_k \, g_k \, z_i^k \right] - g' z_i^{K+1} \right) \frac{\tau^3}{2}, \\ a_R^i &= g' z_i^{K+1} Q. \end{aligned} \tag{2.37}$$

Thanks to the fact that the fermion charges assignment is the same, the neutral couplings have a similar dependence on the electric charge and weak isospin number as in the Standard Model, unlike in some scenarios predicting extra Z bosons with a different coupling structure [26, 27].

Conventionally writing the interaction term as

$$\mathcal{L}_{\text{int.}} \supset Z_\mu \, \bar{\psi} \gamma^\mu \left(a_V - a_A \gamma_5 \right) \psi, \tag{2.38}$$

vector and axial couplings are related to the left and right ones as follows:

$$a_V = \frac{a_L + a_R}{2}, \quad a_A = \frac{a_L - a_R}{2}. \tag{2.39}$$

2.3.2.b Charged couplings and ideal delocalisation

Again, the couplings to the W bosons can be directly read from the Lagrangian (2.35):

$$a_C^i = \frac{1}{\sqrt{2} \sum_{l=0}^K b_l} \sum_{k=0}^K b_k \, g_k \, w_i^k \tag{2.40}$$

where the $\sqrt{2}$ factor is conventional, so that the interaction reads

$$\mathcal{L}_{\text{int.}} \supset a_C \, \psi_L^\dagger \bar{\sigma}^\mu \left(W_\mu^+ \frac{\tau^1 + \imath \tau^2}{2} + W_\mu^- \frac{\tau^1 - \imath \tau^2}{2} \right) \psi_L. \tag{2.41}$$

The W bosons couple exclusively to left-handed fermions: the right-handed ones only interact with $\mathcal{Y}_\mu$, which does not mix with ${V_\mu}^{1,2}$.

For a particular choice of the b_k parameters, one can make the fermions couple to only one of the W resonances (the lightest one, in particular), this is called *ideal fermion delocalisation* [28]. By orthogonality of the eigenvectors w_i^k, setting $b_k\, g_k \propto w_0^k$ makes all the couplings a_C^i vanish except the Standard Model one ($i = 0$). Couplings to the heavy Z' bosons are then also suppressed, and therefore the electroweak corrections are minimised. In such a scenario, the extra W'/Z' are fermiophobic. Constraining the model further — or discovering these resonances — cannot be done in the simplest experimental channels (Drell-Yan).

Further on will be addressed the question of how far from this ideal delocalisation can one go without spoiling EWPT too much; in other words, what are the largest allowed fermion couplings?

2.3.2.c The Fermi constant

In the Standard Model, the Fermi constant is defined as

$$\frac{G_F}{\sqrt{2}} \overset{\text{SM}}{=} \left(\frac{a_C^{\text{SM}}}{2\, m_W^{\text{SM}}}\right)^2, \tag{2.42}$$

but there are now multiple W resonances to be exchanged, and the relation is modified:

$$\frac{G_F}{\sqrt{2}} = \sum_{i=0}^{K} \left(\frac{a_C^i}{2\, m_W^i}\right)^2; \tag{2.43}$$

m_W^i are the masses of the W bosons.

Using the expression for the coupling (2.40), the orthogonality of the w_i^k and the identity

$$w_i = (M_W^2)^{-1}(M_W^2)\, w_i = (m_W^i)^2\, (M_W^2)^{-1}\, w_i, \tag{2.44}$$

one obtains

$$\begin{aligned}\frac{8}{\sqrt{2}}\, G_F &= \frac{1}{\left(\sum_{j=0}^{K} b_j\right)^2} \sum_{i,k,l=0}^{K} b_k g_k\, b_l g_l\, \frac{w_i^k w_i^l}{(m_W^i)^2} \\ &= \frac{1}{\left(\sum_{j=0}^{K} b_j\right)^2} \sum_{k,l=0}^{K} b_k g_k\, (M_W^2)^{-1}_{k,l}\, b_l g_l \\ &= \frac{1}{\left(\sum_{j=0}^{K} b_j\right)^2} (bg)^T (M_W^2)^{-1} (bg)\end{aligned} \tag{2.45}$$

As shown in Appendix A, the dependence on g_k cancels out, and the expression reduces to

$$\frac{8}{\sqrt{2}}\,G_F = \frac{1}{\left(\sum_{j=0}^{K} b_j\right)^2} \sum_{k=0}^{K} \frac{\left(\sum_{l=0}^{k} b_l\right)^2}{f_{k+1}^2}. \tag{2.46}$$

Interestingly, if all the b_k are set to zero (except of course $b_0 \equiv 1$), then the Standard Model relation is automatically recovered, even for non-zero K:

$$\frac{8}{\sqrt{2}}\,G_F \overset{b\to 0}{=} \frac{1}{f^2}, \tag{2.47}$$

where f has been defined earlier (2.23) (*cf.* equation (21.109) [29]).

2.4 Restricting to 4 sites

2.4.1 How many sites should be included?

In principle, the number of hidden symmetries K is arbitrary. As argued at the end of Section 2.2.1, the large K limit is to be associated with an extra-dimensional picture, and may formally correspond to some strong dynamics. At the same time, it has been pointed out that the (unphysical) resonances above the natural cutoff of the model do not play an important role for the basic phenomenology at lower energy. These are unphysical in the sense that the description cannot be trusted any more in the strongly interacting regime: what happens from the point of view of perturbation theory is that higher dimensional operators become more and more important.

In the continuous limit, essentially one only needs to specify a background metric, but the choice is infinite (and is of little importance [23]). So unless a particular geometry is motivated from some stringy scenario [30], the deconstructed picture seems preferable from a purely phenomenological point of view.

The larger K is, the more free parameters there are, something one would want to avoid; there is a trade-off between having a complete extra-dimensional description and the size of the parameter space. However, few sites already reproduce any possible low-energy behaviour well, and one can restrict oneself to minimal cases.

Some attention has been devoted to the case $K = 1$, the original BESS model (Breaking Electroweak Symmetry Strongly) [16] or the 3-Site model [31]. The limited number of parameters makes it easier to discuss properties of the model and possible modifications. It does seem that, in any case, the heavy vector bosons are constrained by EWPT to be fermiophobic.

In the next-to-minimal case — $K = 2$, the *4-Site model* —, however, interplay between the parameters somewhat relaxes this constraint [32], which is the subject of the current discussion. Of course, the downside is that the discussion of the parameter space is not as simple any more. Anyhow, one finds that possible scenarios can be stretched further in terms of fermion couplings compared to minimal models.

With even more sites, the number of free parameters starts becoming prohibitive, and it should not contribute to a much richer phenomenology as the additional resonances would in general be above the cutoff [23].

2.4.2 The parameters

The electroweak sector of the Standard Model depends on three parameters (plus the mass of the Higgs resonance, which we now know to be there): two gauge couplings and a mass scale (the Higgs VEV). With each additional hidden local symmetry, in the setup that has just been described, three new parameters are added: a gauge coupling (g_k), a decay constant (f_k), and a fermion delocalisation parameter (b_k). This means six more parameters compared to the Standard Model in the 4-Site model.

One can impose the gauge sector to be symmetric under a left-right flip, which ensures a definite parity for the gauge bosons:

$$g_k \longleftrightarrow g_{K+1-k}, \quad f_k \longleftrightarrow f_{K+2-k}. \tag{2.48}$$

The number of parameters then gets reduced, and in the 4-Site there are four, and not six additional parameters.

Summarising, the complete list of parameters describing the electroweak sector in the 4-Site model is: three gauge couplings, g, g_1, g'; two dimensionful constants, f_1, f_2; two dimensionless coefficients b_1, b_2.

It is convenient to define certain quantities:

$$M_1 \equiv g_1 f_1, \quad M_2 \equiv g_1\sqrt{f_1^2 + 2f_2^2}, \quad z \equiv \frac{M_1}{M_2}. \tag{2.49}$$

These represent approximatively the masses of the two heavy copies of W/Z bosons, and their ratio. Note that $M_1 < M_2$, therefore $0 < z < 1$; $z \to 1$ would be the degenerate limit (where the masses of the two extra W/Z become close).

Some expressions can be simplified a little by making further redefinitions:

$$A \equiv \frac{m_Z^2}{M_1^2}, \quad \zeta \equiv \frac{1}{z^2} - 1, \quad \xi \equiv \frac{g^2 + g'^2}{2\,g_1^2}, \quad \gamma \equiv \frac{g^2 - g'^2}{g^2 + g'^2},$$
$$c_1 \equiv 1 + b_1, \quad c_2 \equiv 1 + b_1 + b_2, \tag{2.50}$$

with m_Z the mass of the Standard Model Z.

The known vector resonances will be assumed to be the lightest ones, therefore M_1 will be chosen larger than m_Z, thus $0 < A < 1$. In fact, the limit $A \to 0$ should correspond to some *decoupling limit*, where the new physics is sent to an arbitrarily high scale; as will be discussed, expressions are often expanded in A or in some related parameter. It is in this limit that (2.49) are the masses of the heavy resonances. The expansion will be avoided as much as possible, but one has to keep in mind that the model should reduce to the known physics in this limit, which will allow to lift some ambiguities.

From the definition of z, $\zeta > 0$, and the degenerate limit is $\zeta \to 0$. Finally, for the gauge couplings to be real, $\xi > 0$; and a priori $-1 < \gamma < 1$, but it will be shown that for phenomenological reasons γ should not be negative (*i.e.* g should be larger than g').

Typically M_1 will be chosen between a few hundred GeV and $2\text{-}3\,\mathrm{TeV}$, meaning an A of order 10^{-2}-10^{-3}. As for z, usual values range from 0.1 to 0.95, so ζ is between 0.1 and 100.

Furthermore, the following definitions will be useful because these combinations enter the expression for the Fermi constant:

$$C_0 \equiv s_{2\theta}^2 \, \frac{1 + c_2^2 + \frac{2\,c_1^2}{\zeta}}{2\,c_2^2}, \quad C \equiv \frac{1}{\frac{1}{AC_0} - 1}, \tag{2.51}$$

where $s_{2\theta}$ is the sine of twice the Weinberg angle and will be defined in the next chapter; at this point it can just be thought of as an arbitrary constant. C will be required to be positive, which translates as $AC_0 < 1$, in which case

$$C = \sum_{n=1}^{\infty} (AC_0)^n \,. \tag{2.52}$$

2.4.3 Physical quantities

In terms of these parameters, the mass matrix (2.25) reads

$$M_Z^2 = \frac{m_Z^2}{A} \begin{pmatrix} \xi(1+\gamma) & -\sqrt{\xi(1+\gamma)} & 0 & 0 \\ -\sqrt{\xi(1+\gamma)} & 1+\frac{\zeta}{2} & -\frac{\zeta}{2} & 0 \\ 0 & -\frac{\zeta}{2} & 1+\frac{\zeta}{2} & -\sqrt{\xi(1-\gamma)} \\ 0 & 0 & -\sqrt{\xi(1-\gamma)} & \xi(1-\gamma) \end{pmatrix}, \tag{2.53}$$

and again the W mass matrix is just the 3×3 upper-left block. In the limit $\xi \to 0$, both in the W and Z mass matrix, the lowest eigenvalue (besides the photon) goes to zero while the two other ones go to

$$\frac{m_Z^2}{A} \cdot 1 = M_1^2 \quad \text{and} \quad \frac{m_Z^2}{A} \cdot (\zeta + 1) = \frac{M_1^2}{z^2} = M_2^2. \tag{2.54}$$

In order to keep the masses of the Standard Model W/Z finite in that limit, A has to follow ξ to zero, $A \sim \xi$, and thus the two heavier copies of the gauge bosons are sent to infinity. In other words, in the decoupling limit, ξ has to be proportional to A.

The expression for the Fermi constant (2.46) becomes

$$\begin{aligned} \frac{8}{\sqrt{2}}\, G_F &= g_1^2 \frac{A}{m_Z^2} \frac{1 + c_2^2 + \frac{2\, c_1^2}{\zeta}}{c_2^2} \\ \Longrightarrow \quad s_{2\theta}^2\, \frac{\sqrt{2}\, G_F\, m_Z^2}{e^2} &= A C_0 \left(1 + \frac{1}{\xi(1-\gamma^2)} \right) \end{aligned} \tag{2.55}$$

after using relation (2.29):

$$g_1^2 = 2e^2 \left(1 + \frac{1}{\xi(1-\gamma^2)} \right). \tag{2.56}$$

Chapter 3

Electroweak precision tests

3.1 The electroweak sector of the Standard Model

3.1.1 Input parameters and the Weinberg angle

As mentioned before, the electroweak sector of the Standard Model is determined by three parameters only; in the chosen notation, f, g and g'. Three measured quantities are thus enough to fix the model, and all other observables can be compared to theoretical predictions.

The three most precisely known quantities are the electromagnetic charge e, the mass of the Z boson m_Z and the Fermi constant G_F. At tree-level, these are related to the fundamental parameters of the model in a simple way; from equations (2.10), (2.29), (2.47):

$$e = \frac{gg'}{\sqrt{g^2 + g'^2}}, \quad m_Z = f\sqrt{g^2 + g'^2}, \quad G_F = \frac{1}{4\sqrt{2}f^2}. \tag{3.1}$$

Note that these relations are symmetric under the change $g \leftrightarrow g'$; requiring the mass squared of the W to be larger than half the one of the Z lifts the ambiguity, and one has to take the solution for which $g > g'$.

The Weinberg angle is usually defined in terms of the ratio of the W to Z mass,

$$\cos^2\theta_W \equiv \frac{m_W^2}{m_Z^2}, \tag{3.2}$$

but if the fixed physical quantities are the ones above, the W mass is a prediction of the model, not an input. It is useful to define a parameter which is not a prediction and instead a fixed experimental quantity.

$$\sin^2 2\theta_0 \equiv \frac{e^2}{\sqrt{2}\, G_F\, m_Z^2} \tag{3.3}$$

provides a definition in terms of the three input values such that θ_0 coincides with the tree-level prediction of θ_W (choosing the angles in the first quadrant). From now on, unless explicitly stated, only this θ_0 will be used, in common shorthand notations such as $s_{2\theta} \equiv \sin 2\theta_0$ or $c_\theta \equiv \cos\theta_0$.

The reason for including the factor $s_{2\theta}$ in C_0 (2.51) is now clear: the left-hand side of equation (2.55), by definition, reduces to 1.

Finally, since Quantum Electrodynamics (QED) is well established and well understood, pure QED contributions are usually absorbed. More specifically, the vacuum polarization of the photon alone, *i.e.* the running of the electric charge, is taken into account when defining the reference point of the predictions without corrections due to the weak interaction. In practice, the value of e used in defining the Weinberg angle (3.3) is the electromagnetic coupling evaluated at the weak scale (at the Z pole mass), where the other quantities are then measured [33].

3.1.2 Testing the Standard Model and constraining new physics

Besides e, m_Z and G_F, many other electroweak observables are very well measured. The reached precision is enough to test the Standard Model at the level of quantum corrections, which is highly non-trivial. These corrections depend on other Standard Model parameters, most notably on the masses of the top quark and of the Higgs boson. As will be shown, the agreement between theory and experiment is particularly good for a light Higgs, and this is one of the reasons why the recent discovery seems to reinforce further the position of the Standard Model as an effective description of particle physics phenomenology.

This success also means that any extension of the Standard Model is severely constrained: any new ingredients that have anything to do with the electroweak sector will in general modify the predictions, at least at loop-level; or in models such as the 4-Site, where the electroweak gauge structure is directly modified, even the tree-level relations are altered. This means that Beyond the Standard Model scenarios have often to be tuned and are restricted to a specific region of the parameter space, or some mechanism has to play a role in suppressing unwanted corrections. To a certain degree, the $SU(2) \times U(1)$ structure, and in particular the custodial symmetry, have to be preserved in order to have a chance of reproducing the observed phenomenology.

Specifically evaluating the viability of Beyond the Standard Model scenarios requires a parametrisation of the deviation from the Standard Model predictions. This task is pretty much the same as estimating how Standard Model quantum corrections change the tree-level predictions. Thus, the same tools used to describe the success of the Standard Model can be used to place bounds on new physics.

3.2 Matching theory and experiment

3.2.1 The ϵ parametrisation

The most stringent bounds come from measurements of the Z peak during the first run of the Large Electron-Positron collider (LEP), and at the Stanford Linear Collider (SLC), which probed the interaction of the Z boson with fermions. One needs to describe corrections to the couplings relevant to these measurements. The ϵ_i parametrisation is the formalism that will be used in the current analysis [33].

Essentially, fixing e, m_Z, G_F does not determine the W mass and the Z couplings; one can define parameters, vanishing for the tree-level prediction (or rather treel-level+QED, as mentioned at the end of Section 3.1.1), relating these to the input quantities.

The first, Δr_W, is related to the W mass:

$$\Delta r_W \equiv 1 - \frac{\sin^2 2\theta_0}{\sin^2 2\theta_W} = 1 - \frac{s_{2\theta}^2}{4\left(1 - \frac{m_W^2}{m_Z^2}\right)\frac{m_W^2}{m_Z^2}}. \tag{3.4}$$

Two more are defined in terms of the leptonic width of the Z and the leptonic forward-backward asymmetry at the Z peak; in the 4-Site model, since the coupling structure of the Z to the different types of fermions is identical to the Standard Model, it is convenient to directly define $\Delta\rho$ and Δk in terms of the general Z interaction Lagrangian (2.38) (up to the overall sign),

$$\begin{aligned} a_V &= \frac{e}{s_\theta c_\theta}\left(1 + \frac{\Delta\rho}{2}\right)\left(\frac{\tau^3}{4} - s_\theta^2\,(1+\Delta k)\,Q\right), \\ a_A &= \frac{e}{s_\theta c_\theta}\left(1 + \frac{\Delta\rho}{2}\right)\frac{\tau^3}{4}. \end{aligned} \tag{3.5}$$

All three Δ parameters get Standard Model radiative corrections proportional to the top mass squared. It is customary to define linear combinations such that two of the new quantities only depend logarithmically on m_t; these are the ϵ_i parameters,

$$\begin{aligned} \epsilon_1 &\equiv \Delta\rho, \\ \epsilon_2 &\equiv c_\theta^2\,\Delta\rho + \frac{s_\theta^2}{c_{2\theta}}\,\Delta r_W - 2s_\theta^2\,\Delta k, \\ \epsilon_3 &\equiv c_\theta^2\,\Delta\rho + c_{2\theta}\,\Delta k. \end{aligned} \tag{3.6}$$

They are directly related to the alternate parametrisation S, T, U, which is defined in terms of contributions to the vacuum polarisation amplitudes of the electroweak gauge bosons.

The correspondence is

$$\epsilon_1 - \epsilon_1^{\text{REF}} = \frac{e^2}{4\pi}\,T, \quad \epsilon_2 - \epsilon_2^{\text{REF}} = -\frac{e^2}{16\pi s_\theta^2}\,U, \quad \epsilon_3 - \epsilon_3^{\text{REF}} = \frac{e^2}{16\pi s_\theta^2}\,S, \tag{3.7}$$

where the subtracted reference values are the Standard Model corrections (3.8) for some specific value of m_H (and m_t). Further details about these parametrisations are found in Refs. [34–37].

Of course, more parameters would be needed if the predicted couplings do not have the particular structure of the Standard Model, or if flavour universality is not respected. Minimally, an extra coefficient ϵ_b should be added to describe a difference between the charged lepton couplings and the bottom quark ones [38]; the 4-Site model, however, does not contribute to this latter parameter and it is not necessary to consider it [1].

The second run of LEP (LEP2) provided data which is sensitive to the interactions in the gauge sector, and thus further parameters are required for a proper analysis of this additional information, denoted V, X, Y and W [39]. Contributions from the 4-Site model to these parameters should be very much suppressed if the constraints from LEP1 are satisfied, so the discussion will be limited to the standard ϵ_i parameters [32]. Besides, as it should be clear by the end of this discussion, constraints on the gauge sector do not directly limit the c_i, which are the parameters that mainly determine the size of fermion couplings.

Finally, here are approximate expressions of the values predicted by the Standard Model, keeping the dependence on the Higgs mass explicit, and for a fixed top-quark mass, $m_t = 172.7\,\text{GeV}$ [40]:

$$\begin{aligned}
\epsilon_1^{\text{SM}} &= \left(+5.60 - 0.86\,\ln(\frac{m_H}{m_Z})\right)\cdot 10^{-3},\\
\epsilon_2^{\text{SM}} &= \left(-7.09 + 0.16\,\ln(\frac{m_H}{m_Z})\right)\cdot 10^{-3},\\
\epsilon_3^{\text{SM}} &= \left(+5.25 + 0.54\,\ln(\frac{m_H}{m_Z})\right)\cdot 10^{-3}.
\end{aligned} \tag{3.8}$$

As has been mentioned, these corrections are quite sensitive to the top-quark mass, especially ϵ_1 which exhibits a quadratic dependence on it, so choosing a different value for m_t would have an influence on the detail of the results presented here; however it should not matter in terms of general features and in the overall results.

If the light Higgs were to be removed — which is a game one could still play until last summer — the parameter m_H would then be interpreted as the cutoff of the model [39]. This is discussed in more detail later in Section 4.2.1.

3.2.2 Experimental data

The three chosen physical inputs need to be fixed. They are experimentally known to better than per mille level, which means their experimental error can be ignored in what follows. The numbers below are given for reference; they have been taken from [41] (and as a reminder, e is the electromagnetic coupling at the Z peak).

$$e^2 = \frac{4\pi}{128.886}, \quad m_Z = 91.1875\,\mathrm{GeV}, \quad G_F = 1.16637 \cdot 10^{-5}\,\mathrm{GeV}^{-2}. \tag{3.9}$$

As mentioned before, experimentally, the ϵ_i parameters are related to the mass of the W, the width of the Z and the forward-backward asymmetry and can be extracted from these quantities. All three have been measured to be different from zero with a significance larger than 5σ, which can be viewed as a confirmation that the Standard Model description does work at the quantum level.

The following results were obtained by the collaborations working on LEP and SLC, mainly from their measurements of the properties of the Z peak [41, Appendix E]. The fit to the experimental data comprises four free parameters in addition to the three ϵ_i: the Z mass, which is taken as an input here and whose value can safely be fixed as the uncertainty is very small and the correlation with the ϵ_i moderate; the ϵ_b parameter, related to the coupling of the Z to the b quark, which has little relevance to the current discussion [1]; the strong coupling constant and the hadronic contribution to the photon vacuum polarisation, which are not directly related to the electroweak sector. The best fit gives a χ^2 of 15.7 for 9 degrees of freedom (DOF) (corresponding to a probability of 7.2%).

The measured ϵ_i and their uncertainties are

$$\begin{aligned}
\epsilon_1^{\mathsf{EXP}} &= (+5.4 \pm 1.0) \cdot 10^{-3}, \\
\epsilon_2^{\mathsf{EXP}} &= (-8.9 \pm 1.2) \cdot 10^{-3}, \\
\epsilon_3^{\mathsf{EXP}} &= (+5.34 \pm 0.94) \cdot 10^{-3}.
\end{aligned} \tag{3.10}$$

They are not independent observables, though, and their correlation is given by the matrix

$$\rho = \begin{pmatrix} 1 & 0.60 & 0.86 \\ 0.60 & 1 & 0.40 \\ 0.86 & 0.40 & 1 \end{pmatrix}. \tag{3.11}$$

Note that, unlike when given in terms of S, T, U (3.7), these results do not directly depend upon reference values of m_H or m_t.

As a side remark, the best determination of the W boson mass — which is relevant to the determination of the ϵ_i parameters — now comes from the Tevatron experiments [42].

3.2.3 χ^2 test

A comparison between the measured values and the prediction (that can depend on some parameters) has to be done quantitatively, which requires some measure of the agreement between the two. There is arbitrariness in choosing the tools to do so, but the most commonly used merit function is certainly the chi-squared [43]. Given a model and data points, the best fit parameters are the ones minimizing the value of a χ^2 function constructed as below (3.14). If the uncertainties can be assumed to be Gaussian, the χ^2 follows the probability distribution

$$p\left(\chi^2\right) = \left(2^{\nu/2}\,\Gamma\left(\nu/2\right)\right)^{-1}\left(\chi^2\right)^{\nu/2-1}\exp\left(-\chi^2/2\right). \tag{3.12}$$

for $\nu =$ DOF, the number of degrees of freedom (the number of observables minus the number of free parameters).

A good fit is characterised by $\chi^2_{\text{min}} \sim$ DOF, at least for large DOF. A much higher value would mean a poor description of the data by the model; conversely, a much smaller value could point towards an over-parametrisation and a model lacking predictive power, or underestimated errors on the measurements. In the case of the ϵ_i experimental fit [41] — as mentioned in the previous section — the minimum χ^2, 15.7, is just a little less than twice the DOF, 9, which is still considered a fair agreement. The probability associated with the χ^2 taking a value at least as large as this is 7.2%. However, the interpretation of this number is not straightforward, especially when the DOF is small, or when the uncertainties are not Gaussian. Nevertheless, a very large χ^2_{min} (corresponding to a very low probability) is certainly a bad indication.

The property of χ^2 relevant to the current discussion is that the difference to the minimum value,

$$\delta\chi^2 \equiv \chi^2 - \chi^2_{\text{min}}, \tag{3.13}$$

should also follow a chi-squared distribution (3.12) with the DOF equal to the number of parameters allowed to vary. A *confidence region* in the parameter-space of the model under consideration is then defined as the region in which $\delta\chi^2$ is less than a certain level associated to a chosen probability [43]. For instance, with three DOF the $\delta\chi^2$ levels corresponding to probabilities of 68, 95 and 99%, respectively, are 3.5, 7.8 and 11.3.

From (3.10) and (3.11), one can compute the difference in χ^2 from the best fit value when the predicted ϵ_i do not match the experimental central values:

$$\delta\chi^2 = \sum_{i,j}\frac{\delta\epsilon_i}{\sigma_i}\left(\rho^{-1}\right)_{ij}\frac{\delta\epsilon_j}{\sigma_j}, \tag{3.14}$$

where $\delta\epsilon_i$ is the difference between the experimental and theoretical values for ϵ_i, σ_i is the uncertainty on the observed ϵ_i (given in (3.10)), and ρ^{-1} is the inverse of the correlation matrix (3.11). This is the quantity needed to construct confidence regions in the ϵ_i space; contours in 2-dimensional sub-spaces are obtained by minimizing the $\delta\chi^2$ with respect to the parameter one wishes to remove (and choosing levels corresponding to one less degree of freedom). Such confidence regions are shown in Figure 4.2(a).

In order to define confidence regions in the parameter space of the 4-Site model under consideration the ϵ_i are taken as the basic set of indirect observables. The value of (3.14) is then restricted to lie between the minimum it admits within the model and the chosen level. Obviously, if the minimum $\delta\chi^2$ is large to begin with (outside of the range one would pick for a reasonable confidence region in the ϵ_i space), the procedure makes little sense as the model fails to agree well with the data regardless of the value of its parameters.

In the next chapter, the notation will be shifted for more clarity: the quantity defined in (3.14) will be referred to as just χ^2, while $\delta\chi^2$ will mean the difference in χ^2 when varying the 4-Site model parameters.

3.2.4 EWPT and the need of a light Higgs in the Standard Model

Now that the required tool has been defined, theory (3.8) and experiment (3.10) can be compared.

If the corrections due to the weak interaction (3.8) are not taken into account, the predicted ϵ_i vanish, by definition. Since these parameters are measured to be significantly different from zero, a good agreement is not expected, and indeed the corresponding $\delta\chi^2$ is larger than 200. If quantum corrections are considered, the fit can be made considerably better for an appropriate choice of the parameter m_H: $\delta\chi^2_{\text{min}}$ is 2.9 for $m_H \sim 80\,\text{GeV}$, well within the 68% confidence level (CL) region which would correspond to a value of 3.5.

Using the recipe given above, considering the Standard Model to have one free parameter m_H, limits on the mass of the Higgs at, for instance, 99% CL can be set. The corresponding χ^2 value with one degree of freedom is ~ 6.6.

As shown in Figure 3.1, a Higgs with a mass similar to the one of the W/Z bosons is preferred. From this rough estimation, one would exclude a mass larger than about $200\,\text{GeV}$; a complete and more careful analysis loosens this upper bound, which is around $400\,\text{GeV}$ [41].

The message is that the Standard Model provides a good description of the electroweak precision data, on the condition that there is a light Higgs. The fact that the latter has now been observed in this preferred range — at $125\,\text{GeV}$ — makes the Standard Model stronger than ever, and places ever stronger constraints on Beyond the Standard Model scenarios or

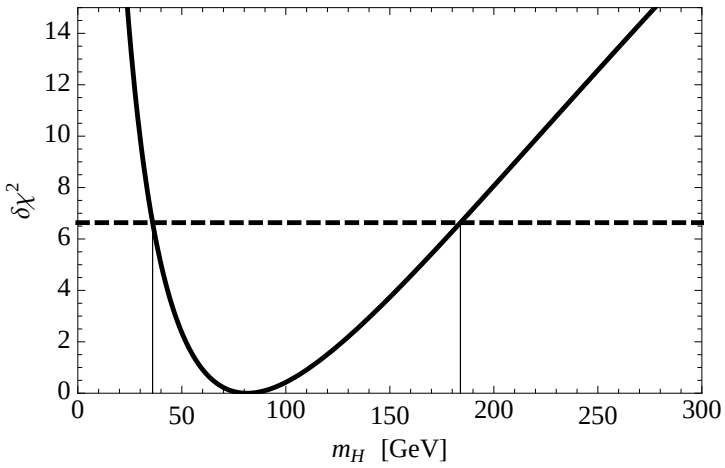

Figure 3.1: $\delta\chi^2$ as a function of the mass of the Higgs, with the 99% CL line.

weakens the reasons for introducing them, as in this 4-Site model. Had this light resonance not been observed, meaning that the parameter m_H would have had to be raised to the TeV region, the poor agreement with the EWPT would have been a very good indication of new physics.

In the next chapter, it will be shown that in the context of the 4-Site model a fair agreement with EWPT would have been possible, even without the light Higgs.

Chapter 4

Constraints on the 4-Site model

4.1 Fixing e, m_Z and G_F

4.1.1 The free parameters in the 4-Site model

The first step in the recipe presented in the previous chapter is to impose the physical input values (3.9). Three of the seven parameters of the model will thus be determined. A convenient choice is to eliminate the gauge couplings, g, g' and g_1 (or, equivalently, ξ, γ and g_1), in favour of the input

$$\{\xi, \gamma, g_1\} \quad \longrightarrow \quad \{e, m_Z, G_F\}\,; \tag{4.1}$$

the four free parameters left can then be taken to be

$$M_1 \text{ or } A; \quad z \text{ or } \zeta; \quad \{b_1,\ b_2\} \text{ or } \{c_1,\ c_2\}\,. \tag{4.2}$$

All these have been defined in Section 2.4.2 of the first chapter.

The reason why M_1 and z are kept as free input parameters is that they correspond well to, respectively, the mass of the first resonance and its ratio to the mass of the second one, as has been mentioned before.

In general, imposing the values of e, m_Z and G_F cannot be done analytically, and one has to either use numerical methods or assume the smallness of a parameter, which can then be expanded in. The 4-Site model, however, is simple enough for an analytical solution to this problem to be found.

The steps and results will be presented with a luxury of details that are not particularly relevant to phenomenology. The goal is to gather as much analytical insight as possible before performing numerical studies. This can provide some understanding useful for optimising computations and help avoiding incorrect results.

4.1.2 The electric charge

It is easy to replace g_1 in terms of e, and the relation has already been used in Section 2.4.3; anticipating equation (4.9), the expression immediately simplifies.

$$g_1^2 = 2e^2\left(1 + \frac{1}{\xi(1-\gamma^2)}\right) = \frac{2e^2}{AC_0}. \tag{2.56}$$

Note that if ξ is small or if γ^2 is close to 1, g_1 becomes large. In particular, the decoupling limit — in which ξ and A go to zero — sees g_1 blow up to infinity. In any case, g_1^2 cannot be smaller than $2e^2$, as ξ has to be positive and also $AC_0 < 1$ as will be shown.

4.1.3 The mass of the Z

The neutral gauge boson mass matrix (2.53) is of rank 3, since there is one zero mode, the photon. The eigenvalue equation for the masses of the three Z bosons is therefore a polynomial of degree three, and not four.

Expressing the Z masses for arbitrary values of the model parameters is not convenient, for the roots of a cubic equation take a somewhat convoluted form. In the context at hand, though, the problem is opposite: the parameters (more precisely just one of them) as a function of the eigenvalue is what is sought after. The equation to be solved,

$$\begin{aligned} A^3 - A^2\left(2+\zeta+2\xi\right) + A\Big((\zeta+1)(1+2\xi) + \left(1-\gamma^2\right)\xi^2\Big) \\ = \zeta\Big(\xi + \left(1-\gamma^2\right)\xi^2\Big), \end{aligned} \tag{4.3}$$

is only quadratic in the parameters, thus easy to solve. It is even linear in γ^2 — it does not depend on γ alone — so the solution can be simply expressed as

$$\gamma^2 = \frac{1-A+\xi}{\xi^2}\left(\xi - A\left(1 + \frac{1}{\zeta - A}\right)\right). \tag{4.4}$$

In principle, A in the previous equation could be any of the three eigenvalues of the matrix $\frac{A}{m_Z^2}M_Z^2$, but as mentioned before, two zero eigenvalues are obtained when $\xi \to 0$, in which case the two other ones are 1 and $\zeta + 1$. In other words, if A is much smaller than 1, it is guaranteed to be the smallest eigenvalue by a continuity argument.

It has been mentioned before that, in the decoupling limit, both A and ξ are expected to vanish together. The (positive) solution to (4.3) for ξ indeed satisfies that property.

Several constrains on what values are acceptable for the parameters can be read from (4.4). A priori ranges have been given in Section 2.4.2, but additional constrains now appear.

If $\zeta < A < 1$, γ^2 is always larger than 1, which has to be rejected as it would correspond to imaginary gauge couplings. Therefore A has to be smaller than ζ in any case, or in terms of M_1 and z,

$$A < \zeta \iff M_1 > m_Z \frac{z}{\sqrt{1-z^2}}. \tag{4.5}$$

Apart from this explicit constraint relating the free parameters M_1 and z, one can derive implicit relations ξ has to satisfy, which are given for the sake of completeness, and so that consistency of the final solution can be checked.

For γ^2 to be indeed smaller than 1, either A has to be in a particular window, determined by some critical value A_c,

$$A > A_c \equiv \frac{1}{2}\left(1+\zeta-\sqrt{1+\zeta^2}\right), \tag{4.6}$$

corresponding to low values of M_1 which are, in practice, never considered, or there is a maximum value for ξ,

$$\xi < \frac{(1-A)A\left(1+\frac{1}{\zeta-A}\right)}{(1-A)-A\left(1+\frac{1}{\zeta-A}\right)}. \tag{4.7}$$

A_c is the value of A for which the denominator of (4.7) vanishes.

Finally, γ itself should not be imaginary, so its square should be positive, which can be expressed as

$$\xi > A\left(1+\frac{1}{\zeta-A}\right). \tag{4.8}$$

4.1.4 The Fermi constant

Thanks to the choice of parametrisation and to the definition of C, the equation that has to be satisfied for the Fermi constant to take the right value is very simple (2.55), and with the definition of the Weinberg angle (3.3) reduces to

$$\begin{aligned} 1 &= AC_0\left(1+\frac{1}{\xi(1-\gamma^2)}\right) \\ &\implies \gamma^2 = 1-\frac{C}{\xi}. \end{aligned} \tag{4.9}$$

Combining it with equation (4.4), it gives a simple linear equation for ξ whose solution is

$$\xi = \frac{(1-A)A\left(1+\frac{1}{\zeta-A}\right)}{(1-A+C)-A\left(1+\frac{1}{\zeta-A}\right)}. \tag{4.10}$$

C cannot take arbitrary values, meaning that the b_k (or c_k) parameters have to be within a certain region. From (4.9) and $0 < \gamma^2 < 1$, C has to be between zero and ξ; for it to be positive, AC_0 has to be less than 1, as had been mentioned before. ξ has to be positive as well, which is automatically satisfied if A is less than A_c, but otherwise gives a lower bound on C:

$$C > A\left(1+\frac{1}{\zeta-A}\right)-(1-A). \tag{4.11}$$

Note that this bound is not necessarily relevant: the smallest C can actually get, when $c_2 \to \infty$, is $1/\left(\frac{2}{As_{2\theta}^2}-1\right)$. At last, making $C < \xi$ explicit yields the condition

$$C < A\left(1+\frac{1}{\zeta-A}\right). \tag{4.12}$$

It is easy to check that the solution for ξ, along with the constraints on C, is compatible with the previously written conditions.

4.1.5 Sign ambiguities

The solution derived in the previous section is completely independent on the sign of some of the parameters, namely γ and the c_k coefficients.

The first of these ambiguities corresponds to deciding whether g or g' is larger, and is completely analogous to the Standard Model case discussed in Section 3.1.1 of the previous chapter: unless γ is chosen positive, the mass of the W will be too low. It is easy to see at least in the decoupling limit (expanding the eigenvalues in ξ), in which the ratio of the W to Z mass squared is, as in the Standard Model, $\frac{1}{2}(1+\gamma) = \frac{g^2}{g^2+g'^2}$.

What will lift the degeneracy in the c_k parameters are the EWPT. Indeed, the only quantities sensitive to the sign of these parameters are the fermion couplings and in particular the Z coupling (2.37). More precisely, e and m_Z — the gauge sector in general — do not explicitly depend on the delocalisation parameters, the solution will therefore only depend on them through the Fermi constant, *i.e.* through the combination C, which in turn only contains c_k^2. As will be discussed further in this chapter, the region of low χ^2 is generally unique and not split into disconnected parts.

4.2 The ϵ parameters and the χ^2

4.2.1 Putting the scalar back, and m_H

To the tree-level contributions of the 4-Site model to the ϵ_i parameters the Standard Model radiative corrections shall be added: they are known to be important and, since only regions of parameter space in which the electroweak sector is not much modified will be considered, should be well approximated by the previously given expressions (3.8). Only the leading order corrections due to the new physics are considered. Indeed, in an effective description such as the 4-Site model, loop-level computations cannot be trusted unless higher dimensional operators are introduced, which introduces even more free parameters. Some arguments can be made about the matching with the low-energy theory, allowing to perform computations at one-loop level [44,45]. The difference between predicted and measured ϵ_i, on which the χ^2 depends, is thus

$$\delta\epsilon = \epsilon^{\text{4-Site}} + \epsilon^{\text{SM}} - \epsilon^{\text{EXP}}. \tag{4.13}$$

In general, if not specified otherwise, it will be understood from now on that ϵ_i and Δ mean the 4-Site contributions alone.

It is necessary at this point to comment on the interpretation of the m_H parameter in (3.8), and thus to also make a few remarks on how a light scalar mode is put back into the model in order to account for the $125\,\mathrm{GeV}$ resonance that has recently been discovered at the LHC [5,6].

Going back to the very beginning — even before new gauge bosons were added — and in particular to equations (2.3) and (2.4), it is not difficult to see that the Standard Model Higgs scalar h, the "radial mode", can be explicitly written out, separated from the "unitary part" of the Σ matrix describing the would-be Goldstone bosons, as

$$\Sigma \longrightarrow \left(1 + \frac{h}{2f}\right)\Sigma, \tag{4.14}$$

where the redefined Σ, on the right-hand side, does not satisfy (2.3) any more but is simply a unitary matrix (as would be the original Σ in the $m_H \to \infty$ limit that was discussed). These two parametrisations are equivalent [46]. In other words, it is just another way to write the Standard Model, and bringing the radial mode back ensures the electroweak symmetry is linearly realised and there are no issues with the loss of perturbative unitarity any more.

The mass matrix for the gauge bosons, which is a quadratic function of Σ, now appears multiplied by an extra factor

$$\mathcal{L}_{\text{mass}} \longrightarrow \left(1 + 2\,\frac{h}{2f} + \frac{h^2}{4f^2}\right)\mathcal{L}_{\text{mass}}. \tag{4.15}$$

The resulting peculiar interactions between the scalar and the gauge bosons, proportional to the masses of the latter, leads to a partial cancellation between the gauge and scalar contributions to the ϵ_i parameters in which the cutoff dependence disappears. Schematically

$$\ln(\frac{\Lambda}{m_Z}) - \ln(\frac{\Lambda}{m_H}) = \ln(\frac{m_H}{m_Z}), \tag{4.16}$$

and this gives the dependence shown in (3.8).

Now moving on to the 4-Site model, where additional gauge bosons are present: from the point of view of EWPT, one would want the interaction between the scalar and the gauge bosons to look just like (4.15). Indeed, since the model is tuned so that the masses and interaction structures of the lighter gauge modes match the Standard Model, this would ensure that the cancellation (4.16) still happens, to good accuracy at least. However, this creates tensions from the point of view of perturbative unitarity. Without a light scalar, the bad behaviour of the scattering of longitudinal gauge bosons is partly fixed by the exchange of the heavier resonances in the model, but these contributions are not needed when the Higgs boson is present, so there may be overcompensation. In order to avoid this situation, the couplings of h may have to depart from the Standard Model values. This is parametrised as follows [47]:

$$\left(1 + 2a\,\frac{h}{2f} + b\,\frac{h^2}{4f^2}\right)\mathcal{L}_{\text{mass}}. \tag{4.17}$$

Good perturbative behaviour would be recovered if one were to start from a fully linearly realised symmetry, *i.e.* including the radial mode corresponding to each Σ^k, resulting in a tower of Higgs bosons. Doing this in the 3-Site and requiring the extra scalar to decouple, one finds that the scattering amplitude vanishes in the high energy limit for $a^2 = b = 1/4$ [48]; this is consistent with the result obtained in the 4-Site model with one extra scalar and setting $z \to 0$ [8]. See also [49–51] for further considerations on similar models.

Back to EWPT, if the couplings of the light scalar differ significantly from the Standard Model values $a = b = 1$, the cancellation (4.16) does not occur any more: the Higgs contribution, the second term on the left-hand side of the equation, comes with an a^2 factor. So unless $a = 1$, a residual dependence on the cutoff remains. One can still write these logarithmic factors as on the right-hand side of (4.16) and re-use (3.8), only m_H should be replaced by some effective m_H^*:

$$\ln(\frac{\Lambda}{m_Z}) - a^2\ln(\frac{\Lambda}{m_H}) \equiv \ln(\frac{m_H^*}{m_Z}). \tag{4.18}$$

One recovers $m_H^* = m_H$, the mass of the Higgs boson, in the limit $a = 1$, while $a = 0$ corresponds to $m_H^* = \Lambda$, the scale of new physics; for intermediate values of a, m_H^* is between these limiting cases.

To summarise, there seems to be a trade-off between delaying the violation of perturbative unitarity and satisfying EWPT. Understanding the details of these effects, including the possible subtleties arising when more scalars are added, is far beyond the original scope of this thesis, however. The results will mainly focus on $m_H^* = 125\,\mathrm{GeV}$ and $3\,\mathrm{TeV}$, the first corresponding to the ideal presence of a purely Standard Model Higgs boson and the second to the originally studied Higgsless picture with a conservatively high cutoff [32]. From now on, m_H should be understood as this effective m_H^*.

4.2.2 The evaluation

Not much is to be said about the evaluation of the 4-Site model contributions to the ϵ_i parameters themselves.

On one hand, the fermion couplings of the lightest Z boson need to be computed from equation (2.37). The corresponding eigenvector — z_0^k — has to be obtained, which can, in principle, be done analytically thanks to the fact that the eigenvalue has been fixed (to be the Z mass); in practice, obtaining it numerically with Mathematica [4] after having fixed the value of all the parameters is enough. Comparing with (3.5), one gets two of the Δ parameters:

$$\begin{aligned}
1+\frac{\Delta\rho}{2} &= \frac{1}{\sqrt{A\left(1+c_2^2+\frac{2\,c_1^2}{\zeta}\right)}} \\
&\qquad \left|\sqrt{\xi(1+\gamma)}\,z_0^0+(c_1-1)\,z_0^1+(c_2-c_1)\,z_0^2-c_2\sqrt{\xi(1-\gamma)}\,z_0^3\right|, \\
\frac{1}{1+\Delta k} &= s_\theta^2\left(1-\frac{\sqrt{\xi(1+\gamma)}\,z_0^0+(c_1-1)\,z_0^1+(c_2-c_1)\,z_0^2}{c_2\sqrt{\xi(1-\gamma)}\,z_0^3}\right).
\end{aligned} \tag{4.19}$$

The absolute value here reflects the fact that the overall sign of the z_0^k can be arbitrarily chosen. In order to recover the conventional sign for the Z couplings, it should be set in such a way that the absolute value in the above expression is unnecessary.

The evaluation of Δr_W (3.4) only requires the computation of the lowest eigenvalue of the charged bosons mass matrix. Again, this can in principle be done analytically, but the complicated expression for cubic roots is not practical and does not provide particular insight; a numerical evaluation is better suited.

4.2.3 Expressions in the decoupling limit

Since the exact analytical evaluation of the ϵ_i parameters does not give particularly simple expressions, it is useful to at least check their behaviour in the decoupling limit, *i.e.* taking A to zero.

First, the solution that has been just derived is, in this limit,

$$\begin{aligned}\xi &= A\left(1+\frac{1}{\zeta}\right)+\mathcal{O}\left(A^2\right),\\ \gamma^2 &= 1-\frac{C_0}{1+\frac{1}{\zeta}}+\mathcal{O}\left(A\right).\end{aligned} \tag{4.20}$$

The mass of the W is

$$\frac{m_W^2}{m_Z^2}=\frac{1}{2}\left(1+\sqrt{1-\frac{C_0}{1+\frac{1}{\zeta}}}\right)+\mathcal{O}\left(A\right), \tag{4.21}$$

or, equivalently

$$\sin^2 2\theta_W=\frac{C_0}{1+\frac{1}{\zeta}}+\mathcal{O}\left(A\right). \tag{4.22}$$

Finally, the properly normalised Z eigenvector is

$$\begin{aligned}\sqrt{\xi(1+\gamma)}\,z_0^0 &= \sqrt{\frac{A}{2\,\zeta}}\left(\sqrt{1+(1-C_0)\zeta}+\sqrt{1+\zeta}+\mathcal{O}\left(A\right)\right),\\ z_0^1 &= \sqrt{\frac{A}{2\,\zeta}}\left(\sqrt{1+(1-C_0)\zeta}+\frac{1}{\sqrt{1+\zeta}}+\mathcal{O}\left(A\right)\right),\\ z_0^2 &= \sqrt{\frac{A}{2\,\zeta}}\left(\sqrt{1+(1-C_0)\zeta}-\frac{1}{\sqrt{1+\zeta}}+\mathcal{O}\left(A\right)\right),\\ \sqrt{\xi(1-\gamma)}\,z_0^3 &= \sqrt{\frac{A}{2\,\zeta}}\left(\sqrt{1+(1-C_0)\zeta}-\sqrt{1+\zeta}+\mathcal{O}\left(A\right)\right).\end{aligned} \tag{4.23}$$

The Δ parameters are then readily derived:

$$\begin{aligned}\Delta\rho &= 2\left(\frac{\left|2c_1+(1+c_2)\zeta\right|}{\sqrt{2\left(1+\zeta\right)\left(2c_1^2+(1+c_2^2)\zeta\right)}}-1\right)+\mathcal{O}\left(A\right),\\ \Delta k &= \left(\frac{2c_2}{2c_1+(1+c_2)\zeta}\,\frac{1+\zeta-\sqrt{(1+\zeta)(1+(1-C_0)\zeta)}}{1-\sqrt{1-s_{2\theta}^2}}-1\right)+\mathcal{O}\left(A\right),\\ \Delta r_W &= \left(1-s_{2\theta}^2\,\frac{1+\frac{1}{\zeta}}{C_0}\right)+\mathcal{O}\left(A\right)=\left(1-\frac{2c_2^2\left(1+\zeta\right)}{2c_1^2+(1+c_2^2)\zeta}\right)+\mathcal{O}\left(A\right),\end{aligned} \tag{4.24}$$

and the ϵ_i parameters themselves are combinations of these (3.6).

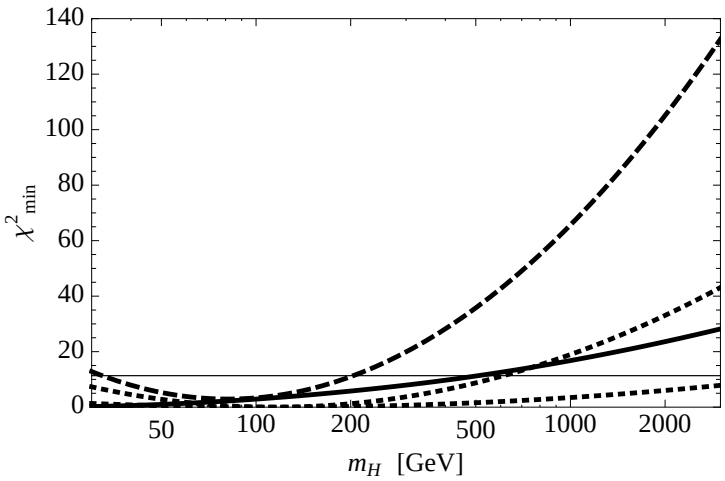

Figure 4.1: χ^2_{min} as a function of m_H; the continuous line is the 4-Site model, the dashed line the Standard Model, and the dotted lines are obtained setting ϵ_1 to zero and either tuning $\delta\epsilon_{2,3}$ to the best values (the lower line) or setting them to zero (the upper line). The horizontal line is the 99% CL (for three DOF).

4.2.4 The minimum χ^2

In order to establish a confidence region in the parameter space, the first ingredient needed is the minimum value χ^2 can take within the model for a given m_H. The Higgs mass will not be considered as a free parameter but only as some fixed number determining the size of the Standard Model radiative corrections to the ϵ_i (and interpreted as argued in Section 4.2.1). Two cases will be specifically discussed: $m_H = 125\,\text{GeV}$, where the Higgs boson actually is, and $m_H = 3\,\text{TeV}$, the cutoff scale of the effective description, as considered in previous analyses [1,2] and corresponding to the absence of a light scalar. It will be shown that, without the Higgs boson, new dynamics on top of the Standard Model would certainly have been required and that, even though the 4-Site model can improve the agreement with the EWPT, other additional ingredients would have been expected below the cutoff.

Anticipating the results, for the physical Higgs mass, the χ^2_{min} in the 4-Site is about 3.7, marginally smaller (20%) than in the Standard Model. Removing the Higgs — setting $m_H = 3\,\text{TeV}$ — the χ^2 can be reduced by a factor 5, bringing it down from 130 to 30; it is still too high, corresponding to being only on the edge of a 5σ confidence region in the ϵ_i space (*i.e.* at 99.9999% CL), but certainly much better than in the Standard Model in which one would be over 10σ away from the best fit. The result for arbitrary m_H is shown in Figure 4.1.

It is instructive to project onto the ϵ_3-ϵ_1 (or S-T) plane and see where the models sit relative to the confidence region. This is shown in Figure 4.2(a). Although the 4-Site model appears to sit almost within the 99% CL region at $m_H = 3\,\text{TeV}$ (corresponding to a χ^2 of about 11 when considering the 3-dimensional ϵ_i space), because ϵ_2 cannot simultaneously be tuned to the right value, the χ^2 is in fact much higher, at 28, as shown in Figure 4.2(b). At the other end of the m_H range, note that although the Standard Model point is close to the

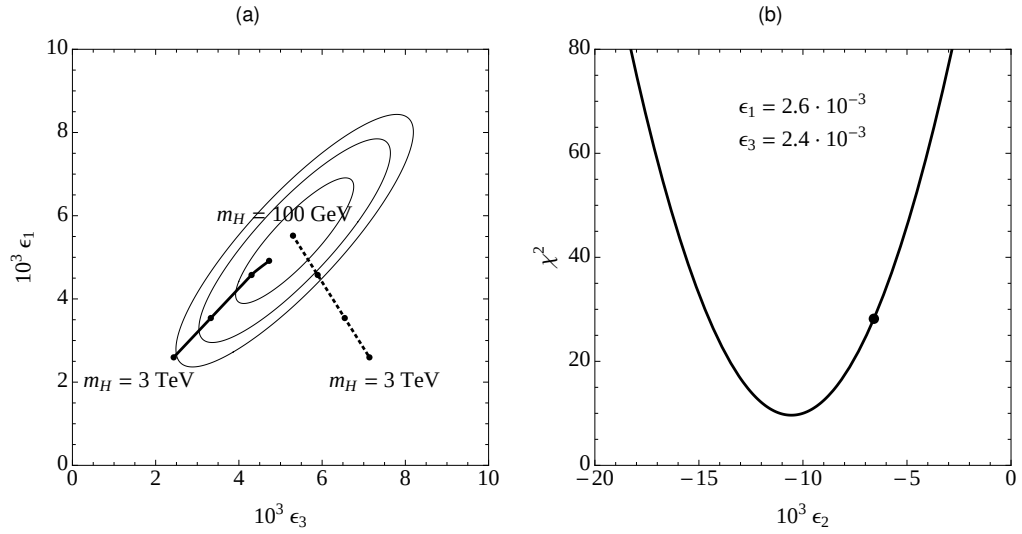

Figure 4.2: (a) The concentric ellipses delimit the confidence regions at 68, 95 and 99% CL (from the smallest to the largest) in the ϵ_3-ϵ_1 (S-T) plane. The thick lines are the model predictions as a function of m_H; the dots correspond to $m_H = 100\,\mathrm{GeV}$, $300\,\mathrm{GeV}$, $1\,\mathrm{TeV}$ and $3\,\mathrm{TeV}$. The solid line shows the 4-Site prediction while the dashed one is for the Standard Model alone. In the 4-Site, the points are obtained by minimizing the overall χ^2 (3.14) with respect to the four free parameters as will be discussed in this section. (b) χ^2 in the ϵ_2 direction at the point corresponding to $m_H = 3\,\mathrm{TeV}$ in the 4-Site model. The black dot corresponds to the 4-Site model value.

centre of the region, the overall χ^2 is lower in the 4-Site, again because of ϵ_2. What the figure highlights is how, when considering larger m_H, it is possible to tune the value of ϵ_3 in the 4-Site model to go back in the alignment of the ellipse and significantly reduce the χ^2. On the other hand, this is not possible with ϵ_1 and it takes the same value as in the Standard Model for m_H above a few hundred GeV. If no Higgs boson had been discovered at the LHC, the 4-Site model would have helped fixing the agreement with EWPT, but other contributions would still have been required, for instance to ϵ_1 (or T) indeed; large contributions to that parameter, unlike in the case of ϵ_3, imply a violation of custodial symmetry [39], thus adding operators breaking this symmetry might have been required in order to construct a physically viable model.

The 4-Site contributions to the ϵ_i parameters allow to push the 99% CL upper bound on m_H to about $500\,\mathrm{GeV}$ (compared to just a couple of hundred GeV in the Standard Model alone), as seen from Figure 4.1. For a larger m_H, the 4-Site model on its own is incomplete as it fails the EWPT, and further ingredients would be required; as argued in the previous paragraphs, there is a significant improvement over the Standard Model nevertheless, and limited additions might be enough. Even though the model is ruled out for $m_H = 3\,\mathrm{TeV}$, results will still be discussed in that case. Considering the extreme limits $m_H = 125\,\mathrm{GeV}$ and $3\,\mathrm{TeV}$ (in the sense discussed in 4.2.1), which may both be unphysical, allows to explore to what extent the phenomenology of the 4-Site can vary. The main results,

concerning the validity of approximate evaluations of the ϵ_i parameters, and the general conclusion that heavy electroweak gauge boson resonances do not need to be fermiophobic are unchanged.

In any case, one still has to find where the minimum χ^2 sits in the parameter space, and it will help to start with a few observations.

First, an obvious statement that has to be made nevertheless is that, in the decoupling limit — $A \to 0$ *and* $c_1 = c_2 = 1$ —, all three 4-Site ϵ_i contributions vanish. Indeed they have to, if the 4-Site model is to reduce to the Standard Model in that limit. The corollary of that statement is that χ^2_{min} has to be at least as low as the corresponding Standard Model value. In particular for large values of the Higgs mass, the χ^2 can be significantly reduced compared to the Standard Model.

Second, for a low χ^2, meaning a good agreement with the data, the ϵ_i parameters need to be small, of order 10^{-3}. Choosing arbitrary (allowed) values for the c_k parameters does not guarantee this at all, some tuning is therefore required. In practice, interesting regions in parameter space may be very localised, there may be flat directions (*i.e.* extended regions in parameter space along which the quantities of interest are practically constant), and there may be degeneracies, meaning that the task of numerically minimising the χ^2 can benefit from some analytical guidance. Such a better understanding also helps identifying the region of interest in the c_1-c_2 plane when the other parameters are fixed.

Next, it appears that the true χ^2_{min} is always obtained at $A = 0$. Perturbing around that point and scanning the parameter space only seems to increase the χ^2; although no analytical proof is offered, the remarks made in this section should provide arguments that it is unlikely for that minimum to be local only, the global one being at some finite value of A. This is where the expressions given in the previous section will prove useful.

Another important observation presented here without formal proof but only as a numerically checked property is that $\Delta\rho = \epsilon_1$ cannot be positive for any valid parameters in the model; more precisely, it is bounded between -2 and zero. The vector which is dotted with the Z eigenvector in equation (4.19) can have a norm larger than one, but it is then necessarily misaligned with z_0^k such that the scalar product is always less than 1. Even when going to limiting cases (*e.g.* maximum or minimum allowed values for C), this appears to be true. It is easy to check that this holds for $A = 0$ at least (4.24).

Given the data (3.10) and the Standard Model contributions (3.8), the preferred value for ϵ_1 is positive as soon as m_H is larger than about a hundred GeV and increases monotonically. The previous point, however, was that the 4-Site model tree-level contribution is at best zero, by no means positive. A strict lower bound on χ^2_{min} follows: it will not be possible to do better than setting ϵ_1 to zero and adjusting the two other ones in order to minimise the χ^2, at least for a large m_H. Note that, because of correlation, the optimal values are not simply $\delta\epsilon_{2,3} = 0$. The ϵ_i in the 4-Site model are not entirely independent, however, making it

impossible to reach this minimum; on the other hand, it turns out that it is possible to obtain a slightly better result, for large m_H, than making the $\delta\epsilon_{2,3}$ vanish, as shown in Figure 4.1.

Finally, in most cases, χ^2_{min} does not depend on ζ. It is instructive to further simplify the expressions (4.24) by sending ζ to either zero or infinity and to understand these limiting cases.

4.2.4.a The degenerate limit

If A has been sent to zero, it is safe to do the same with ζ next. The order here matters indeed, since A has to be smaller than ζ. Similarly, the condition on C (4.12), which becomes

$$C_0 = s_{2\theta}^2 \, \frac{1 + c_2^2 + \frac{2\,c_1^2}{\zeta}}{2\,c_2^2} < 1 + \frac{1}{\zeta}, \tag{4.25}$$

needs to hold asymptotically. So when $\zeta \to 0$,

$$s_{2\theta}^2 < \frac{c_2^2}{c_1^2}. \tag{4.26}$$

Now $\epsilon_1 = \Delta\rho$ identically vanishes in this limit, which is good for large m_H, as has been just argued. The other two Δ simplify and only depend on the ratio c_2/c_1, not on the magnitude of the parameters:

$$\begin{aligned} \Delta k \;&\longrightarrow\; \frac{c_2}{c_1} \, \frac{1 - \sqrt{1 - \frac{c_1^2}{c_2^2}\, s_{2\theta}^2}}{1 - \sqrt{1 - s_{2\theta}^2}} - 1, \\ \Delta r_W \;&\longrightarrow\; 1 - \frac{c_2^2}{c_1^2}. \end{aligned} \tag{4.27}$$

Obviously, they both vanish if this ratio is 1 (since it should happen for $c_1 = c_2 = 1$), and χ^2_{min} has to be close to that point. A negative ratio is strongly disfavoured, as it would mean a large Δk.

Minimising the χ^2 in this limit does yield the true χ^2_{min} if m_H is large enough. However, this minimum may only be local for smaller m_H, namely when the fit starts preferring a negative (rather than zero) contribution to ϵ_1. This happens even before $\epsilon_1^{\text{EXP}} - \epsilon_1^{\text{SM}}$ becomes negative because of correlations; it is the case in particular when m_H is set to the physical Higgs mass. The true minimum can be reached in this degenerate limit with small m_H nevertheless, on the condition that the c_k parameters also scale with ζ and are not kept finite. The way to do so while keeping the other Δ under control is by making both vanish in

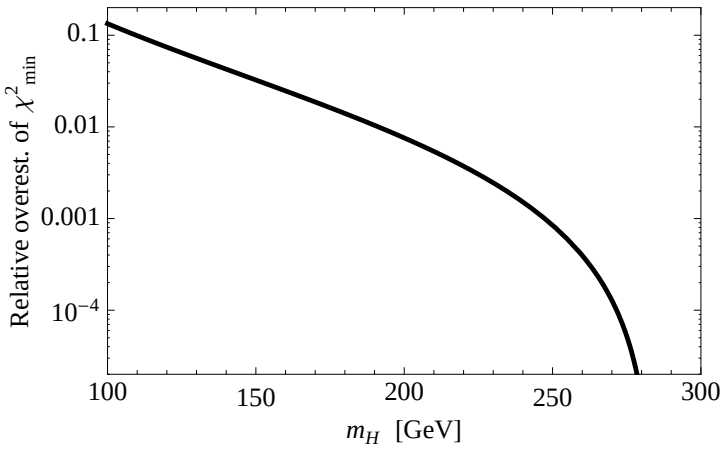

Figure 4.3: Relative difference between the minimum χ^2 obtained in the $\zeta \to 0$ limit keeping the c_k parameters finite or not, as a function of m_H.

the following way:

$$c_1 \equiv \sqrt{\zeta}\,\tilde{c}_1, \quad c_2 \equiv \sqrt{\zeta}\,\tilde{c}_2, \tag{4.28}$$

where the $\tilde{c}_i$ are finite. The condition (4.25) then becomes

$$s_{2\theta}^2 < \frac{2\tilde{c}_2^2}{1+2\tilde{c}_1^2}, \tag{4.29}$$

and the Δ parameters go to

$$\begin{aligned}
\Delta\rho &\longrightarrow 2\,\frac{\sqrt{2}\,|\tilde{c}_1|}{\sqrt{1+2\tilde{c}_1^2}} - 2, \\
\Delta k &\longrightarrow \frac{\tilde{c}_2}{\tilde{c}_1}\,\frac{1-\sqrt{1-\frac{1+2\tilde{c}_1^2}{2\tilde{c}_2^2}\,s_{2\theta}^2}}{1-\sqrt{1-s_{2\theta}^2}} - 1, \\
\Delta r_W &\longrightarrow 1 - \frac{2\tilde{c}_2^2}{1+2\tilde{c}_1^2}.
\end{aligned} \tag{4.30}$$

Sending these $\tilde{c}_i$ to infinity while keeping their ratio fixed brings the expressions back to the previous case, of course. The difference now is that there is an extra handle controlling the size of $\epsilon_1 = \Delta\rho$.

Compared to keeping the c_k finite, a lower χ^2 value can be obtained this way when m_H is below $\sim 300\,\mathrm{GeV}$, but the effect is small: even for $m_H = 125\,\mathrm{GeV}$, the difference is less than 10%, as shown in Figure 4.3.

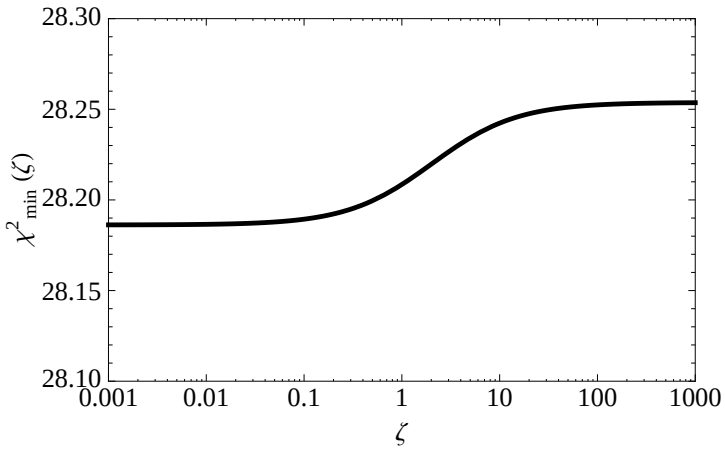

Figure 4.4: Minimum value of the χ^2 obtained at fixed value of ζ, for $m_H = 3\,\mathrm{TeV}$.

4.2.4.b The large ζ limit

The opposite limit, $\zeta \to \infty$, can also be taken; again, the c_k parameters are kept finite at first. This time all c_1 dependence is washed away, and c_2 alone is left as a parameter:

$$\begin{aligned}
\Delta\rho &\longrightarrow \frac{\sqrt{2}\,|1+c_2|}{\sqrt{1+c_2^2}} - 2, \\
\Delta k &\longrightarrow \frac{2c_2}{1+c_2}\,\frac{1-\sqrt{1-\frac{1+c_2^2}{2c_2^2}\,s_{2\theta}^2}}{1-\sqrt{1-s_{2\theta}^2}} - 1, \\
\Delta r_W &\longrightarrow 1 - \frac{2c_2^2}{1+c_2^2} = \frac{1-c_2^2}{1+c_2^2}.
\end{aligned} \tag{4.31}$$

Condition (4.25) still has to be satisfied and reads

$$s_{2\theta}^2 < \frac{2c_2^2}{1+c_2^2}. \tag{4.32}$$

Since only one parameter is left, there is not much freedom to tune the model. In particular going away from $c_2 = 1$ makes the value of $\epsilon_1 = \Delta\rho$ smaller, which reduces the agreement with data when m_H is large. As a result, the minimum obtained for $m_H = 3\,\mathrm{TeV}$ is slightly larger than the one obtained in the degenerate limit. Figure 4.4 shows this mild ζ dependence.

Allowing c_1 to follow ζ to infinity by making the same replacement as before (4.28) (this time only for c_1, in order to avoid trivial cancellations), some additional control is gained.

The expressions become

$$\begin{aligned}
\Delta\rho &\longrightarrow \frac{\sqrt{2}\,|1+c_2|}{\sqrt{1+c_2^2+2\tilde{c}_1^2}} - 2, \\
\Delta k &\longrightarrow \frac{2c_2}{1+c_2}\,\frac{1-\sqrt{1-\frac{1+c_2^2+2\tilde{c}_1^2}{2c_2^2}\,s_{2\theta}^2}}{1-\sqrt{1-s_{2\theta}^2}} - 1, \\
\Delta r_W &\longrightarrow 1 - \frac{2c_2^2}{1+c_2^2+2\tilde{c}_1^2},
\end{aligned} \tag{4.33}$$

with the condition

$$s_{2\theta}^2 < \frac{2c_2^2}{1+c_2^2+2\tilde{c}_1^2}. \tag{4.34}$$

In that way, ϵ_1 can only be decreased further, though. Therefore, it does not help in the large m_H case; for small m_H, however, it does. In fact, expressions (4.30) and (4.33) are equivalent up to a redefinition of the c_k parameters. Making the replacement

$$\tilde{c}_1^2 \longrightarrow \frac{(1+c_2)^2}{2\left(4\tilde{c}_1^2+(1-c_2)^2\right)}, \quad \tilde{c}_2^2 \longrightarrow \frac{2c_2^2}{4\tilde{c}_1^2+(1-c_2)^2} \tag{4.35}$$

while matching the signs of $\frac{\tilde{c}_2}{\tilde{c}_1}$ and $\frac{2c_2}{1+c_2}$ turns the first set of expressions into the second. This transformation does not map the entire $\tilde{c}_1$-$\tilde{c}_2$ plane, though, and in particular it is impossible to go back to the $\zeta \to 0$ with finite c_k case, starting from the opposite limit. It means that, contrary to what happens for large m_H, the same χ^2 can be reached at low m_H in both $\zeta \to 0$ and ∞ limits. Furthermore, this is true for any finite value of ζ: there is a strict flat direction, provided that m_H is small enough.

4.2.5 The region of interest

The analysis done on χ^2_{min} should help understand where the region of low χ^2 — the physically relevant region — sits in the c_1-c_2 plane. Most elements needed to discuss this question have now been given; one just needs to thread them together and try to develop the picture, considering finite ζ and A.

4.2.5.a Finite ζ

The preferred region is generally a narrow strip whose orientation mainly depends on ζ: for small values, it is concentrated around $c_1 \approx c_2$ (*i.e.* $b_2 \approx 0$) while, for large values, it lines-up with $c_2 \approx 1$ (*i.e.* $b_1 + b_2 \approx 0$). In the strict limits that were considered, the extension of these regions is infinite; at finite values of ζ, though, the region of interest must interpolate

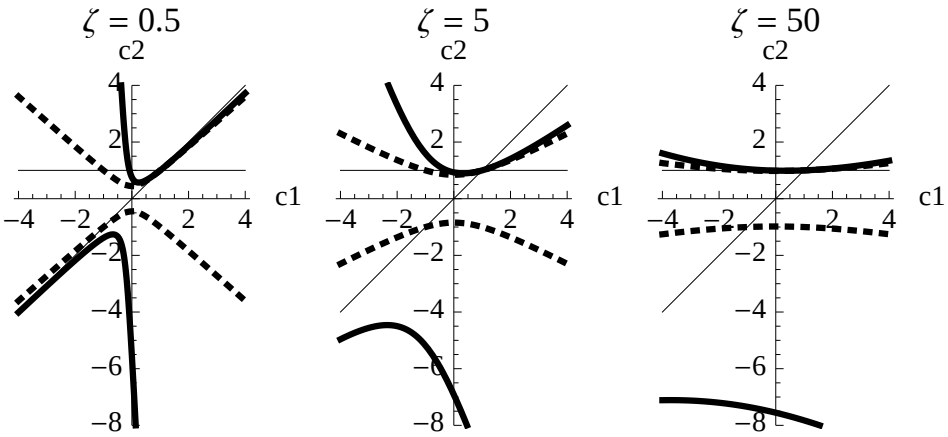

Figure 4.5: Points in the c_1-c_2 plane for which Δk (solid line) or Δr_W (dotted line) vanishes, at $A = 0$ and different values of ζ. The χ^2 can only be low where the curves meet. The thin lines give the $\zeta \to 0$ and ∞ limits of the intersection, as a reference.

between the two lines, and in the process it becomes finite. It is also clear that $c_1 = c_2 = 1$ is a special point, as it is the intersection of the two limiting cases, thus it should always be at least in the vicinity of the low χ^2 region. Only when A is increased, does it start producing a significant shift, since for any ζ the ϵ_i parameters vanish at that point when $A = 0$.

One can get a good feel for what the orientation and, to some extent, the size of the region is by looking for points where both Δk and Δr_W are close to zero. In the limit $A \to 0$ (4.24), it is easy to analytically solve $\Delta k = 0$ and $\Delta r_W = 0$ (separately), and then plot the resulting curves to see where they are close to each other, as shown in Figure 4.5. The reason why the region of interest has to be in this vicinity is that the gradient of the Δ perpendicular to these curves is steep.

In terms of the ϵ_i parameters, it has been noted before [32] that the preferred direction manifests itself mainly in ϵ_3, since it has a Δk dependence; in ϵ_2, on the other hand, it plays against Δr_W, resulting in a reduced sensitivity. What then sets the extension of the allowed region is mainly ϵ_1, as the tension with the experimental data is stronger than for ϵ_2.

An additional point to make here is that this relation between c_1 and c_2 roughly corresponds to fixing the value of C, since the W mass (thus Δr_W) only depends on the delocalisation parameters through that precise combination. Since $c_1 = c_2 = 1$ should be at least close to the low χ^2 region, the preferred value for C should be close to what it is at that point, *i.e.* $C_0 \approx s_{2\theta}^2 \left(1 + \frac{1}{\zeta}\right)$. Moreover, the entire gauge sector also depends on C only and not on the c_k explicitly, implying that, for a given ζ and A, all gauge self-couplings are determined (up to overall signs) and, within the allowed region, depend very little on the c_k.

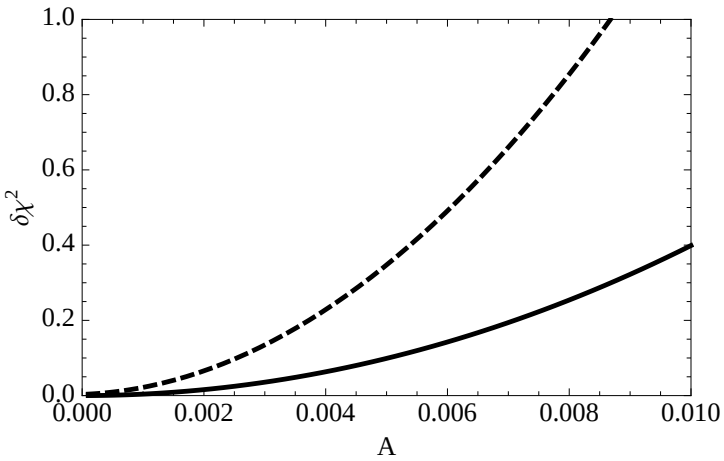

Figure 4.6: Minimum χ^2 difference for $\zeta = 1$ and fixed A. The solid line and dashed lines are, respectively, for $m_H = 125\,\mathrm{GeV}$ and $3\,\mathrm{TeV}$.

4.2.5.b Finite A

Now that the χ^2_{min} has been found for $A = 0$, the vicinity of that point can be explored to check that it is indeed a local minimum, at least. At finite A, not only is there a minimum allowed value for ζ, but a slight preference for larger values of ζ also appears. Nonetheless, since there is pretty much a flat direction along ζ at zero A, the dependence on this parameter is not too strong if it is large enough compared to A. Thus, fixing the value of ζ for simplicity still allows to get a good idea of the behaviour of the χ^2. Figure 4.6 shows difference between the χ^2 and its minimum value, obtained at fixed A and ζ, which indeed grows with A.

There can be marginal regions where the χ^2 goes back down for larger values of A. The corresponding masses of the new vector bosons then receive important corrections and are actually larger than $\sim M_1$. What happens then is that, compared to the small A limit where the Standard Model gauge bosons are mainly located at the extremities of the Moose diagram, the role of the $SU(2)$ factors gets inverted, so to speak. These cases will not be discussed here, though; only the region of small A will be under consideration.

As for the effect of A on the region of low χ^2 in the c_1-c_2 plane, it is mainly an upwards shift, as shown in Figure 4.7; for simplicity, only the $\Delta r_W = 0$ contour is shown, but it is indicative of where the region of interest lies indeed.

4.3 Limits on physical quantities

Now that χ^2_{min} has been established, $\delta\chi^2$ (3.13) can be computed. Surfaces of constant $\delta\chi^2$ in the 4-dimensional parameter space delimit confidence regions. The value of $\delta\chi^2$ corresponding to a given confidence level is here given by the value of the cumulative χ^2

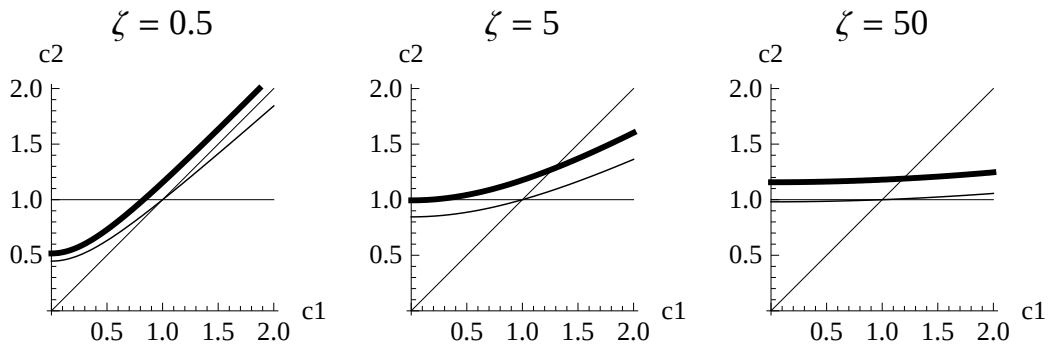

Figure 4.7: The $\Delta r_W = 0$ curve in the region of interest for $A = 0$ (thin line) and $A = 0.1$ (thick line), at different values of ζ.

distribution with 4 degrees of freedom. Mainly the 95% CL will be considered, which is $\delta\chi^2 = 9.49$.

Of particular interest are the points in the allowed region where the couplings to the new vector resonances are largest. These are expected to be somewhere on the surface of the region, since bigger new physics effects should imply more important deviations from the Standard Model, thus a larger χ^2.

For the sake of comparison with previous works [1, 32], the parameter space will be described in terms of (z, M_1, b_1 and b_2) rather than (ζ, A, c_1 and c_2); translating from one to the other is straightforward, though, using (2.50).

4.3.1 b_k dependence and degeneracy

Figure 4.8 shows a typical situation and illustrates the discussion of Section 4.2.5 about the shape and size of the region of interest, only now shown in the b_k rather than c_k plane. It allows to make several remarks.

First, the delocalisation parameters b_k introduced in Section 2.3.1 are necessary even for low m_H, if M_1 is not taken particularly large (in the decoupling limit $M_1 \to \infty$ the Standard Model, which agrees well with data at low m_H, is recovered for vanishing b_k): one can see that the $b_k = 0$ point is excluded from the allowed region.

Second, there is indeed an exact ideal delocalisation point, where $a_C^1 = a_C^2 = 0$, *i.e.* where the two thick lines cross in Figure 4.8, but it is not necessarily inside the confidence region.

Third, the largest allowed couplings correspond to points at the extremities of the ellipse. Due to the interplay between the two decoupling parameters, the fermion couplings can be made significantly larger than if they were restricted to be close to the ideal delocalisation.

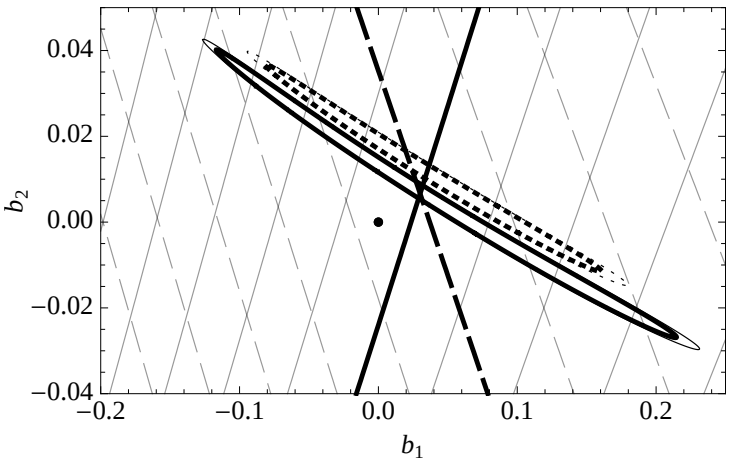

Figure 4.8: Slice of parameter space at $z = 0.8$ and $M_1 = 1\,\mathrm{TeV}$. The straight diagonal lines represent contours of given charged fermion current couplings (dashed: a_C^1; solid: a_C^2), normalised to the Standard Model coupling; the lines are separated by 0.2 and the thick ones correspond to zero (they are the bottom of "valleys": the absolute value of the couplings increases in both directions). The thick and thin ellipses are, respectively, the 95% and 99% CL contours; the solid one is for $m_H = 125\,\mathrm{GeV}$, the dotted one for $m_H = 3\,\mathrm{TeV}$. The dot show the $b_1 = b_2 = 0$ point.

Next, the couplings to the first and second resonance are not independent; fixing the size of one approximately determines the other one.

Last, there seems to be an approximate degeneracy in parameter space: the confidence region is centred around the vicinity of the ideal delocalisation, and on either side are points with sensibly the same charged fermion couplings. It does not directly appear in the figure, but what distinguishes these two sides is the *relative* sign between the fermion couplings and the trilinear and quartic gauge couplings. As mentioned in the previous section, the magnitude of the gauge self-couplings is fairly constant within the ellipses, but in order to preserve their sign, the fermion couplings have to change sign across the zero contour.

The neutral current couplings (2.37) also deserve a few comments.

The coefficient giving the Q dependence is, just like the trilinear and quartic gauge couplings, fixed by the value of C, and thus varies very little inside the confidence region; the right-handed couplings a_R cannot be tuned by varying the c_k parameters. The coefficient of τ^3 is constructed the same way as the charged couplings, and it has a very similar dependence on c_k, including the sign difference between the two regions. The first of these two coefficients is small compared to the largest allowed values for the second, thus the approximate degeneracy observed for the charged couplings still appears to some degree (the picture gets modified most for large z and small M_1, *i.e.* small ζ and large A). At the extremities of the ellipse, the heavy Z bosons couple predominantly to left-handed fermions; around the ideal delocalisation, they have small but non-vanishing photon-like couplings (*i.e.*

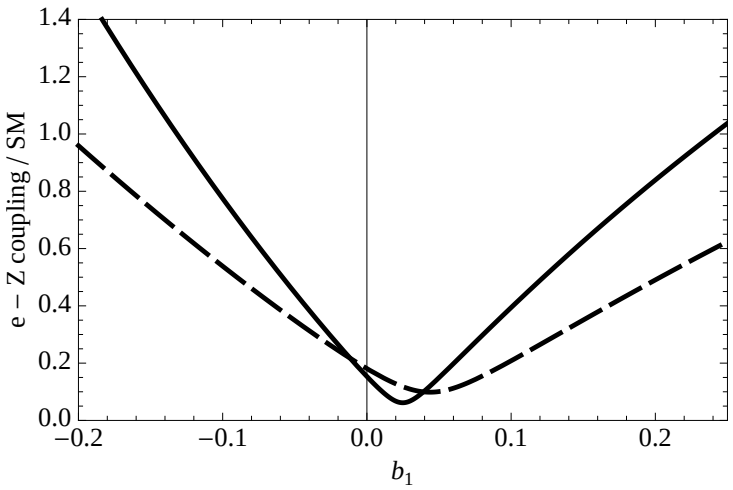

Figure 4.9: The combination $\sqrt{(a_V^i)^2 + (a_A^i)^2}$ for the electron, normalised to the Standard Model value, as a function of b_1, picking points along the minimum χ^2 valley. The dashed line is for the first heavy Z, the solid line for the second. The other parameters have been set to $z = 0.8$, $M_1 = 1\,\mathrm{TeV}$ and $m_H = 125\,\mathrm{GeV}$.

$a_R = a_L$). Furthermore, the sizes of the couplings to the first and second resonances are linked in the same way as in the charged case. The situation is illustrated in Figure 4.9.

For most interesting regions of parameter space, there is thus a certain degeneracy in terms of fermion couplings; a physical difference would only appear in processes involving gauge boson self-interactions. No particular attention will be given to that specific feature, though, as the focus of the discussion is solely on fermion couplings.

4.3.2 Maximum allowed couplings

One can search for the point on the surface of the confidence region that yields the largest coupling for a given resonance mass, having fixed z. Results are presented in terms of the charged gauge bosons, but the general picture in the neutral sector is exactly the same.

Figure 4.10 compares the limits on the two resonances. Not surprisingly, the heavier the resonances, the more strongly can they couple to the Standard Model without spoiling the EWPT substantially. At a same mass-point, the couplings to the second heavy W can in general be made larger compared to the first. Besides, the overall improvement of the fit for smaller m_H relaxes the bounds.

A broader view of the parameter space, including the z dependence, is shown in Figure 4.11. For most intermediate values of z and M_1, the largest allowed a_C^2 mainly depends on the mass of the resonance. What happens with the first resonance, though, is that as the second one is pushed away to higher energies (lowering z), it has to couple less and less to fermions. One can therefore imagine cases where the first heavy gauge boson has a low mass but suppressed fermion couplings, making its visibility very low, while the second one

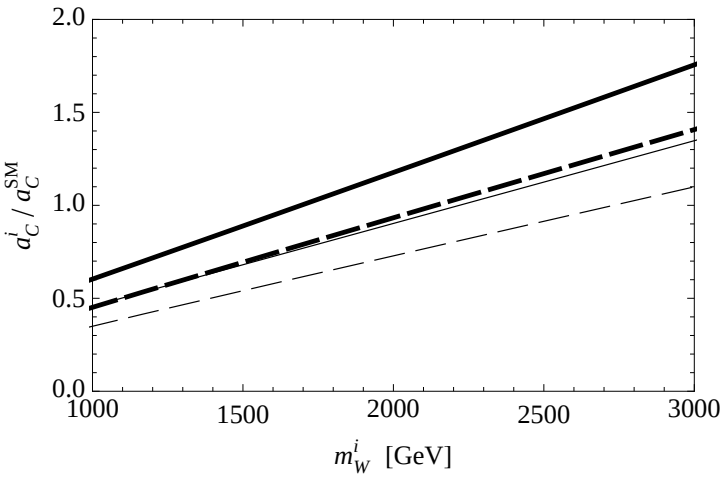

Figure 4.10: Maximum allowed charged current couplings at 95% CL, for $z = 0.8$, as a function of the mass of the gauge bosons. The solid and dashed lines are, respectively, the limits corresponding to the heavier and the lighter of the two extra W resonances. The thick lines are for $m_H = 125\,\mathrm{GeV}$ and the thin ones for $m_H = 3\,\mathrm{TeV}$. The value of the couplings is normalised to the Standard Model one.

could have Standard Model-like couplings. For both resonances to have sizeable couplings while staying below the cutoff scale, they cannot be too far apart.

4.3.3 Fermion couplings in the 3-Site model

In the extreme case $z \to 0$, the second resonance disappears from the picture completely. In fact, the model then formally reduces to a 3-Site model, with a $\sqrt{2}$ rescaling of g_1. The tendency shown in Figure 4.11, that for a fixed mass the largest allowed coupling to the first resonance decreases when going to smaller values of z, is confirmed in the exact limit, and the 3-Site model indeed has to be fermiophobic [31]: the limits on the coupling are shown in Figure 4.12 and they are one or two orders of magnitude smaller than in the 4-Site model, when extra freedom in parameter space is gained from having an additional $SU(2)$ factor. The dependence on m_H is also inverted, and at large values of the cutoff, there is even a minimum allowed coupling.

The simplest experimental channels, who rely on a sizeable direct coupling between the new resonances and the Standard Model fermions (in particular Drell-Yan), will therefore not necessarily provide the strongest exclusion bounds on such a fermiophobic scenario [52, 53].

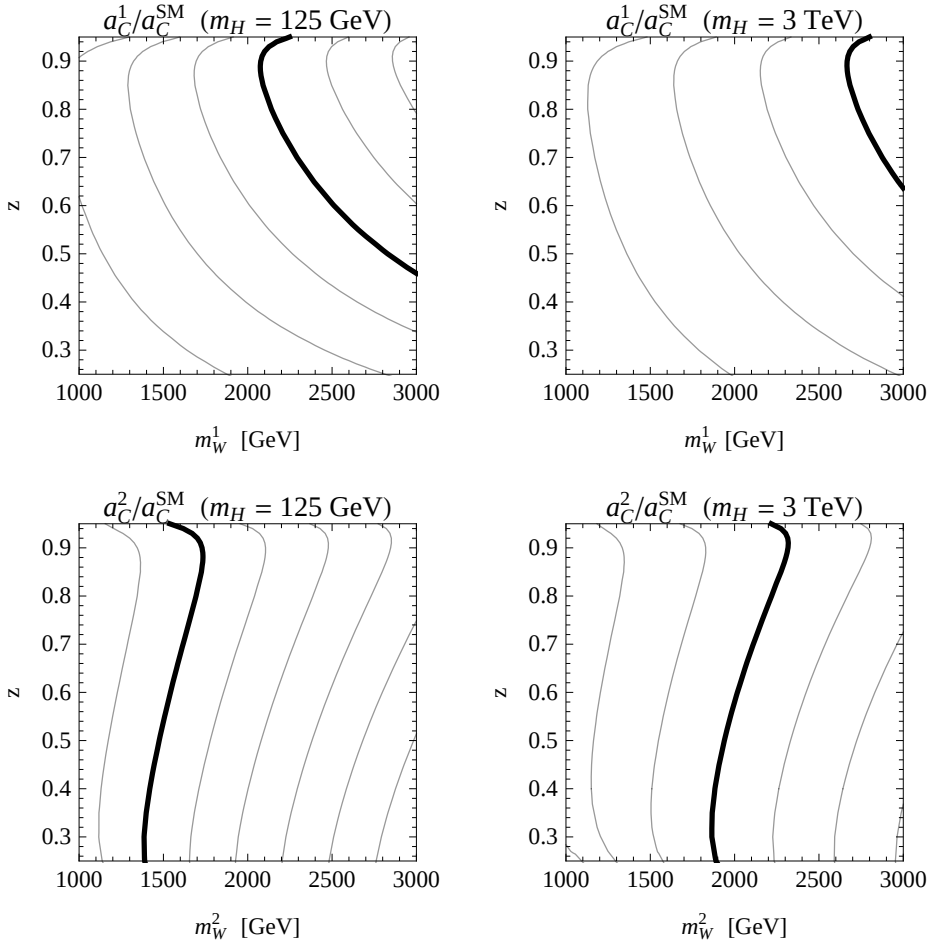

Figure 4.11: Maximum allowed fermion couplings to the extra charged resonances, as a function of their mass and of z, at 95% CL. The thick line indicates where a coupling as large as the corresponding Standard Model one is allowed; contours are separated by 0.2 in units of a_C^{SM}, increasing with the mass.

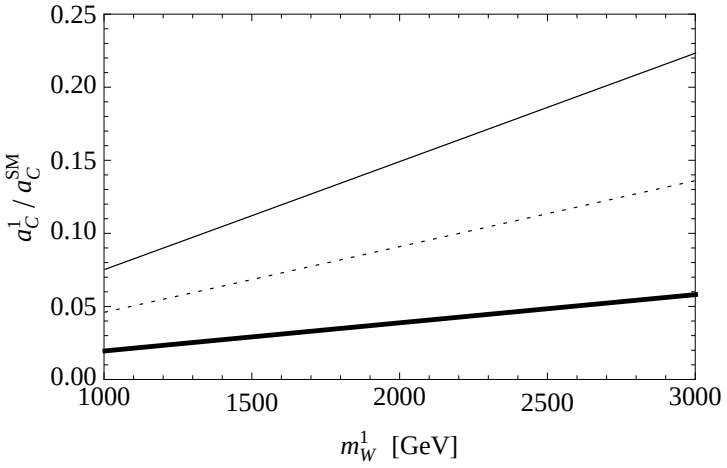

Figure 4.12: 95% CL limit on the fermion coupling of the extra charged resonance in the 3-Site model, as a function of its mass, normalised to a_C^{SM}. The thick line is for $m_H = 125\,\text{GeV}$ and the thin ones for $m_H = 3\,\text{TeV}$. In the latter case, there is a minimum allowed coupling as well, indicated by the dotted line.

4.4 A not-so-good approximation

Previously, these computations in the 4-Site model had only been performed in the decoupling limit, keeping few next-to-leading-order (in the decoupling limit expansion) corrections [32].

As mentioned before, the 4-Site model is expected to reduce to the Standard Model if the parameter A is sent to zero, having fixed the b_k parameters to zero as well (or equivalently the c_k to 1); only in this limit is there a formal identity between the gauge couplings g and g' in the two models.

Since the Standard Model should not be dramatically modified, interesting regions of parameter space are not expected to span too far away from this limit, which has been shown to be true for most of the parameter space in the previous sections. Instead of being computed exactly, expressions in this class of models are commonly expanded in some parameter (or several) related to deviations from the decoupling, and therefore assumed to be small [25, 31].

Such an approximation works well in the 3-Site case; in the 4-Site model, however, the series expansion of the ϵ_i parameters do not behave as well [1].

One should not be too surprised that it may happen. In the region of interest, the value of the ϵ_i must be of order 10^{-3}, meaning that in a trustworthy expansion, the leading term cannot be larger than that. Consequently, unless some particular mechanism makes sure all the series coefficients are equally suppressed, terms should be kept at least up to the order at which the expansion parameter guarantees an unimportant correction compared to the small leading order.

Quantities other than the EWPT parameters — masses and couplings — don't suffer from the same problem; approximate expressions give mostly good estimations.

4.4.1 The expansion parameter

While the choice of expansion parameter is not unique, it should not be critical either. A will be used here, as it depends on only one of the free parameters, M_1, and thus makes for a simpler choice in terms of controlling its value. Furthermore, all expressions have now been given in terms of this parameter, and the limit $A \to 0$ has been presented already.

Another possible expansion parameter is e^2/g_1^2 [1] which is, using equations (2.56) and (4.9),

$$\frac{e^2}{g_1^2} = \frac{AC_0}{2} < \frac{1}{2}. \tag{4.36}$$

It is proportional to A, therefore is an equivalent choice. In fact, since A and g_1^2 are inversely proportional to each other, one can think of the decoupling limit as either $A \to 0$ or $g_1^2 \to \infty$.

Other combinations that could be used include $g^2/g_1^2 = \xi(1+\gamma)$, and indeed ξ also vanishes in the decoupling limit while γ is finite (as it should be) (4.20). As a consistency check, when $c_1 = c_2 = 1$,

$$C_0 \overset{c_k=1}{=} s_{2\theta}^2 \left(1 + \frac{1}{\zeta}\right), \tag{4.37}$$

and the Standard Model relations between the electric charge, the gauge couplings g and g', and the Weinberg angle are recovered in the limit $A \to 0$.

Coming back to the argument made at the beginning of this section, the size of the expansion parameter at the lower end of the considered mass-range, $M_1 \sim \mathrm{TeV}$, is of order 10^{-2}, which is larger than the typical ϵ_i correction. Furthermore, alternative expansion parameters that also depend on z (and on the b_k) may become even bigger in other limits, for instance as z gets closer to 1: g^2/g_1^2 is of order 10^{-1} for $z = 0.95$ and $M_1 = 1\,\mathrm{TeV}$.

Some expressions up to order A are given in Appendix B.

4.4.2 Expansion in the decoupling parameters

On top of the expansion in the (inverse of the) new physics energy scale, expressions in the previous studies of the 4-Site model were also approximated for small decoupling parameters [32]. More precisely, terms at most quadratic in b_k were kept generally. In addition, terms of order g^2/g_1^2 (*i.e.* A) were only evaluated at $b_k = 0$, and anything containing $b_k\, g^2/g_1^2$ or higher powers were disregarded.

In this approximation, the first two ϵ_i are only evaluated at $A = 0$, and they depend on b_k^2:

$$\epsilon_{1,2} = \left(-\frac{(1-z^2)\left((b_1+b_2)^2 + z^2(b_1-b_2)^2\right)}{4} + \mathcal{O}\left(b_k^3\right) \right) + \mathcal{O}\left(A\right); \tag{4.38}$$

the order A correction vanishes at $b_k = 0$. Note that the Weinberg angle has been neglected and set to zero in ϵ_2.

As a side remark, yet another approximation has been made when presenting the expression for Δr_W, compared to the original definition (3.4),

$$\Delta r_W \approx \frac{c_{2\theta}}{s_\theta^2} \left(1 - \frac{m_W^2}{c_\theta^2\, m_Z^2}\right). \tag{4.39}$$

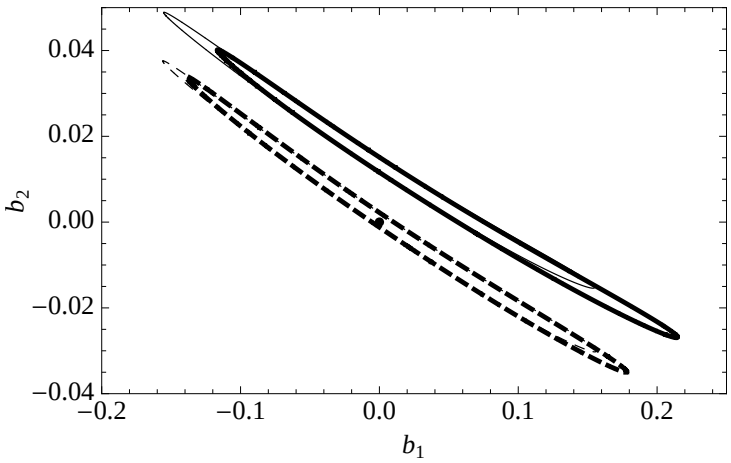

Figure 4.13: 95% CL contours for $z = 0.8$, and $m_H = 125\,\mathrm{GeV}$. The thick lines are complete calculations, the thin ones obtained using expressions from the previous reference [32]; solid lines are for finite A ($M_1 = 1\,\mathrm{TeV}$), and the dashed lines correspond to the limit $A \to 0$. The dot indicates the point $b_1 = b_2 = 0$.

These two definitions agree at leading order in the expansions considered but are not equivalent. However, Δr_W only contributes to ϵ_2, which is the least important in the χ^2 fit, therefore it matters little.

On the other hand, some order A correction was considered in ϵ_3. The expression (rewritten in terms of A instead of g^2/g_1^2) that was used is

$$\begin{aligned}\epsilon_3 = &\left(-\frac{b_1 + b_2 - (b_1 - b_2)z^2}{2(1 + b_1 + b_2)} + \mathcal{O}\left(b_k^2\right)\right) \\ &+ A\left(c_\theta^2(1 + z^2) + \mathcal{O}\left(b_k\right)\right) + \mathcal{O}\left(A^2\right). \end{aligned} \tag{4.40}$$

A remark about this expression is that the b_k in the denominator of the first term are technically higher order corrections, so should actually not be kept.

4.4.3 The confidence region

Computing the ϵ_i parameters using such approximations can shift the position of the confidence region, and ultimately modify the limits on fermion couplings. Figure 4.13 shows how the position of the allowed region in the b_1-b_2 plane indeed changes.

What happens is that, because part of the $\mathcal{O}(A)$ contribution to ϵ_3 has been kept, the approximate region is well *aligned* with the exact one, but shifted along the preferred direction. The corrections received by the couplings are not as important, and therefore the limits should change, as one can see by comparing directly with Figure 4.8. The figure also shows that, because of the expansion in the decoupling parameters, the approximate result does not converge to the exact one, even in the limit $A \to 0$.

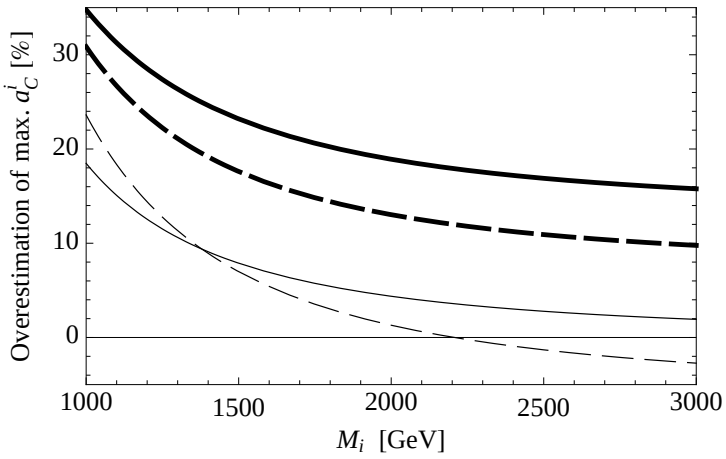

Figure 4.14: Overestimation of the 95% CL bound on the charged current couplings for $z = 0.8$ and $m_H = 125\,\mathrm{GeV}$, plotted as a function of the parameters M_1 or M_2. The dashed lines are for the first resonance, the solid ones for the second. The thick lines are calculations based on previously used approximate expressions [32], and for the thin ones, the χ^2 has been computed exactly in the limit $A \to 0$.

Interestingly, taking into account all $\mathcal{O}(A)$ terms consistently, without expanding in b_k, does reproduce the exact result well at these values of z/M_1: the approximation only breaks down at larger z / smaller M_1.

The observed shift also means that the confidence region is no longer centred around the ideal delocalisation region; a certain relative sign of the fermion couplings would also appear to be much preferred, which is artificial, as the ϵ_i are not directly sensitive to it.

4.4.4 Maximum couplings

The location of the confidence region is not particularly well described by the approximate expressions, but what matters in the end is whether or not it has an important effect of the prediction of physical quantities.

If one computes the maximum allowed W couplings using the same procedure as in the previous section, only using now approximate expressions for both the χ^2 and the fermion couplings (but keeping the same value for χ^2_{min}, though), the limit is generally overestimated, as shown in Figure 4.14.

Using approximate expressions not only for the χ^2 but for the couplings as well can, depending on the case, partially compensate for the shift in parameter space. The limit on couplings is still predicted to be too large, though.

In order to highlight the effect of the expansion in the decoupling parameters, these limits were also computed in the $A \to 0$ limit with the full dependence on the b_k. In this limit, the couplings diverge, therefore only the χ^2 has been evaluated at zero A, determining

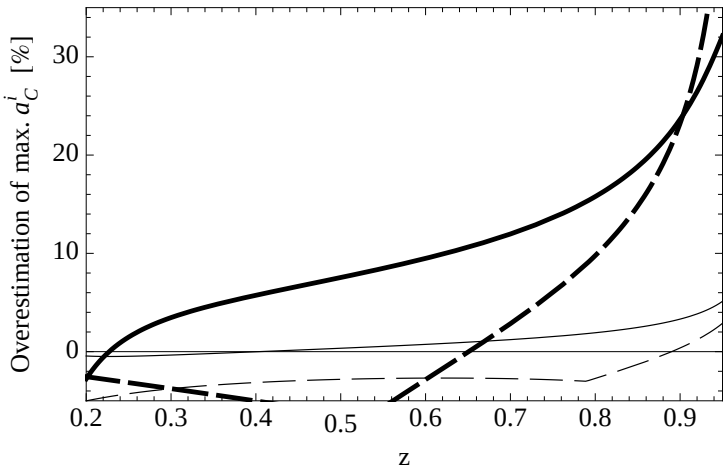

Figure 4.15: Same as Figure 4.14, except this time M_1 and M_2 are fixed to $3\,\mathrm{TeV}$ while z is varied. The dashed lines are for the first resonance, the solid ones for the second. The thick lines are calculations based on previously used approximate expressions [32], and for the thin ones, the χ^2 has been computed exactly in the limit $A \to 0$.

the allowed region in the b_1-b_2 plane, while the complete expression has been used for the couplings themselves. At lower masses, the approximation is of course expected to perform badly, and indeed the difference with the complete calculation becomes large. However, going to higher masses does not makes the approximate result converge to the exact one if only the leading order terms in b_k are considered. Note that the limit on a_C^1 computed at $A = 0$ does increase again and converge at larger masses, even though it appears here not to do so. This error due to the expansion in the decoupling parameters depends on z rather than on A, and the dependence is shown in Figure 4.15.

The fact that the expansion in the b_k worsens the situation considerably also explains why such an expansion has a better hope to be trustworthy in the 3-Site model: there is only one decoupling parameter, so it has to be small by itself, as there cannot be any compensation as in the 4-Site model.

4.5 Summary

It has been argued why heavier copies of the Standard Model W and Z bosons could exist and have properties such as described by the 4-Site model, in particular if the Higgs mechanism is related to strong dynamics.

The simplest realisation of these models is excluded by EWPT constraints, but introduction of direct couplings between the left-handed fermions and the extra gauge groups allows to ease these tensions. These additional couplings need to be moderately tuned.

Only considering one extra gauge factor, the extra resonances are necessarily fermiophobic. It is not the case however if the extension is of multi-resonance nature: compensations between the new contributions allow more freedom within the EWPT constraints and the resonances might couple to fermions as strongly as the corresponding Standard Model ones.

Previous computations of the limits on allowed fermion couplings were performed using an expansion in some of the model parameters [32]. This expansion, and in particular the expansion in the decoupling parameters, does modify the picture significantly, though. With this approximation, the limits on fermion couplings are typically overestimated by $\mathcal{O}(10\%)$, and inconsistently exhibit a strong preference for one particular relative sign [1].

The fact that the fermion couplings can be sizeable means that limits from Drell-Yan searches at the LHC do provide additional constraints compared to the EWPT alone [2]. Further constraints come from more complicated processes, such as di-boson channels [8].

Drell-Yan searches for extra heavy copies of the Standard Model W and Z are thus particularly relevant to the 4-Site model, and they will be presented in the second part of this discussion. In the interpretation of the experimental data, however, yet another approximation is made: the interference between the Standard Model contribution and the new physics is disregarded. The goal of the second part is therefore also to investigate the consequences and importance of this approximation.

Part II

The effect of interference in searches for new resonances in the Drell-Yan channels

Chapter 5

Interference in Drell-Yan

5.1 Interference

A discussion on interference should start with a clear definition of what is meant by *interference*.

"Interference" usually evokes waves. The prime example that comes to mind has to be Young's double-slit experiment: light is shone through two (or more) narrow slits, and on a screen placed behind appears an alternation of bright and dark fringes, an *interference pattern*. Describing light as a propagating wave naturally leads to this effect: there are spots where the waves coming from the two slits are in phase and reinforce each other, and spots where there are in anti-phase and cancel each other.

More precisely, the propagation of the waves can be described by an amplitude $\sim \mathrm{e}^{\imath\,\delta}$ (where δ is proportional to the distance travelled). The corresponding intensity of the light is the modulus squared of the amplitude. If there are two sources, the total intensity is not just the sum of both individual intensities (which would just be a constant), but the norm squared of the sum of the amplitudes:

$$\left|\,\mathrm{e}^{\imath\,\delta_1}+\mathrm{e}^{\imath\,\delta_2}\,\right|^2=\left|\,\mathrm{e}^{\imath\,\delta_1}\,\right|^2+\left|\,\mathrm{e}^{\imath\,\delta_2}\,\right|^2+2\,\mathrm{Re}\left(\mathrm{e}^{\imath(\delta_1-\delta_2)}\right)=2\left(1+\cos\left(\delta_1-\delta_2\right)\right) \tag{5.1}$$

The interference pattern is entirely due to the cross-term between the two amplitudes, which gives the cosine in the final expression; such a contribution is therefore called an *interference term*.

Interference is a generic wave-mechanics phenomenon. Since any quantum mechanical system exhibits wave-like properties, interference also occurs in this context. This of course is true for particle physics, where the transition amplitude is given by the *matrix element* $\mathcal{M}$

of the process under consideration

$$\mathcal{M} = \sum_i \mathcal{M}_i \quad \Rightarrow \quad \left|\mathcal{M}\right|^2 = \sum_i \left|\mathcal{M}_i\right|^2 + \sum_{i<j} 2\,\mathrm{Re}\left(\mathcal{M}_i^* \mathcal{M}_j\right) \tag{5.2}$$

Again, the probability of the process depends not only on the individual probabilities of all the sub-processes (if they each were the only one contributing), but also on cross-terms, or interference terms. One can paint an analogy with the double-slit experiment in the sense that, in both cases, there is interference because the process can happen via multiple paths; the difference is that, in one case, these paths are separated in real-space while in the other it is in momentum-space.

The implicit assumption here is that all the contributions $\mathcal{M}_i$ — in the language of perturbation theory, one would say "diagrams" — contribute to the *exact same* process, defined by specific initial and final states. Often, many formally different processes are summed over and combined: momenta are integrated, helicities and polarisations are averaged over, different colour combinations are added together, etc. It may therefore happen that, within the set of all considered processes, no two diagrams ever simultaneously contribute. An example of such a peculiar situation in the context of the current discussion is the case of an extra purely right-handed W on top of the Standard Model left-handed W.

What determines the presence or absence of interference, as well as its size and sign, can be — somewhat arbitrarily — separated into two categories.

First, model details; in particular the coupling structure of the different particles at play, *i.e.* what precise states they couple to, as *this* is what decides whether there *is* interference or not to begin with. Overall, coupling sizes will influence the relative importance of the different contributions; masses essentially set the kinematic dependence. This all means that interference is highly model dependent; interference effects might in some cases be the only way (or at least the best) to discriminate between models [54, for instance].

The second ingredient is kinematics: the different amplitudes will in general not all have the same dependence on some kinematic variables. In fact, kinematic variables of interest are precisely constructed in order to have separate regions where one contribution or the other dominates the process. This implies that, somewhere between two such regions (and provided the dependence on kinematics is smooth), these contributions need to be of the same importance; thus, interference between them is *not* kinematically suppressed at this point, and furthermore it is enhanced compared to the sub-dominant contribution outside of the intermediate kinematic range. To put it in a simplistic way: if a^2 and b^2 are comparable in size, so should $a\,b$ be; if a^2 is much larger than b^2, $a\,b$ can be expected to sit in between. Therefore, unless there is a strong overall suppression because of a particular interaction structure, there has to be a kinematic region where the interference is important.

The final remark about interference is that, unlike the other terms which are moduli squared and therefore positive definite, it can be negative. This is indeed what happens in Young's experiment: destructive interference leads to the observed shaded areas.

5.2 The Drell-Yan processes

The specific example that will be discussed here are Drell-Yan processes: the production of a pair of (light) leptons in a hadron collision [55], considering both neutral and charged final states. The production of e^+e^- or $\mu^+\mu^-$ will be referred to as *neutral Drell-Yan* or simply the neutral channel, while the final states of the charged processes are $e^\pm\nu_e$ and $\mu^\pm\nu_\mu$. Detecting electrons and muons are two distinct problems for an experimentalist; from a theoretical point of view, though, in such a process where both can safely be considered massless, there is no practical difference. The whole discussion is therefore equally applicable to both cases.

This type of process is particularly relevant now, as the LHC is collecting data and probing higher and higher energies. The signals of the Drell-Yan channels are among the cleanest one can hope for in the difficult environment that is a high-energy hadron collider. The final state one tries to identify is purely leptonic and stands out from the very busy Quantum Chromodynamical (QCD) activity. No colour charge in the final state also means less diagrams, making it a simple process to study. On the other hand, it means that the cross-section is lower than, for instance, the one of b-$\bar{b}$ production (comparing here Standard Model rates). Less backgrounds and easier identification ensure a high efficiency, though, which largely compensates for the lower event-rate.

There is a difference between the neutral and charged channels. In the former, both outgoing particles are seen by the detector, and the invariant mass of the pair can be fully reconstructed. In the latter, however, the neutrino escapes unseen, and since the individual momenta of the initial partons are unknown, the same cannot be done; one has to settle for only part of the kinematic information, and the next best available observable is the *transverse mass*. The analysis of the neutral channels is therefore more complicated and suffers from more uncertainty; the cross-section is however typically larger than in the neutral channel.

Drell-Yan processes are of great historical importance: the discoveries of the Standard Model W and Z resonances at the Super Proton Synchrotron (SPS) in 1983 were indeed made in these channels [56–59], ten years after the first observation of neutral current interactions [60]. If heavier particles with similar properties do exist and are not fermiophobic, they should be visible in the same way, and their first observation could also be in Drell-Yan. It has been argued in the first part of this discussion that these hypothetical new gauge bosons could very well couple significantly to fermions, thus the study of these processes at the LHC is most relevant.

From now on, heavy copies of W and Z bosons shall generically be denoted as *W'* and *Z'*, and the letters without the prime shall exclusively refer to the Standard Model particles. By "copies", it is here implied that all properties of Z'/W' bosons are identical to the ones of the Z/W except for their mass and, possibly, the size and chiral structure of their interaction with fermions; the details of their self-interactions will not be discussed and can, a priori, also differ from the Standard Model.

5.2.1 What about interference?

If there are new particles contributing to the Drell-Yan process, the modification of the Standard Model prediction is, in general, not only the addition of an extra resonance peak but also of some interference with the known states.

A similar interference effect — between the photon and the Z boson (not in Drell-Yan, though) — allowed a glimpse of the Z before the resonance peak itself was accessible, in 1978 [61]. This was done by observing parity-violating asymmetries that would not have been present assuming only QED.

There are some prospects of measuring such effects in asymmetries at the LHC [62], but it is unlikely to allow a Z' discovery before the actual observation of the expected peak in the invariant mass distribution, at least not in standard scenarios [63]. The current discussion will focus on the invariant/transverse mass distribution, which current search strategies are based on.

The reason why it makes sense to reiterate and emphasise the properties of interference in the context of Drell-Yan, even though — from a theoretical point of view — they are in principle well known and understood [54, 62–68], is that this contribution has long been completely disregarded in the interpretation of new physics searches when extracting limits on models [69–77]. The goal is simply to increase awareness of the possible issues when neglecting interference, mainly by clarifying the domain of applicability of the approximation and its model-dependence.

The experimental community has taken note of these concerns and is starting to explore the consequences of interference [78–80], also thanks to studies of specific models where the effect is large [66]. Interestingly, the effect of interference in a different but related channel (production of a top- and a bottom-quark [68]) has been included in analyses for a longer time now [81, 82].

5.2.2 The matrix element squared

Drell-Yan processes are among the simplest one can think of: at leading order, a single (class of) diagram contributes to the hard scattering, shown in Figure 5.1. Furthermore, the

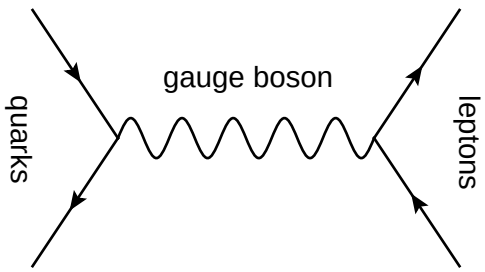

Figure 5.1: The only type of Feynman diagram contributing at leading order to Drell-Yan processes.

masses of all the external particles are much smaller than the typically considered energies and can safely be neglected.

Following the convention introduced in (2.38) for the vector and axial-vector couplings, the associated unpolarised matrix element squared is (including the explicitly written color and helicity averaging factors, and neglecting the masses of the external states)

$$\begin{aligned}\left|\mathcal{M}\right|^2 &= \frac{1}{3}\cdot\frac{1}{4}\sum_{i,j}\left|\mathcal{M}_i^*\mathcal{M}_j\right| \\ &= \frac{\hat{s}^2}{3}\sum_{i,j}\left|P_i^*(\hat{s})P_j(\hat{s})\right|\Bigg(\left(1+c\hat{\theta}^2\right)\left(a_V^i\,a_V^j+a_A^i\,a_A^j\right)_l\left(a_V^i\,a_V^j+a_A^i\,a_A^j\right)_q \\ &\qquad + \,2\,c\hat{\theta}\,\left(a_V^i\,a_A^j+a_A^i\,a_V^j\right)_l\left(a_V^i\,a_A^j+a_A^i\,a_V^j\right)_q\Bigg),\end{aligned} \tag{5.3}$$

where the summation is over all the different states contributing to the process (*e.g.* photon, Z, Z', etc.). $\hat{s}$ is the Centre of Mass (CoM) energy squared of the partonic process, $c\hat{\theta}$ the cosine of the scattering angle in the CoM, here defined as the angle between the incoming and outgoing particles (or anti-particles), and the products of couplings to leptons and quarks are labelled with, respectively, l and q. The $P_i(\hat{s})$ are the propagator factors:

$$P_i(\hat{s}) \equiv \frac{1}{\hat{s}-m_i^2+\imath\,m_i\,\Gamma_i} = \frac{\hat{s}-m_i^2-\imath\,m_i\,\Gamma_i}{\left(\hat{s}-m_i^2\right)^2+m_i^2\,\Gamma_i^2}, \tag{5.4}$$

and $|P|^2$ is the Breit-Wigner distribution; m_i and Γ_i are the mass and width of the resonance i. The particular case of the photon corresponds to $a_A = 0$ and $a_V = Q\,e$, where Q is (2.36); a purely left-handed W boson is $a_V = a_A = \frac{a_C}{2}$, with the definition (2.41).

Echoing a remark made at the beginning of the chapter, this expression does not just represent a single process but any combination of left- or right-handed initial or final states. Interference terms ($i \neq j$) can therefore vanish if, for instance, particle i has left-handed couplings ($a_V = a_A$) while particle j only couples to right-handed fermions ($a_V = -a_A$). For generic couplings, there is interference, though. How the situation can change depending on the details of the model will be discussed mainly in the context of the neutral channel, in Chapter 7.

5.2.3 The cross-section

The full process under consideration involves hadrons in the initial state; the prediction for the partonic process needs to be convoluted with Parton Distribution Functions (PDF) of the proton, $f_q(x;\mu)$. The total cross-section is

$$\sigma = \int \mathrm{d}x_1\,\mathrm{d}x_2\,\frac{\mathrm{d}c\hat{\theta}}{32\pi\,\hat{s}}\,\sum_{q,\bar{q}}\Big(f_q(x_1;\mu)\,f_{\bar{q}}(x_2;\mu)\,\left|\mathcal{M}_q\right|^2 + f_{\bar{q}}(x_1;\mu)\,f_q(x_2;\mu)\,\left|\mathcal{M}_q\right|^2\{c\hat{\theta}\to -c\hat{\theta}\}\Big), \tag{5.5}$$

where the quark and anti-quark flavours have been explicitly separated and are respectively denoted by q and $\bar{q}$. In the neutral case, the process will be considered flavour-diagonal, *i.e.* the possible quark combinations are u-$\bar{u}$, d-$\bar{d}$, c-$\bar{c}$, etc. while in the charged process, the flavour structure is given by the Cabibbo-Kobayashi-Maskawa (CKM) matrix. x_i are the momentum fraction carried by the two initial partons — each coming from a specific direction along the beam axis — and range from 0 to 1; μ is the chosen factorisation scale. Here $c\hat{\theta}$ is defined with respect to the direction of parton 1, so that it has a unique meaning in the chosen reference frame; its sign has therefore to be changed in the expression (5.3) when the incoming particle and anti-particle are swapped. Finally, a subscript q has been added to the matrix element squared to emphasise that the couplings on which it depends may differ according to the quark type.

The PDF set that has been used in the computation of all these results is the CTEQ6L [83]. The factorisation scale μ has been conventionally fixed to $\sqrt{\hat{s}}$ in computations of the neutral channel and $m_T/2$ (defined later in (5.11)) in the charged channel: the quantity chosen should be related to the energy scale of the hard process. Some checks have been performed using other sets, and changing the factorisation scale; the results are generally insensitive to these details.

5.2.4 Kinematic variables

The momentum fractions x_i relate the the partonic CoM energy squared $\hat{s}$ to the one of the hadronic system s,

$$\hat{s} = x_1\,x_2\,s. \tag{5.6}$$

Since all external particles in the process are considered massless, the invariant mass squared of the lepton pair is simply $\hat{s}$. Note that this is only true at leading order: next-to-leading order (NLO) QCD corrections include initial state radiations that take away some of the CoM energy of the hard process. In the current discussion, however, the invariant mass and $\sqrt{\hat{s}}$ will be considered synonyms.

Being interested in invariant mass distributions, it is convenient to abandon x_1 and x_2 in favour of $\hat{s}$ (or $\sqrt{\hat{s}}$), and to choose as a second variable the rapidity difference between the partonic and the hadronic CoM reference frames, y,

$$y = \frac{1}{2} \log \frac{x_2}{x_1}. \tag{5.7}$$

The change of variables and of integration domain is

$$\int_0^1 \mathrm{d}x_1 \int_0^1 \mathrm{d}x_2 = \frac{1}{s} \int_0^s \mathrm{d}\hat{s} \int_{-\log\sqrt{s/\hat{s}}}^{+\log\sqrt{s/\hat{s}}} \mathrm{d}y. \tag{5.8}$$

y is the quantity that relates $c\hat{\theta}$ to the scattering angle in the lab-frame $c\theta$. The relation is best expressed in terms of the pseudorapidities η and $\hat{\eta}$, defined as

$$\tanh\eta \equiv c\theta, \quad \tanh\hat{\eta} \equiv c\hat{\theta}. \tag{5.9}$$

y is then simply the difference between the two, or

$$\eta = \hat{\eta} - y. \tag{5.10}$$

As explained at the beginning of the section, in the charged Drell-Yan processes, the invariant mass cannot be measured because the outgoing neutrino escapes the experiment undetected (and because the total longitudinal momentum — or y — is not known). The only kinematic properties of the process one can infer from the detection of the charged lepton alone are quantities invariant under longitudinal boosts. The most commonly used kinematic variable in that context is the *transverse mass* m_T, defined as

$$m_T^2 \equiv 2\, p_T^l\, p_T^\nu\, (1 - \cos\Delta\phi)\,, \tag{5.11}$$

where p_T^l is the momentum of the charged lepton, p_T^ν is the missing energy (associated with the neutrino leaving the detector), and $\Delta\phi$ is the azimuthal angle between the two. The reason for including a dependence on $\Delta\phi$ is to make it robust to QCD corrections [84]. At leading order, however, the prediction is simply

$$m_T^2 = \hat{s}\,(1 - c\hat{\theta}^2) \tag{5.12}$$

and the transverse mass ranges from zero to $\sqrt{s}$.

5.3 General remarks

5.3.1 Relative size and sign of the contributions

In the first section of the chapter, it was argued that one should think separately about the influence of the coupling structure on the interference and the kinematic dependence. What was meant appears now clearly in (5.3): essentially, the interference factorises into two parts. One depends on the couplings, the structure of the interactions; the other is a product of propagators, and it determines the dependence on $\hat{s}$, the kinematic variable that provides the best separation between a region where physics is believed to be well understood and a region where new phenomena could manifest themselves.

The overall size of the effect, controlled by the coupling factor, will depend on the chiral structure of the new gauge bosons. Note that a global rescaling of the W'/Z' couplings acts quadratically on the resonant term, but only linearly on the interference: the relative importance of the interference term compared to the pure new physics contribution thus increases if the couplings are reduced.

For a given model, *i.e.* given couplings, what matters next is the propagator factor. Non-interference terms are Breit-Wigner distributions, thus are kinematically enhanced when $\hat{s}$ is close to the resonance mass. Away from the resonances, however, there is no reason why any of the contributions should dominate. Furthermore, an interference term containing the product of two propagators, it increases when approaching *both* resonant peaks, albeit less than the corresponding pure Breit-Wigner term.

There is something to be said about the sign of the interference, too. It is easy to see that the propagator factor of the interference term is negative in the region between the two corresponding resonance peaks. So unless the coupling factor is negative as well — which, in particular, is not the case if the couplings of the two resonances are proportional to each other —, the interference contributes destructively in the intermediate region. It also changes sign at both resonances; this means it can sharpen the features of the peaks.

5.3.2 Aspects that will not be discussed

A few potentially important aspects will be left out of the present analysis. They are thus briefly commented on here.

5.3.2.a Angular dependence

First, no angular distributions nor asymmetries will be presented. As mentioned in Section 5.2.1, such observables are not an improvement over invariant mass distributions in terms

of discovery potential in the most common scenarios such as the ones considered in the present discussion [63]. All current experimental analyses are indeed based on invariant/-transverse mass distributions.

No rapidity cuts will be considered either. LHC experiments only include events if the scattering angle is within, typically, $|\eta| < \eta_c \sim 2.5$, but most events are concentrated in this central region anyway. A rapidity cut would have an influence through the angular dependence of the cross-section, which factorises in (5.3) separately for the $c\hat{\theta}$-even and $c\hat{\theta}$-odd parts. If no cut is performed, all angles are integrated over, and one immediately sees that the $c\hat{\theta}$-odd terms cancels; however, a more careful discussion is useful when considering a cut on η.

One has to separately discuss the charged and neutral cases, here: indeed, in the former, since the neutrino remains undetected, its rapidity cannot be determined, thus cannot be cut out; only the rapidity of the charged lepton is constrained.

In the neutral case, it is easy to show that imposing the rapidity of both outgoing leptons to be less than some η_c amounts to limiting the integration range of the CoM rapidity to

$$\hat{\eta} \in [-\eta_c + |y|, \eta_c - |y|]. \tag{5.13}$$

In other words, the integration over the CoM angular variable is still done over a symmetric domain, therefore the $c\hat{\theta}$-odd term vanishes.

To discuss the charged case, it is useful to first express the cross-section in the following way, in terms of the lab-frame rapidity of the charged lepton, η (choosing the sign of $c\hat{\theta}$ appropriately):

$$\begin{aligned}\frac{\mathrm{d}\sigma}{\mathrm{d}\hat{s}} \propto \int \mathrm{d}y \, \frac{\mathrm{d}\eta}{\cosh^2(\eta + y)} \sum_{q,\bar{q}} \Big(& f_q(\hat{s}, y; \mu)\, f_{\bar{q}}(\hat{s}, -y; \mu)\, \left|\mathcal{M}_q\right|^2 \{c\hat{\theta} \to \pm \tanh(\eta + y)\} \\ & + f_{\bar{q}}(\hat{s}, y; \mu)\, f_q(\hat{s}, -y; \mu)\, \left|\mathcal{M}_q\right|^2 \{c\hat{\theta} \to \mp \tanh(\eta + y)\}\Big)\end{aligned} \tag{5.14}$$

A cut on the charged lepton rapidity then translates directly into limits on the integration interval of η. If the rapidity of the other lepton were also constrained, y would then have to be integrated over a limited range, but as this other lepton is a neutrino, it is not the case. y is simply integrated over the range given in (5.8), and after performing the change of variable $y \to -y$ and $\eta \to -\eta$ in the second term, one gets

$$\frac{\mathrm{d}\sigma}{\mathrm{d}\hat{s}} \propto 2 \int \mathrm{d}y \, \mathrm{d}\eta \sum_{q,\bar{q}} f_q(\hat{s}, y; \mu)\, f_{\bar{q}}(\hat{s}, -y; \mu) \left(\frac{\left|\mathcal{M}_q\right|^2}{\cosh^2(\eta + y)} \{c\hat{\theta} \to \pm \tanh(\eta + y)\} \right). \tag{5.15}$$

If there is no rapidity cut, η gets integrated from $-\infty$ to ∞, thus the shift in y is irrelevant, and the $c\hat{\theta}$-odd term does cancel out, but no symmetry guarantees the cancellation otherwise.

As a result, unless an important rapidity cut is imposed in the charged channel, the $c\hat{\theta}$-odd term in (5.3) can be neglected when computing cross-sections and transverse mass distributions. In the neutral case, the $c\hat{\theta}$ odd terms always cancel out when the angular variable is integrated over, even with a rapidity cut. Considering only the $c\hat{\theta}$-even term, the angular dependence completely factorises, in which case a rapidity cut cannot have an influence on the importance of interference.

5.3.2.b Next-to-leading order QCD corrections

The next important comment to make is about NLO QCD corrections (namely the potential radiation of jets from the initial state), since only leading order predictions are presented in this discussion. As for angular dependencies, one can argue that these corrections have to approximately factor out: they only come in on the quark side — the "production" side of the process — and should not be too different for the various contributions. A complete computation does confirm that point [67].

5.3.2.c Flavour structure

Finally, flavour interaction structures different from the Standard Model one will not be considered. Deviations of this kind are highly constrained, especially in the neutral sector. Considering such cases is anyway not relevant to the points raised in the current discussion and would only be unnecessary complications.

Chapter 6

The charged channel

Much of this chapter's content appears as it does in the published version of this discussion, with minimal adjustments [3].

6.1 Preliminary remarks

6.1.1 Models of W'

Heavy charged W' bosons arise in a number of theories that extend the Standard Model gauge group. Essentially, there needs to be an extra $SU(2)$ symmetry that joins the known fermions together in pairs in a similar way than $SU(2)_L$ does in the Standard Model.

The Left-Right symmetric (LR) class of models [85–87], based on the enlarged symmetry $SU(2)_L \otimes SU(2)_R \otimes U(1)$, is an old and popular example; within these models the discovery reach of the LHC has been recently re-investigated [88–90] and bounds have been derived using results published by the LHC collaborations [91]. A second class is represented by extra-dimensional theories [10, 11, 92], where W' bosons emerge as Kaluza-Klein excitations of the SM gauge bosons. Within the ADD (Arkani-Hamed, Dimopoulos, Dvali) model, the phenomenology of signals from extra charged gauge bosons at the LHC have been discussed in Refs. [93, 94]. In the RS1 (Randall, Sundrum) model with gauge bosons in the five-dimensional (5D) bulk and fermions on the ultraviolet brane, analogous results are published in Refs. [95, 96]. Five-dimensional models can also be deconstructed to the usual four-dimensional space-time [21, 97–104], where they are described by chiral Lagrangians with extended gauge symmetries. Within this framework, Higgsless theories find their natural 5D interpretation. The simplest deconstructed model is the 3-Site model that has been presented in the first part (also called minimal Higgsless model), and represents the 5D interpretation of the old BESS model (Breaking Electroweak Symmetry Strongly) [16, 105]. As argued in Section 4.3.3, the tension between electroweak precision tests (EWPT) and

unitarity requirements constrain the W' boson to be almost fermiophobic [25, 106–109]. Its next-to-minimal extension, the 4-Site model that has been extensively described in the first part (see also [1, 2, 27, 32, 110, 111]), relaxes the above-mentioned dichotomy thus allowing sizeable couplings between extra W' bosons and SM fermions as predicted by more general extra-dimensional theories. Technicolor models represent the last class of theories implying the existence of new heavy charged gauge bosons [112]. This class, which historically provides an alternative electroweak symmetry breaking (EWSB) mechanism to the Higgs procedure, predicts multiple extra W' (and Z') bosons [113]. For a recent phenomenological study, see [114].

Experimental searches for a W' boson at the Tevatron and the LHC are usually interpreted in the context of a benchmark scenario inspired by Ref. [115]. This model just includes one extra charged vector boson with couplings to fermions identical to those of the corresponding SM W boson, and no mixing with the EW SM bosons; this scenario is referred to as the Sequential Standard Model (SSM). It is the standard W' paradigm, thus results will be presented within that framework. To show how interference contributions add up when there is more than one resonance, the 4-Site model is also considered.

Contrary to the case of Z' bosons, which can couple differently to up/neutrino and to down/charged lepton particles, a W' needs to have a constrained structure; there is much less freedom in playing with the interaction of a W'. Forbidding any deviations from the flavour structure of the Standard Model, as discussed at the end of the previous chapter, only two things can be changed. First, how much the W' couples to left- and right-handed particles (for right-handed lepton couplings to exist, one would have to introduce extra neutrinos); this has an influence on the overall size of the interference effect as only the left-handed coupling would contribute. Second, whether the W' distinguishes between quarks and leptons; in the Un-unified Standard Model [116], for instance, there is a sign difference between the two, which leads to a negative coupling factor in (5.3) for the interference, meaning that it is constructive between the W and W'.

Studying the qualitative behaviour of the standard SSM scenario only should therefore suffice to acquire a basic understanding of the more general case.

6.1.2 Objectives

The aim is to discuss more specifically experimental searches and strategies used to extract and present exclusion bounds on the W' mass. In most experimental analyses performed to date, the expected signal is calculated taking into account only the pure W' boson contribution. Although the search is conducted in a limited higher-energy region (by using minimum transverse mass cuts) where the importance of the interference terms is indeed reduced, the results, which are formally limits on the cross-section in the high-energy search window only, are then extrapolated and expressed as limits on the complete cross-section without

any kinematic cuts [69, 71, 73, 75, 76, 78]. However, the interference between W' and Standard Model background results in a significant change in the signal prediction: the Beyond the Standard Model contribution to the total cross-section can even be negative. Thus, this latter quantity is not, for a generic model, representative of what the signal is in the search-window, and expressing the observed limit in terms of it is not the most convenient choice. It is therefore argued that the way of presenting 95% CL upper limits on the W' boson production cross-section could be improved, and that leaving in a kinematic cut on the dilepton transverse mass would be more meaningful and useful to theorists.

What has to be stressed is that, unlike other effects such as NLO QCD corrections, the interference contribution varies over the kinematic range; it does not simply shift the prediction by an overall factor. In the region of interest — close to the Beyond the Standard Model resonance peak — the interference is negligible as expected, therefore taking it into account should not significantly shift the value of exclusion bounds on W' boson masses. Outside of this range, however, it becomes important; thus it is fundamental in determining an appropriate search-window.

Although the interpretations of current searches are perfectly valid assuming a purely right-handed W', transposing these results to a more general case is not trivial because of the interference. The message is also that, in *any* search where interference may occur and not only in this particular W' example, its importance has to be established.

6.1.3 The importance of an m_T cut and/or including the interference

Based on the discussion so far, it is not difficult to anticipate some of the results and to enunciate a few expectations.

When considering hadron collisions, thus integrating the partonic cross-section (convoluted with PDFs) over the whole energy range, the interference can be the dominant contribution to the BSM signal, making the predicted total cross-section smaller than in the SM. The pure BSM term alone cannot properly represent the new physics contribution to the total cross-section simply because the interference term contains a SM factor, which becomes large at lower energy. Indeed, the PDFs greatly enhance the lower energy dynamics compared to the higher energy region. Note that the interference is in general a very large contribution to the total BSM prediction, due to the enhancement of the lower energy region where it dominates the signal, independently on whether it is destructive or constructive.

In order to isolate new physics, one should cut out the low-energy region where the SM dominates (and where subsequently the interference term becomes large compared to the pure BSM contribution). In the case of a W' boson search in charged lepton plus neutrino final states, this means implementing a minimum m_T requirement. This is indeed a common approach in experimental search strategies.

Observed experimental limits are currently expressed in terms of the contribution of the pure BSM term alone to the total cross-section, as a means of making them independent of any kinematic cuts. As has just been argued, the meaning of this particular quantity is not straightforward when considering a model in which the interference does not vanish.

Furthermore, what is not necessarily obvious and has to be stressed is how extrapolating the results so that limits are given on the total cross-section (without kinematic cuts) is not useful from a theoretical point of view. If one wants to compare an observed limit with a complete BSM prediction that includes destructive interference, imposing a high enough m_T cut is a necessity. Knowing the value of the m_T cut used in the data analysis, it is in principle possible to undo the extrapolation step and obtain at least an estimate of the limit on the cut cross-section by rescaling the limit on the total cross-section according to the fraction of pure BSM contribution in the search-window. This might only be an approximation if additional corrections enter the extrapolation procedure experimentalists use. More importantly it is only possible to recover limits corresponding to the specific values of the m_T cut used in the experimental analyses. For some models (in general for a high enough W' boson mass), the provided cuts might not be optimal, *i.e.* the predicted BSM cross-section including the interference would be larger for a higher m_T cut. This theoretical cross-section might even be negative for the given cuts; one would then have to extrapolate the provided limit to a higher m_T cut in order to make a comparison, which should lead to an underestimation of the bound on the mass of a W' boson. Conversely, neglecting the interference in such a case would result in a too strict mass exclusion limit.

As the optimal m_T cut strongly depends on the model, one suggestion would be that the observed limit on the BSM cross-section should be presented *as a function of* a minimum m_T cut. The theoretical prediction (including the interference) could be then accordingly computed keeping the m_T cut dependence. Note that the theoretical cross-section for the complete BSM signal is maximal when choosing the m_T cut such that the differential cross-section (in m_T) is zero at the cut, thus integrating over the positive region only.

This section is concluded with a few additional side remarks.

As argued above, it is important to implement an m_T cut, whether it is to make sure the interference can reasonably be neglected or in order to guarantee the predicted cross-section to be positive.

One might expect that more sophisticated search techniques, involving fitting to the distribution rather than simply cutting and counting, exhibit a certain sensitivity to the predicted shape of the differential cross-section in the intermediate energy-range where the interference is an important contribution and cannot be ignored.

Finally, because of the interference, a reduction of events will be predicted below the region where the BSM peak starts to emerge over the background. If the deviation is significant enough, this might actually be a useful way to probe hypothetical resonances whose

mass is beyond reach otherwise, although it could be difficult [63]. It might at least have an effect on how the background should be estimated, and thus care would be required in that respect as well.

6.1.4 Note on the computation

Computing the cross-section of the process (5.5) involves a 3-dimensional integral, but only two variables need to be integrated over to get the differential cross-section $\mathrm{d}\sigma/\mathrm{d}m_T$. One should change variable from $\hat{s}$ (or $c\hat{\theta}$) to m_T using the relation (5.11) and perform the remaining integrals, over $c\hat{\theta}$ (or $\hat{s}$) and y. Prior to using the transverse mass, the integrals nicely factorise: the rapidity y only enters in the PDFs, and the matrix element factor contains all the dependence on the scattering angle. This would allow to perform them separately, and then in a second step combine the pieces as a function of $\hat{s}$.

Unfortunately, the consequence of switching to m_T is that the PDF factor now also depends on $c\hat{\theta}$. There is still no y dependence in the matrix element squared, the piece that contains all the model dependence, though. It is useful to perform the integral over y separately, giving a *parton luminosity* factor depending on m_T and $c\hat{\theta}$; having sampled the value of this integral, it will not be necessary to recompute it when changing the model parameters.

The integrations are performed using Mathematica [4].

6.2 Heavy charged gauge bosons at the LHC

In this section, quantitative examples of destructive interference are given. Two reference models are considered: the SSM and the 4-Site. The impact of the interference terms on W' boson searches at the $7\,\mathrm{TeV}$ LHC is analysed.

6.2.1 The benchmark model

In the benchmark model inspired by Ref. [115], the W' boson is considered a heavy analogue of the SM W boson with the same couplings to left-handed fermions. Thus, W' decay modes and branching ratios are very similar to those of the SM W boson, with the only exception being the top-bottom quark channel which opens up for W' masses above $180\,\mathrm{GeV}$. No mixing (or interaction) with SM gauge bosons or other heavy gauge bosons such as Z's is assumed. Its width (neglecting the top-quark mass) is therefore simply

$$\Gamma_{W'} = \frac{4}{3}\frac{m_{W'}}{m_W}\Gamma_W. \tag{6.1}$$

As discussed previously, the prediction of this model does contain interference. One could imagine a similar model in which the interference vanishes by making the W' right-handed: this would require either the inclusion of light (sterile with respect to other interactions) right-handed neutrinos or have the extra bosons couple purely to right-handed quarks while still coupling to left-handed leptons. Current analyses performed without the inclusion of any interference thus formally correspond to testing such a model instead of the benchmark model with left-handed coupling, which is sometimes but not always specified.

Within this benchmark framework, CDF [69] and D0 [71] searched for a W' boson in the electron-neutrino final state, and extracted an exclusion limit on the W' mass at 95% confidence level (CL) equal to $1.12\,\mathrm{TeV}$ [69]. Recently, searches in the combined electron-neutrino and muon-neutrino final states by both ATLAS and CMS notably extended the lower limit to: $m_{W'} \geq 2.55\,\mathrm{TeV}$ and $3.10\,\mathrm{TeV}$ (or $3.35\,\mathrm{TeV}$ without interference), respectively [73, 79].

These analyses are based on the production of W' bosons and their subsequent decay into a charged lepton (electron or muon) and a neutrino, with an individual branching fraction of about 8.5%. As neutrinos give rise to missing transverse momentum in the detector, the selection criteria require candidate events with at least one high transverse momentum lepton. The off-peak, high-end tail of the SM W boson production and decay constitutes the irreducible background, which is the primary source of noise. Reducible backgrounds are also considered (see Ref. [79] and references therein for details). The present discussion, however, focuses on the signal and its irreducible background, that is on the process:

$$pp \to W, W' \to l\nu_l \tag{6.2}$$

with $l = e, \mu$ and $l\nu_l = l^-\bar{\nu}_l + l^+\nu_l$, and at $7\,\mathrm{TeV}$ CoM energy. Experimental analyses use several large Monte Carlo (MC) samples to evaluate signal and background efficiencies. They use MC samples for both the W' signal and its electroweak irreducible background, produced using PYTHIA at LO [117]. A mass dependent K-factor for the next-to-next-to-leading order (NNLO) correction is calculated and applied to the LO cross-section. The W' contribution and the irreducible background are evaluated separately as events are generated using PYTHIA, in which the interference has not been implemented for this process.

Because the neutrino cannot be measured, the experimental analysis must rely on the transverse mass of the leptonic system instead of its invariant mass, making a potential W' peak less prominent. Wide search-windows are thus generally used, in which the interference might matter.

As an illustration, Fig. 6.1 shows the differential cross-section in the electron-neutrino transverse mass, $m_T(e\nu_e)$, at LO in both electroweak and QCD interactions, for the LHC at $7\,\mathrm{TeV}$ (using CTEQ PDF). One representative value for the W' boson mass is considered: $m_{W'} = 2.4\,\mathrm{TeV}$. The distribution obtained summing up SM irreducible background and

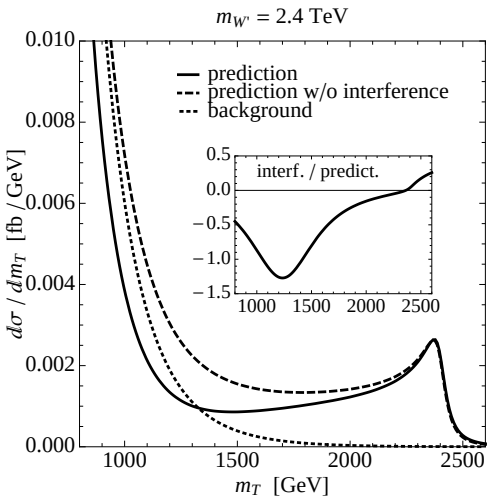

Figure 6.1: Differential cross-section in the dilepton transverse mass for $m_{W'} = 2.4\,\mathrm{TeV}$, considering $7\,\mathrm{TeV}$ pp collisions. The dashed line shows the SM background plus the pure W' boson contribution (without interference, as in the PYTHIA implementation used by experimentalists [73,75,76]). The solid line gives the complete theoretical distribution, including the interference term between W and W' bosons. The dotted line represents the SM irreducible background as reference. The inset plot displays the interference term normalised to the complete theoretical prediction.

pure W' contribution, corresponding to what is produced by PYTHIA (dashed line), is compared with the full result including the interference term (solid line). The SM background is displayed as reference (dotted line). Owing to the destructive interference pattern, there is a sizeable reduction of the differential cross-section: around $1\,\mathrm{TeV}$, the predicted distribution can go down to about half of what would be expected when neglecting the interference, as can be read from the inset plot.

Clearly, the inclusion of the interference term brings an important change in the shape of the m_T distribution compared to the prediction obtained by summing up SM background and pure signal. Only at around $100\,\mathrm{GeV}$ before the W' boson Jacobian peak does the interference drop down to a few percent and become negligible. The approximation adopted by the experimental collaborations (as the interference has not been implemented in PYTHIA) has then a restricted validity domain. Neglecting the interference outside the above-mentioned domain has three main consequences. First of all, the choice of the optimal minimum m_T cut to enhance the signal over background ratio can favour too low a value compared to the complete calculation. Secondly, in the commonly used "counting strategy", the number of expected events collected from above the m_T cut is overestimated (see Table 6.1 at the end of the section), which skews any estimate of the deviation from the SM prediction. Lastly, changes of the distribution in lower m_T regions which are considered to be new physics free could be missed if the irreducible background is estimated from data in such regions.

As shown in Fig. 6.2, which displays the m_T distribution of the model prediction normalised to the SM background, if one neglects the interference term (dashed line) the m_T

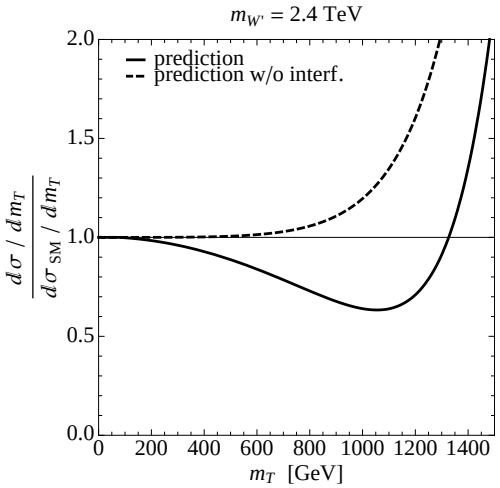

Figure 6.2: Ratio between the differential cross-section in the dilepton transverse mass for the prediction of the model and the SM irreducible background, considering $7\,\mathrm{TeV}$ pp collisions. The solid line shows the ratio obtained when including the interference. The dashed line represents the ratio without taking into account the interference. $m_{W'}$ is set to $2.4\,\mathrm{TeV}$.

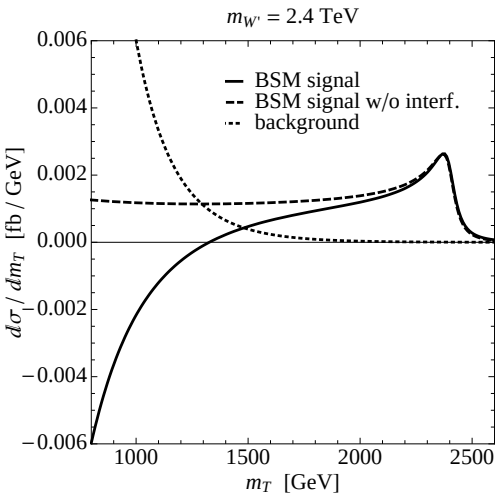

Figure 6.3: Differential cross-section in the dilepton transverse mass for $m_{W'} = 2.4\,\mathrm{TeV}$, considering $7\,\mathrm{TeV}$ pp collisions. The dashed line shows the pure W' boson signal (*i.e.* as implemented in PYTHIA). The solid line gives the theoretical distribution of the BSM signal, including the interference term between W and W' bosons. The dotted line represents the SM irreducible background as reference.

region which can be assumed to be BSM physics free can extend up to around $600\,\mathrm{GeV}$. Within that approximation, the BSM physics contribution is indeed apparently below the 5% level in that range. However, if one includes the interference (solid line) the situation changes. The m_T region where the BSM physics contribution can be considered negligible shrinks down to about $300\,\mathrm{GeV}$ for the chosen W' boson mass.

Now concentrating more specifically on the W' boson signal (*i.e.* the contribution of new

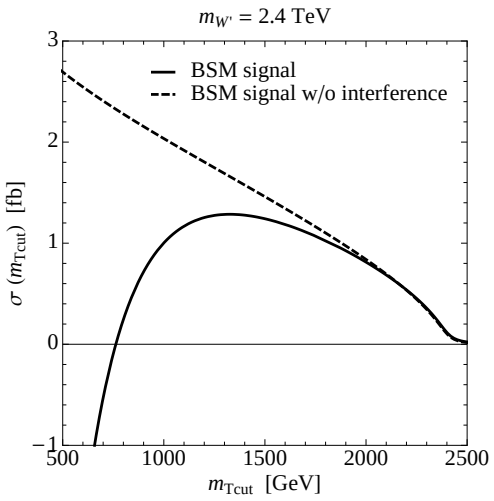

Figure 6.4: W' signal cross-section as a function of the minimum m_T cut for $m_{W'} = 2.4\,\mathrm{TeV}$, considering $7\,\mathrm{TeV}$ pp collisions. The dashed line shows the the pure W' boson contribution without interference (*i.e.* as implemented in PYTHIA). The solid line gives the BSM signal, including the interference term between W and W' bosons.

physics to the cross-section, $\sigma_{\text{total}} - \sigma_{\text{SM}}$), the differential cross-section in the dilepton transverse mass is plotted in Figure 6.3. The W' signal predictions with and without the interference term are compared. As already anticipated, the complete signal becomes negative below a certain m_T value, while the approximate result is positive-definite over all the m_T range. In most LHC searches, the mass dependent K-factor for the NNLO correction is calculated and applied to the LO "pure" signal cross-section; its value varies for instance from 1.14 to 1.36 [79]. Since the effect of the interference is significant, it would be advisable to refer instead to the computation given in Ref. [67] where this term is taken into account. As argued in Section 5.3.2, the picture is not expected to change significantly, since the QCD corrections affect the "production side" of the process, while the interference effect has to do with the propagator factor in the partonic cross-section.

To quantify these effects on the integrated signal cross-section, in Figure 6.4 the cumulative result is plotted as a function of the lower cut on the dilepton transverse mass, $m_{T\text{cut}}$. As before, approximate and complete calculations are compared for a representative value of the W' mass: $m_{W'} = 2.4\,\mathrm{TeV}$. As the m_T cut is decreased, the divergence between the two predictions increases. Below a critical m_T cut, the new physics signal cross-section even becomes negative. Two pieces of information can be extracted from this figure.

If a lower m_T cut is imposed, the approximation can overestimate the signal cross-section by an amount which depends on how far from the Jacobian peak the m_T cut is chosen. This is summarised in Table 6.1, where the relative overestimation of the W' boson signal cross-section due to the approximation is given. The values for the m_T cut and $m_{W'}$ have been chosen according to a previous CMS analysis [118]. For the selected W' boson masses and integration windows, the discrepancy can range from 4% to 64%. Such an overestimation

$m_{W'}$ [GeV]	$m_{T\text{cut}}$ [GeV]	$\sigma\,(m_{T\text{cut}})$ [fb] signal no interf.	signal with interf.	diff. in %	SM backgr.	σ total [fb] signal no interf.	signal with interf.
1400	1000	67.4	65.0	3.7	1.1	131.1	−30.1
1600	1100	31.3	29.7	5.5	0.6	60.1	−59.3
1800	1100	16.1	14.6	10	0.6	28.5	−63.4
2000	1100	8.0	6.8	18	0.6	14.0	−59.0
2200	1100	3.9	3.0	32	0.6	7.1	−52.3
2400	1100	1.9	1.2	64	0.6	3.7	−45.6

Table 6.1: From left to right, the columns indicate the W' boson mass value, the minimum m_T cut, the cross-section for the W' boson without interference calculated from the m_T lower cut on, the cross-section for the W' boson with interference from the m_T lower cut on, the difference in percent between these two normalised to the latter, the SM irreducible background from the m_T lower cut on, the total cross-section for the W' boson signal without and with interference. Computed for $7\,\mathrm{TeV}$ pp collisions. No efficiency and acceptance factors are included.

of the new physics signal leads to placing a too strict exclusion bound on the mass of a W'. Some of the most recent CMS analyses present improved results where interference has been taken into account, and the difference on the excluded mass limit is of $\mathcal{O}\,(5-10\%)$: the latest limit on an SSM W' mass is $3.10\,\mathrm{TeV}$ with and $3.35\,\mathrm{TeV}$ without interference [78, 79].

The second piece of information is related to the existence of a critical m_T cut below which the BSM signal cross-section becomes negative. This implies, as anticipated in section 6.1.3, that the fully integrated signal cross-section is negative in most cases of interest (the contribution below the W peak is large enough to make the total result positive only for W' masses below about $1.3\,\mathrm{TeV}$ in this model). Values are given in the last column of Table 6.1. This illustrates the point made in section 6.1.3 that this quantity does not reflect the prediction of the model in the search region as it can be dominated by the qualitatively different behaviour of the interference at lower energy.

6.2.2 The 4-Site model

The first part of this thesis has been devoted to presenting the 4-Site model and how it is constrained by EWPT. In particular, it has been shown that sizeable fermion couplings, comparable to the Standard Model ones, are allowed.

The 4-Site model has thus the potential of being detected during the early stage of the LHC experiment in the Drell-Yan channel. As for the spectrum, EWPT imposes a lower limit on the mass of the extra gauge bosons. The minimum mass can range between 250 and $600\,\mathrm{GeV}$, depending on the z-parameter value (see Ref. [1] for computational details). The maximum allowed value for the mass of the extra gauge bosons is instead fixed by the

requirement of perturbative unitarity. In [32,110,111], all vector boson scattering amplitudes, which are the best smoking gun for unitarity violations are computed, with the conclusion that the 4-Site model should preserve unitarity up to around $3\,\mathrm{TeV}$. Thus, the allowed mass-range for the 4-Site model is roughly $[250, 3000]\,\mathrm{GeV}$.

A parton level analysis of the search for the two extra charged bosons present in the 4-Site model, W_1 and W_2, in the Drell-Yan channel at the $7\,\mathrm{TeV}$ LHC was recently presented in Ref. [2], and it shows how direct searches can further constrain the parameter space of the model compared to the limits given by EWPT. In this thesis, however, the focus is specifically on the effect of the interference between extra heavy $W_{1,2}$ and the SM W bosons on the observables used in the experimental analysis of the final state with a charged lepton and a neutrino rather than on the actual collider constraints; the 4-Site model merely serves as a second example, after the SSM, in which the importance of interference is investigated. The analysis presented in the previous section is repeated in this new context to show how the interference contributions can add up when multiple resonances are present.

In Figure 6.5, the differential cross-section in the dilepton transverse mass at LO in both EW and QCD interactions is displayed. The same representative mass as in the case of the SSM is chosen for the heavier charged gauge boson: $m_{W_2} = 2.4\,\mathrm{GeV}$. The distribution is plotted for a fixed value of the z-parameter, $z = 0.8$, and for the maximal couplings between extra gauge bosons and SM fermions allowed by EWPT at 95% CL with $m_H = 3\,\mathrm{TeV}$, even though it corresponds to a point disfavoured by EWPT. In this setup, the mass of the lighter charged gauge boson is fixed to be $m_{W_1} = 1920\,\mathrm{GeV}$. As one can see, the multi-resonance peaking structure is quite visible, especially when the interference is included (solid line).

A direct comparison with the benchmark SSM model predictions given in the previous section shows that in the 4-Site model the impact of the interference term on the $m_T(l\nu_l)$ distribution is stronger. In the TeV region, the expected number of events gets indeed depleted by more than a factor of four with respect to the theoretical prediction without interference (dashed line). Once again, accounting for the interference brings an important change in the shape of the $m_T(l\nu_l)$ distribution as compared to the prediction obtained by summing up SM background and pure $W_{1,2}$-boson contribution. In the high energy scale region used for BSM physics searches, only starting from the lighter resonance Jacobian peak the interference drops down to a few percent level, and becomes negligible as shown in the inset plot. This suggests that the minimum $m_T(l\nu_l)$ cut, which defines the search window, should be chosen around that value if one wants to work in the approximation where the interference is neglected. If too low, it could indeed bring to an overestimation of the predicted number of events within the adopted approximation.

Analogously, in the low $m_T(l\nu_l)$ region used for shaping the irreducible SM background from observed data, the interference drops down to a few percent level only below $m_T(l\nu_l) \simeq 200\,\mathrm{GeV}$. The BSM physics free region is shown in Figure 6.6 for $z = 0.8$ and $m_{W_2} = 2.4\,\mathrm{TeV}$. As for the benchmark model presented in the previous section, the ratio between

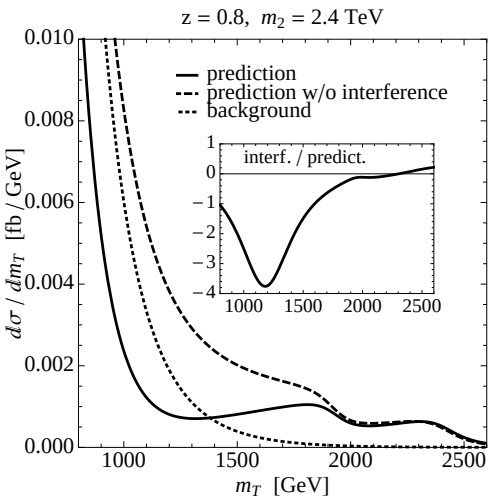

Figure 6.5: Differential cross-section in the dilepton transverse mass for $z = 0.8$ and $m_{W_2} = 2.4\,\mathrm{TeV}$, considering $7\,\mathrm{TeV}$ pp collisions. The dashed line shows the SM background plus the pure $W_{1,2}$-boson contribution. The solid line gives the complete theoretical distribution, including the interference term between W and $W_{1,2}$-bosons. The dotted line represents the SM irreducible background as reference. The inset plot displays the interference term normalised to the complete theoretical prediction.

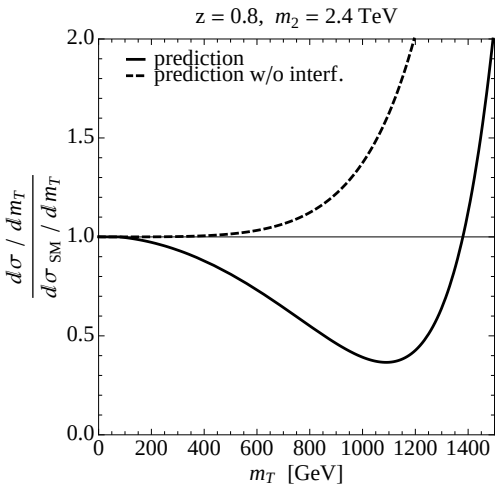

Figure 6.6: Ratio between the differential cross-section in the dilepton transverse mass for the prediction of the model and the SM irreducible background, considering $7\,\mathrm{TeV}$ pp collisions. The solid line shows the ratio obtained when including the interference. The dashed line represents the ratio without taking into account the interference. $z = 0.8$ and $m_{W_2} = 2.4\,\mathrm{TeV}$ are considered.

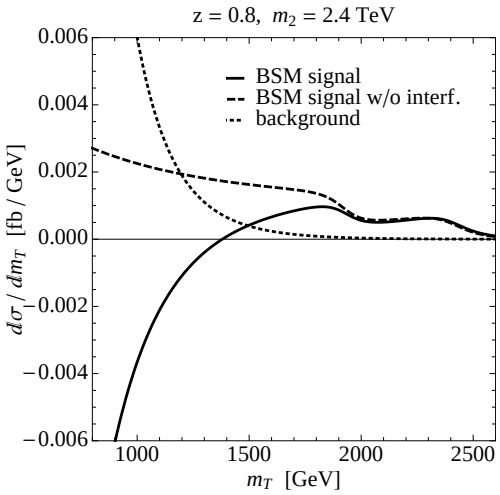

Figure 6.7: Differential cross-section in the dilepton transverse mass for $z = 0.8$ and $m_{W_2} = 2.4\,\mathrm{TeV}$, considering $7\,\mathrm{TeV}$ pp collisions. The dashed line shows the pure $\mathrm{W}_{1,2}$-boson contribution. The solid line gives the theoretical distribution of the BSM signal, including the interference term between W and $\mathrm{W}_{1,2}$-bosons. The dotted line represents the SM irreducible background as reference.

the m_T distribution for the BSM model and the SM irreducible background is displayed. The results obtained with (solid line) and without (dashed line) interference terms between $\mathrm{W}_{1,2}$ and W bosons are compared. Also in this case, neglecting the interference leads to an overestimation of the BSM physics free region. Within this approximation, the $\mathrm{W}_{1,2}$-boson contribution would indeed remain below the order of 5% up to $m_T(l\nu_l) \simeq 600\,\mathrm{GeV}$. The complete prediction suggests instead that in order to perform a model independent analysis one should only take data in a restricted range below $m_T(l\nu_l) \simeq 200\,\mathrm{GeV}$ to fit the functional form of the SM background.

Figure 6.7 shows the m_T distribution for the $\mathrm{W}_{1,2}$-boson signal with (solid line) and without (dashed line) interference between $\mathrm{W}_{1,2}$ and W bosons (*i.e.* after subtracting the SM background). The curves displayed support the result obtained previously for the benchmark model. Also within the 4-Site model in fact the $\mathrm{W}_{1,2}$-boson signal becomes negative below a certain m_T value, while the approximate result is always positive-definite. The total cross-section for the $\mathrm{W}_{1,2}$-boson signal can become negative as well. This is displayed in Figure 6.8, where a comparison between the total cross-section for the $\mathrm{W}_{1,2}$-boson signal with (solid line) and without (dashed line) interference terms between $\mathrm{W}_{1,2}$ and W bosons is shown as a function of the minimum cut on the dilepton transverse mass.

The consequences of this behaviour are summarised in Table 6.2, the analogue of Table 6.1 in the 4-Site model. For the minimum m_T cuts imposed by previous experimental analyses [118], the signal event overestimation induced by neglecting interference terms ranges between 6% and 266% in the considered mass spectrum. Compared to the previously discussed benchmark model, the 4-Site displays a much stronger impact of the interference terms on the extraction of exclusion limits. As shown in the last column of the table, the

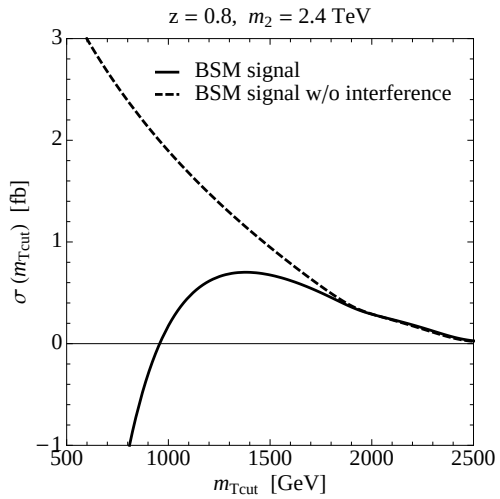

Figure 6.8: $W_{1,2}$ signal cross-section as a function of the minimum m_T cut for $z = 0.8$ and $m_{W_2} = 2.4\,\mathrm{TeV}$, considering $7\,\mathrm{TeV}$ pp collisions. The dashed line shows the pure $W_{1,2}$-boson contribution. The solid line gives the BSM signal, including the interference term between W and $W_{1,2}$-bosons.

m_2 [GeV]	$m_{T\,\text{cut}}$ [GeV]	$\sigma\,(m_{T\,\text{cut}})$ [fb] signal no interf.	signal with interf.	diff. in %	SM backgr.	σ total [fb] signal no interf.	signal with interf.
1400	1000	11.6	10.9	5.7	1.1	27.0	−66.9
1600	1100	7.0	6.2	12	0.6	17.8	−65.4
1800	1100	4.9	3.7	31	0.6	12.4	−59.7
2000	1100	3.4	2.1	62	0.6	9.3	−51.5
2200	1100	2.3	1.1	121	0.6	7.4	−41.5
2400	1100	1.7	0.5	266	0.6	6.2	−30.3

Table 6.2: From left to right, the columns indicate the W_2-boson mass value, the minimum m_T cut, the cross-section for the $W_{1,2}$-boson without interference calculated from the m_T lower cut on, the cross-section for the $W_{1,2}$-boson with interference from the m_T lower cut on, the difference in percent between these two normalised to the latter, the SM irreducible background from the m_T lower cut on, the total cross-section for the $W_{1,2}$-boson signal without and with interference. $z = 0.8$ is assumed. Computed for $7\,\mathrm{TeV}$ pp collisions. No efficiency and acceptance factors are included.

complete signal cross-section is negative, just as in the W' benchmark model, and provides another illustration of the discussion in section 6.1.3.

6.3 Summary

The interference between SM and BSM contributions is a priori expected to be sizeable and negative in the intermediate energy range between the resonance peaks, in particular if the

extra bosons couple universally to left-handed fermions. Quantitative statements about the implications of these effects have been made in the context of two reference models: the SSM and the 4-Site model.

The present study confirms that the interference is minimal only around the Jacobian peak of the distribution in the dilepton transverse mass $m_T(l\nu_l)$, the key observable used in experimental analyses. Away from the peak, it is substantial. It can decrease the $m_T(l\nu_l)$ differential cross-section by more than a factor of four compared to the result with no interference included. The size of this effect is model dependent and varies with the W' boson mass. Nevertheless, there is up to a factor of two difference already for $m_{W'} \simeq 2\,\mathrm{TeV}$ [3].

Neglecting the interference has several consequences. It should affect the estimate of the optimal cut on the $m_T(l\nu_l)$ variable to enhance the signal over background ratio, leading to an underestimation of the value of this cut. In addition, one generally overestimates the number of predicted signal events in the search window when using this approximation. The direct implication is that the extracted 95% CL exclusion bound on the mass of the heavy W' boson in published analyses is likely to be too strict.

Another consequence concerns the estimate of the $m_T(l\nu_l)$ range which can be assumed to be new physics free and thus used to derive a functional form describing the SM background via a fit to the observed data. The derived SM background is then extrapolated to the high energy range where new physics effects are expected to appear. In the cases considered, the above-mentioned new physics free range shrinks by roughly a factor three when including interference terms, its upper bound going from $600\,\mathrm{GeV}$ down to $200\,\mathrm{GeV}$. This implies that only the range strictly around the Jacobian peak of the SM W boson can formally be considered to be new physics free. Even though points outside this range are taken into account, it can be expected that they do not contribute much to the fit, since most points lie in the lower-end of the range. Nevertheless, one should be aware of this effect and use appropriate care.

Lastly, the predicted signal cross-section for the production and decay of extra heavy W' boson(s) can be negative if the interference with SM background is included and no kinematic cut is applied. More precisely it is negative because it is dominated by the SM contribution through the interference term, therefore is not indicative of the characteristics of the new physics. Therefore, presenting exclusion bounds on the W' boson mass in terms of this quantity does not have a clear direct meaning. Currently, the interpretation of experimental results is expressed via the 95% CL upper bound on the cross-section for the W' boson production and decay. This limit is cleaned up from any kinematic cuts, efficiency and acceptance factors in order to simplify its comparison with the theoretical signal cross-section and extract exclusion bounds on the W' mass for any possible model. This choice makes sense if the new physics contribution to the cross-section is positive-definite and independent of the SM, which is only true if the interference vanishes or if it is neglected.

A possible suggestion would be that the cut on $m_T(l\nu_l)$ used for the data analysis should be kept in the definition of the 95% CL upper bound on the new physics cross-section. Presenting limits as a function of this cut would allow for better comparisons with arbitrary models, in particular including interference effects, by providing means to choose the optimal cut case by case.

The message conveyed in this discussion is progressively being heard, and some of the recommendations made have indeed been taken into account in more recent experimental analyses by CMS. The interference does not seem to make a big difference in terms of the exclusion limit on the W' mass: in the limits quoted by these analyses, the effect is only a shift down of about $100\,\mathrm{GeV}$ from $2.5\,\mathrm{TeV}$ and $250\,\mathrm{GeV}$ from $3.35\,\mathrm{TeV}$ [78, 79]. The latest published exclusion bounds on the SSM W' mass (neglecting the interference) from ATLAS and CMS are respectively $2.55\,\mathrm{TeV}$ and $3.10\,\mathrm{TeV}$ (or 3.35 without interference) [73, 79].

Chapter 7

The neutral channel

7.1 Preliminary remarks

7.1.1 Models of Z'

Contrary to the case of W', a simple extra $U(1)$ gauge factor is enough for neutral gauge bosons to appear in Beyond the Standard Model scenarios. Their interaction structure is also less constrained. For a complete review of models of Z', see [26].

Results will mainly be presented in the context of a Sequential Standard Model (SSM) extension, where the Z' has exactly the same couplings as the Z, just as in the analysis of

$\frac{2}{g_{Z'}}\ a_{V,A}$		E_6	GLR	GSM
u,c,t	V	0	$\frac{\cos\phi}{2}+\frac{\sin\phi}{3}$	$\frac{\cos\alpha}{2}+\frac{4\sin\alpha}{3}$
	A	$\frac{\sin\theta_6}{\sqrt{6}}-\frac{\cos\theta_6}{\sqrt{10}}$	$-\frac{\cos\phi}{2}$	$\frac{\cos\alpha}{2}$
d,s,b	V	$-\sqrt{\frac{2}{5}}\cos\theta_6$	$\frac{\sin\phi}{3}-\frac{\cos\phi}{2}$	$-\frac{\cos\alpha}{2}-\frac{2\sin\alpha}{3}$
	A	$\frac{\cos\theta_6}{\sqrt{10}}+\frac{\sin\theta_6}{\sqrt{6}}$	$\frac{\cos\phi}{2}$	$-\frac{\cos\alpha}{2}$
e,μ,τ	V	$\sqrt{\frac{2}{5}}\cos\theta_6$	$-\frac{\cos\phi}{2}-\sin\phi$	$-\frac{\cos\alpha}{2}-2\sin\alpha$
	A	$\frac{\cos\theta_6}{\sqrt{10}}+\frac{\sin\theta_6}{\sqrt{6}}$	$\frac{\cos\phi}{2}$	$-\frac{\cos\alpha}{2}$
ν_e,ν_μ,ν_τ	V	$\frac{3\cos\theta_6}{2\sqrt{10}}+\frac{\sin\theta_6}{2\sqrt{6}}$	$-\frac{\sin\phi}{2}$	$\frac{\cos\alpha}{2}$
	A	$\frac{3\cos\theta_6}{2\sqrt{10}}+\frac{\sin\theta_6}{2\sqrt{6}}$	$-\frac{\sin\phi}{2}$	$\frac{\cos\alpha}{2}$

Table 7.1: The couplings of the Z' to the different species of fermions in the three different classes of models: E_6 Grand Unified Theories, Generalised Left-Right symmetric models, and Generalised sequential Standard Model. The parameter $g_{Z'}$ in the three cases is set to, respectively, $\frac{e}{c_\theta}\sqrt{\frac{5}{3}}$, $\frac{e}{c_\theta}\sqrt{\frac{1}{s_\theta^2}+\frac{s_\theta^2}{c_{2\theta}}-2}$ and $\frac{e}{c_\theta\, s_\theta}\sqrt{1+s_\theta^4}$.

the charged process. However, twelve other cases will also be discussed, that are representative of three different classes of models [27].

First, in theories where Grand Unification is achieved through an E_6 gauge group, there are commonly two $U(1)$ factors that can survive down to lower energies, and the gauge boson corresponding to one combination of these could then be a light enough and observable Z' [119, 120]. The charge assignment in these models leads to the fermion couplings given in Table 7.1, which depend on the mixing angle between the two $U(1)$ factors just mentioned, θ_6 (the subscript is added to avoid confusion with the other θ used previously). Note that the convention for this angle is the one used in [27]; the one in [119] is recovered by making the replacement $\theta_6 \to \theta_6 - \pi/2$. The overall gauge coupling strength is set to $g_{Z'} = \frac{e}{c_\theta}\sqrt{\frac{5}{3}} \approx 0.46$.

Second, models where both $SU(2)_R$ and $U(1)_{B-L}$ are gauged and break down to $U(1)_Y$ also predict a Z' (and W'), corresponding to the combination orthogonal to hypercharge. Again, the alignment of the breaking can be parametrised by a mixing angle, ϕ. The resulting couplings to the different species of fermions are given in Table 7.1, for $g_{Z'} = \frac{e}{c_\theta}\sqrt{\frac{1}{s_\theta^2} + \frac{s_\theta^2}{c_{2\theta}} - 2} \approx 0.59$. It is a generalisation of Left-Right symmetric models (GLR) [26, 27].

Last, one can generalise the idea of the SSM by allowing a different dependence on τ^3 and Q of the couplings, parametrising it with an angle α. The Standard Model (and thus the SSM) corresponds to choosing $\alpha \approx -0.072\pi$. Again, the charge assignments are given in Table 7.1 under GSM, and the gauge coupling is fixed to $g_{Z'} = \frac{e}{c_\theta\, s_\theta}\sqrt{1 + s_\theta^4} \approx 0.76$ [27].

A selection of various representative values can be chosen for the mixing angles θ_6, ϕ and α [27]. In all these models, the Z' are not considered to couple to the Standard Model gauge bosons; they can only directly decay into the Standard Model fermions, via the couplings given in Table 7.1. If the Z' are taken heavy enough, one can neglect the mass of the top-quark and their width is simply

$$\Gamma_{Z'} = \frac{m_{Z'}}{4\pi}\left(3\left((a_V^u)^2 + (a_A^u)^2 + (a_V^d)^2 + (a_A^d)^2\right) + (a_V^e)^2 + (a_A^e)^2 + (a_V^\nu)^2 + (a_A^\nu)^2\right). \tag{7.1}$$

7.1.2 Objectives

As in the discussion on the charged Drell-Yan process, the goal is to present some of the features of interference and clarify under what assumptions this contribution can be neglected or not.

From the general discussion in Chapter 5, and with the results presented in the previous one, the qualitative behaviour of interference in the differential cross-section is not expected

	name of resonance	mixing angle	up-type γ	up-type Z	up-type Z'	down-type γ	down-type Z	down-type Z'
QED	γ		$\mathbf{1}$			0.25		
Weak int.	Z		0.02	0.32		0.01	0.41	
E_6	χ	0	0	0.05	0.03	-0.16	-0.02	0.17
	ψ	0.5π	0	-0.07	0.02	0	0.07	0.02
	η	-0.29π	0	-0.02	0.03	-0.06	0.02	0.02
	S	0.129π	0	0.03	0.01	-0.14	0.01	0.19
	I	0.21π	0	0	0	-0.1	0.04	0.17
	N	0.42π	0	-0.07	0.02	-0.01	0.08	0.04
GLR	R	0	0.34	0.1	0.45	0.17	0.05	0.45
	$B-L$	0.5π	0.45	0.01	0.2	-0.22	-0.01	0.2
	LR	-0.129π	0.03	0.11	0.12	0.03	0.02	0.22
	Y	0.25π	0.84	0.02	1.1	0.08	0.05	0.31
GSM	SSM	-0.072π	0.02	0.32	0.32	0.01	0.41	0.41
	T_{3L}	0	0.56	0.44	1.2	0.28	0.53	1.2
	Q	0.5π	5.9	0.09	$35.$	1.5	0.08	8.8

Table 7.2: Value of the factor (7.2) for all contributions in a variety of models specified by a certain mixing angle, normalised to the pure photon factor (top-left entry). In the case of both the up- and down-type quark factors, the three columns are, respectively, the interference with the photon, the interference with the Z, and the pure Z' factor. The first two rows are the corresponding values in the Standard Model.

to be particularly different in the neutral Drell-Yan. Due to the variety of different Z' models, some subtleties might arise, though. How various coupling structures of the Z' can influence the interference will therefore be discussed first.

The main point of this discussion will be the investigation of the commonly used Narrow Width Approximation (NWA), whose validity is not systematically checked [121]: it is a very convenient approximation, but, as will be shown, it does not yield as good results as one would expect from performing computations without taking the interference into account.

7.1.3 The model dependence of the interference

Much can be said about how — and how much — the interference will contribute by simply computing the coupling factor present in the different terms of the matrix element squared (5.3):

$$\left(a_V^i\, a_V^j + a_A^i\, a_A^j\right)_l \left(a_V^i\, a_V^j + a_A^i\, a_A^j\right)_q . \tag{7.2}$$

The value of this factor is given in Table 7.2, computed in a variety of models. In a certain sense, it is a generalisation of the c_u, c_d parameters [27], with the inclusion of the extra

quantities relevant to the interference. All the values have been normalised to the pure photon factor in the up-type quark process, which is $e^4 Q_u^2$. The factors (7.2) are different for the processes involving up- and down-type quarks. The first row of the table shows the QED couplings in these two processes. In the second row are the couplings to the Standard Model Z as well as the relative sizes of the interference between the photon and the Z. For the rest of the table, the columns labelled with γ or Z are, respectively, the magnitude (7.2) of the interference between the photon or the Standard Model Z and the Z'; the third column of each group is the coupling strength of the Z', *i.e.* corresponds to the parameters c_u and c_d.

One sees immediately that, in the Standard Model itself, there is a substantial attenuation of the interference between the Z and the photon: the coupling factor of the interference is much smaller than the diagonal one. In other models, however, this is not necessarily the case; the interference can even be enhanced with respect to the pure Z' contribution, as in the ψ, N and $B - L$ models. In these latter models however, the up- and down-quark contributions have opposite sign, therefore will (partially) cancel each other, suppressing the overall effect.

An important feature to have in mind when reading these numbers is that, in proton collisions, the luminosity of the up-quark process is larger than the down-quark one. This implies for instance that in the ψ model, the interference effect will be constructive, as the negative coupling factor associated with the up-quark will dominate; conversely, in $B - L$, the opposite happens.

The ratio of up- and down-type quark luminosities is not a constant: it generally increases with the momentum fractions, thus with the CoM energy of the hard process. At low invariant mass, it is of order one, but it increases rapidly and is about an order of magnitude larger around half of the hadronic CoM energy, for instance. As a consequence, in models such as χ or S, the interference exhibits an additional change of sign which has nothing to do with the propagator factor: the up- and down-quark contributions compete against each other in such a way that, at lower energies, the down-quark wins while the situation changes at some higher energy.

To summarise, all the E_6 models exhibit constructive interference. The effect is suppressed however, because of competing contributions from the up- and down-type quark processes. In some cases — the χ and S models — the sign of interference changes at higher energies, when the up-quark contribution starts dominating.

In all other models, the interference is destructive between the Standard Model region and the Z' peak; even in the $B - L$ model, again, because the down-quark contribution is less important.

As a last remark, consider the SSM: the interference with the Z in this case is obviously not suppressed nor enhanced — by construction — but, on the other hand, the one with

the photon is very small. The overall effect of interference is thus somewhat reduced. If, on the other hand, an second heavy neutral resonance with exactly the same coupling structure as the photon were added, there would not be any such suppression. This is why in models with Kaluza-Klein excitations of both Standard Model gauge bosons, the interference is large compared to models such as the ones considered here where only one resonance is added [66]: a single Z' cannot maximally interfere with both the Z and the photon simultaneously.

7.1.4 Note on the computation

Contrary to the case of the charged Drell-Yan process, where the cross-section is computed as a function of the transverse mass of the outgoing leptons, in the neutral channel, one is interested in the invariant mass of the lepton pair, which considerably simplifies the computation, at least when considering the process at leading order only. Indeed, the angular integral, over $c\hat{\theta}$ and the one over y can be completely factorised and performed separately. In particular, the model-independent PDF factor only has to be computed once, as a function of $\hat{s}$, when considering the invariant mass distribution of several models.

The integrations are performed using Mathematica [4].

7.2 Heavy neutral gauge bosons at the LHC

In this section, quantitative statements are made in the context of $7\,\mathrm{TeV}$ collisions of protons as an illustration of how the interference changes certain properties of the signal of potential new physics in the neutral Drell-Yan channel. The model mainly considered for this purpose is the usual SSM benchmark, as it is a widespread paradigm and it exhibits a fairly large interference effect compared to other similar models.

7.2.1 Invariant mass distributions

Even though in the previous discussion about the charged Drell-Yan process it was the transverse mass that was used as a kinematic observable, and one is now interested in the invariant mass, $\sqrt{\hat{s}}$, even though the relative importance is somewhat reduced, as discussed in Section 7.1.3, the visible features of the interference in differential cross-section distributions are no different than in the W' case.

A typical case, considering the SSM with a Z' of mass $m_{Z'} = 3\,\mathrm{TeV}$, is shown in Figure 7.1. At the resonance peak, the interference does not matter. However, at lower energies it starts dominating the BMS prediction and drives it negative.

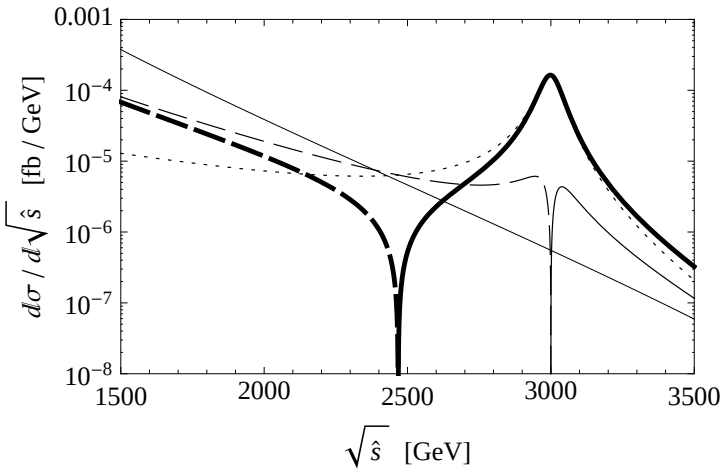

Figure 7.1: Invariant mass distribution for a SSM Z' of mass $m_{Z'} = 3\,\mathrm{TeV}$ in $7\,\mathrm{TeV}$ pp collisions. The thick line is the new physics contribution to the differential cross-section, the dashed line indicates where it is negative. The thinner line and the dotted line are, respectively, the interference and the pure Z' contributions alone. The falling thin solid line is the SM background.

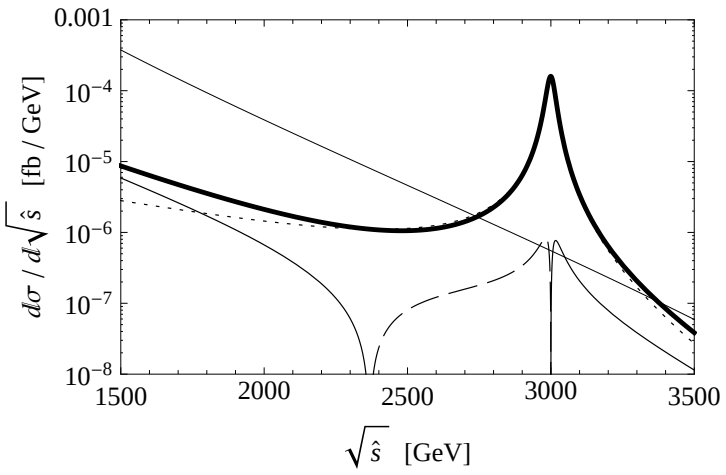

Figure 7.2: Invariant mass distribution for an $E_6\,\chi$ Z' of mass $m_{Z'} = 3\,\mathrm{TeV}$ in $7\,\mathrm{TeV}$ pp collisions. The thick line is the new physics contribution to the differential cross-section, the dashed line indicates where it is negative. The thinner line and the dotted line are, respectively, the interference and the pure Z' contributions alone. The falling thin solid line is the SM background.

In a less typical case that has been anticipated in the general discussion of Section 7.1.3, the interference can change sign between the resonances. Figure 7.2 shows an example of this feature, with a Z' of mass $m_{Z'} = 3\,\mathrm{TeV}$ as predicted in the $E_6\,\chi$ model. The interference changes sign at the resonance peak, as expected, but it does so again a little below that point, where the up-type quark destructive interference contribution becomes large enough to overcome the down-quark constructive one. Since these two contributions compete, the overall effect of the interference is substantially suppressed: it becomes the dominant part of the new physics signal only below $\sim 1.8\,\mathrm{TeV}$, where the Standard Model background is already much larger anyway.

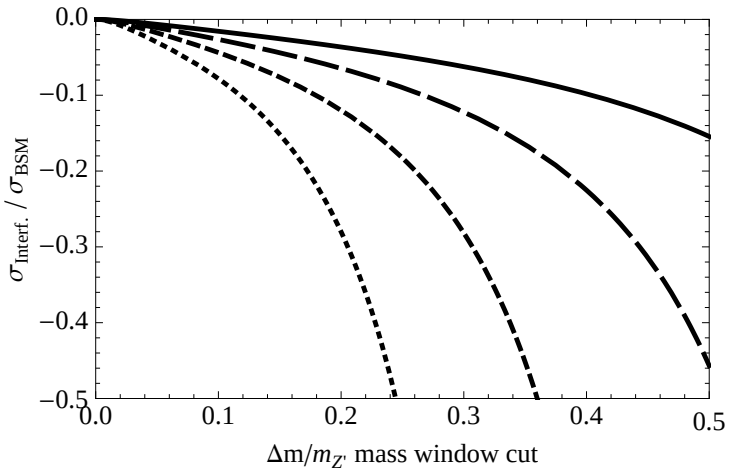

Figure 7.3: The relative size of the interference contribution to the BSM cross-section, in the region determined by $\Delta m/m_{Z'}$. The solid line corresponds to a SSM Z' of mass $m_{Z'} = 1\,\text{TeV}$ and the dotted line to a $4\,\text{TeV}$ one. The two dashed lines in between are for $m_{Z'} = 2$ and $3\,\text{TeV}$.

7.2.2 The relative size of interference

More interestingly, one can wonder how much the interference contributes to the new physics signal when integrating the differential cross-section over the peak region. Symmetric integration windows will be considered, defined by

$$\left|\sqrt{\hat{s}} - m_{Z'}\right| < \Delta m, \tag{7.3}$$

and results shown as a function of $\Delta m/m_{Z'}$.

Considering again the SSM, for masses ranging between 1 and $4\,\text{TeV}$, it appears clearly in Figure 7.3 that, although the effect is indeed small in the close vicinity of the resonance peak, it becomes substantial when considering larger regions. The effect is also increasing when considering heavier Z'.

If the couplings of the Z' are rescaled (along with a consistent rescaling of the width), the effect can be shifted. However, the picture almost does not change if the couplings are made smaller (and the Z' narrower); it only significantly changes when the Z' peak is made very large and broad. In Figure 7.4, the couplings have been rescaled by a factor 5, and the width therefore by a factor 25. The effect of interference is then pushed away from the peak. This is due to the fact that, when the coupling is made larger, the relative importance of the interference decreases, simply because it contains less powers of the Z' coupling; and inversely, of course. In fact, changing the width while keeping the couplings fixed has an opposite effect: increasing it means the interference contribution becomes large for a smaller integration window. This is illustrated by Figure 7.5.

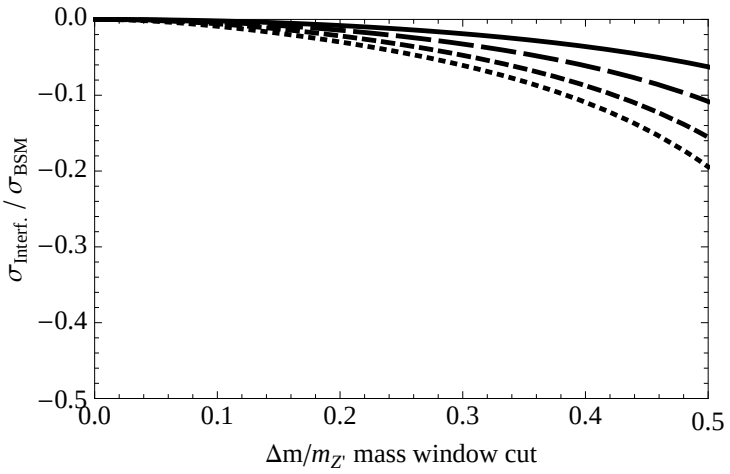

Figure 7.4: The relative size of the interference contribution to the BSM cross-section, in the region determined by $\Delta m/m_{Z'}$. The solid line corresponds to a SSM Z' with couplings scaled up by a factor 5 of mass $m_{Z'} = 1\,\text{TeV}$ and the dotted line to a $4\,\text{TeV}$ one. The two dashed lines in between are for $m_{Z'} = 2$ and $3\,\text{TeV}$.

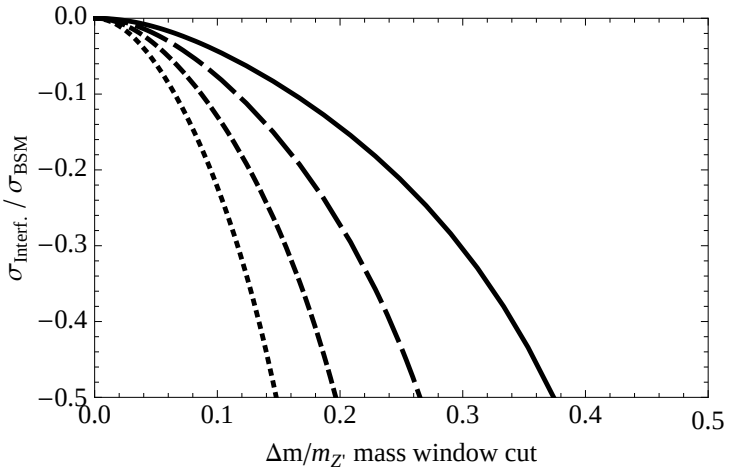

Figure 7.5: The relative size of the interference contribution to the BSM cross-section, in the region determined by $\Delta m/m_{Z'}$. The solid line corresponds to a SSM Z' of mass $m_{Z'} = 1\,\text{TeV}$, whose width has been scaled up by a factor 5 while keeping the fermion couplings constant, and the dotted line to a $4\,\text{TeV}$ one. The two dashed lines in between are for $m_{Z'} = 2$ and $3\,\text{TeV}$.

7.2.3 On the validity of the Narrow Width Approximation

With some sense of how much the interference contributes to the signal of new physics, one can then ask a more specific question: considering this effect, which is a purely off-shell effect, how valid is the popular Narrow Width Approximation (NWA)?

Very often, cross-section estimations of particular processes are made assuming the intermediate state is only produced on-shell: the computation then factorises into a production cross-section and a branching ratio, *i.e.* the probability that the produced state indeed decays into the desired final state.

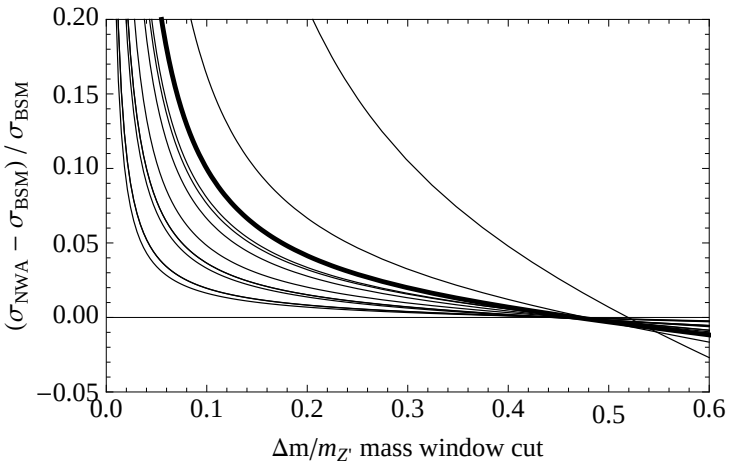

Figure 7.6: Relative difference between the NWA and a full computation, neglecting the interference, as function of the integration window, at a fixed Z' mass $m_{Z'} = 1\,\mathrm{TeV}$. All the models considered are plotted; the thick line indicates the SSM.

The cross-section, in the NWA, is

$$\sigma_{\text{NWA}} = \frac{1}{s}\int_{-\log(\sqrt{s}/m_{Z'})}^{\log(\sqrt{s}/m_{Z'})} \mathrm{d}y \sum_{q,\bar{q}} \left(f_q(m_{Z'}^2, y; \mu)\, f_{\bar{q}}(m_{Z'}^2, y; \mu)\, \frac{\pi}{3} \left((a_V^q)^2 + (a_V^{\bar{q}})^2 \right) \right) \times \text{BR}, \tag{7.4}$$

where the branching ratio, BR, is equal to the partial width to the considered leptons divided by the total width of the Z'.

If the interference is neglected, the difference between the NWA and a full computation of the BSM cross-section is just in how the kinematic dependence on $\hat{s}$ (entering in the evaluation of the PDF) is treated. In the NWA, only $\hat{s} = m_{Z'}^2$ contributes to the Z' cross-section while in a finite width computation one has to integrate a Breit-Wigner resonance over a certain invariant mass range. The model dependent coupling factor is, however, the same in both cases. As a result, one can match the two predictions by choosing an appropriate integration window for the full computation, and this window will essentially be model independent for a fixed Z' mass (as long as models with similarly small widths are considered). Figure 7.6 shows this "magic" cut for a mass of $m_{Z'} = 1\,\mathrm{TeV}$. An agreement between the two results is indeed reached for the same cut of about 50% in all models. Only the Q model, which has very large couplings and width, agrees slightly less with the rest. This was pointed out previously [27], and subsequently quoted by experimentalists [77].

The problem is, the interference spoils this nice feature. Figure 7.7 shows the same result as Figure 7.6, but properly taking into account the interference. The mass dependence of this result is shown in Figure 7.8; the shift of the would-be "magic" cut can be seen from the result without interference. Note that at a mass of $4\,\mathrm{TeV}$, a point where the NWA result can be obtained in the full computation appears.

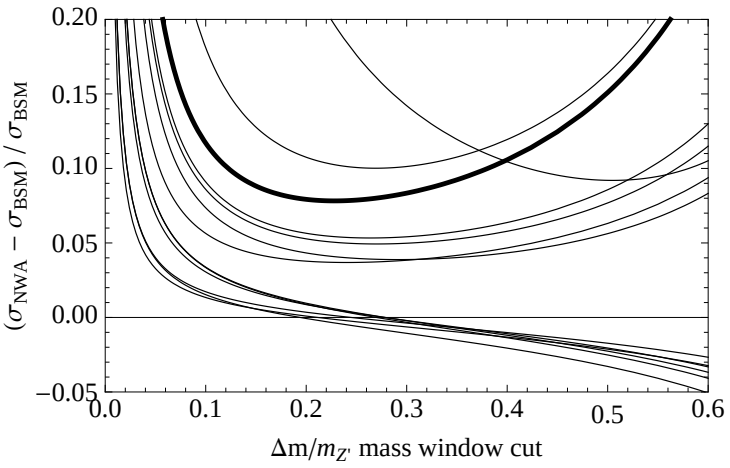

Figure 7.7: Relative difference between the NWA and a full computation, including the interference, as function of the integration window, at a fixed Z' mass $m_{Z'} = 1\,\mathrm{TeV}$. All the models considered are plotted; the thick line indicates the SSM. The lines that cross the axis correspond to the E_6 models featuring constructive interference.

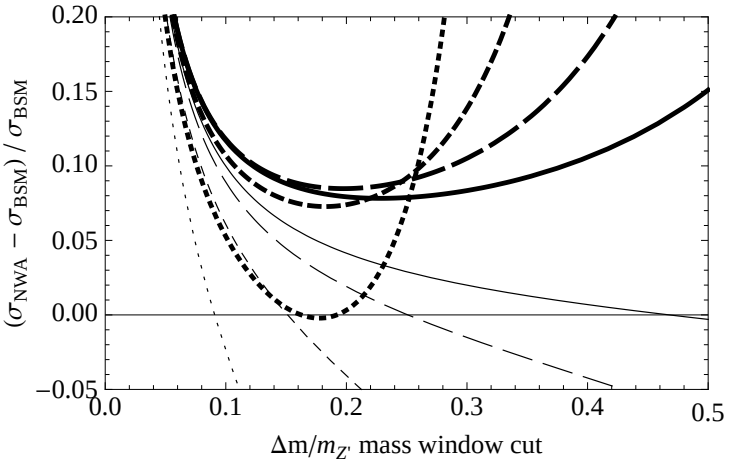

Figure 7.8: Relative difference between the NWA and a full computation as function of the integration window. The solid line corresponds to a SSM Z' of mass $m_{Z'} = 1\,\mathrm{TeV}$ and the dotted line to a $4\,\mathrm{TeV}$ one. The two dashed lines in between are for $m_{Z'} = 2$ and $3\,\mathrm{TeV}$. The thick and thin lines are, respectively, the result with and without interference.

The conclusion is that the model dependent interference matters in this context. In general, when there is destructive interference, the NWA result is an overestimation and can only represent the true cross-section up to, in cases here considered, about $5 - 10\%$, no matter what integration window around the peak is chosen.

One can wonder if, reducing the couplings of the Z' and thus its width, one can get to a point where there is perfect agreement with the NWA. Figure 7.9 shows what happens in the SSM with couplings ten times smaller: if the interference is neglected, any large enough cut gives practically the same result, equal to the NWA; with interference, on the other hand,

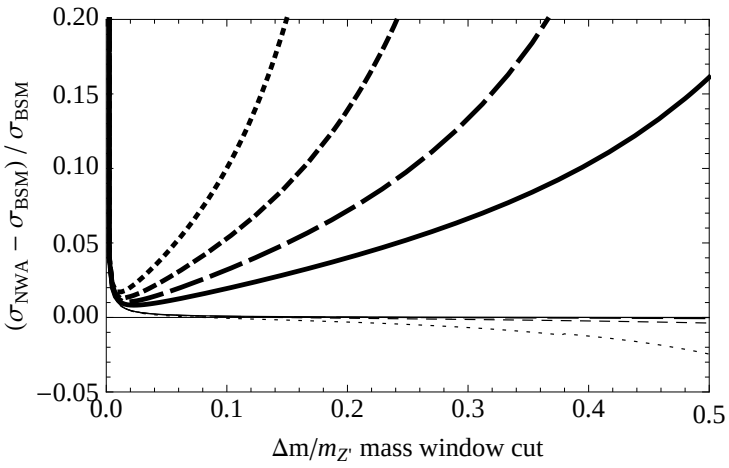

Figure 7.9: Relative difference between the NWA and a full computation as function of the integration window. The solid line corresponds to a SSM Z' with couplings reduced by a factor 10^{-1} of mass $m_{Z'} = 1\,\mathrm{TeV}$ and the dotted line to a $4\,\mathrm{TeV}$ one. The two dashed lines in between are for $m_{Z'} = 2$ and $3\,\mathrm{TeV}$. The thick and thin lines are, respectively, the result with and without interference.

if a narrow integration window does indeed give back the NWA result, as soon as the cut is extended, the off-shell contribution becomes important and the approximation fails.

7.3 Summary

Although a single Z' cannot maximally interfere as does a left-handed W', because the Standard Model neutral sector consists of two particles with different chiral structures, the Z and the photon, the interference is still an important effect in the neutral channel when considering the new physics prediction over the entire kinematic range.

It has been shown that, depending on the details of the Z' couplings, the interference can be constructive in the intermediate energy region (in the E_6 models) or destructive (in the GLR and GSM classes of models). Cancellation between the contributions from the up- and down-type quark processes may occur and partially suppress the interference, and, in some particular cases, lead to an extra sign change.

The interference is highly model dependent, both in terms of the Z' couplings and mass; the width also plays an important role. If the resonance is made very narrow, the interference still contributes significantly to the BSM prediction if a large search window is considered. It might not have a big influence on the visibility of the peak, as the Standard Model background is likely to drown anything away from the resonance region. It is important to understand this effect, however, to avoid relying on properties a Z' signal does not have.

A particularly striking result is that the NWA does not perform as good as one would expect: because of negative interference, it is in general not possible to find a special kinematic

window in which the predicted cross-section is equal to the NWA estimation. In some cases, no matter what invariant mass cut is applied, the NWA overestimates the Z' cross section by at least $5 - 10\%$. The most important point, though, is that the NWA (in particular, but actually neglecting the interference in general) gives a false sense of model-independence of the qualitative features of the new physics signal in Drell-Yan.

As in the charged case, experimental search strategies seem to be sufficiently robust against these effects and, as a result, one can hope that the proper treatment of interference would not have a considerable impact on the extracted mass limits of potential Z'. Only one recent analysis mentions the interference effect, that is taken into account for the analysis of some models where it is expected to be important [80]. The most up to date limits from ATLAS and CMS are, for the SSM, $m_{Z'} > 2.86$ and $2.96\,\mathrm{TeV}$ [74, 77]. Limits on E_6 models are also given and are about $m_{Z'} > 2.4 - 2.6\,\mathrm{TeV}$. These are derived without taking into account interference.

Chapter 8

Conclusion

Two subjects have been discussed in the present work.

In the first part, EWPT constraints on the 4-Site model have been carefully computed. The results generally correspond to previous estimations [32], namely that the extra heavy W and Z gauge bosons present in this model can have sizeable fermion couplings without spoiling the success of the Standard Model in describing electroweak precision data too much.

In the details, however, some inconsistencies due to a poor approximation were present that had been missed: the allowed couplings were somewhat overestimated; and asymmetric confidence regions were obtained, leading in a seemingly preferred sign for the couplings.

In the second part, searches in the Drell-Yan channels for new heavy gauge resonances, such as the ones predicted in the 4-Site model, were discussed. The subject is of particular interest at present, with the LHC running, collecting data, and allowing to place more and more stringent exclusion limits on these models. Currently, standard copies of W and Z bosons (Sequential Standard Model) are excluded for masses up to around $3\,\mathrm{TeV}$.

The interpretation of experimental searches for deviations from the Standard Model predictions in terms of a specific model requires the evaluation of what the signal of new physics is. Here again, approximation is required.

Commonly, the interference contribution between the new particles and the Standard Model is neglected. It has been shown that the approximation is indeed reasonable when restricting oneself to the kinematic region where the new physics dominates, which is the region most relevant to experimental searches. Outside such a region, however, the approximation may dramatically break down.

The conclusion is that, although the effect on current search strategies might be limited, it is important to keep in mind the qualitative features that fail to appear in the approximation.

It also shows the limits of commonly used concepts in this context, namely the NWA, which cannot properly represent the prediction of all models.

The awareness of these effects is currently increasing, and if most recent analyses do not consider interference at all [73, 74, 77], in some cases there has been an effort to take it into account at least when discussing certain models [78–80].

Appendix A

Derivation of the expression for the Fermi constant

The goal here is to prove (2.46) starting from the equation before. This can be restated as

$$(bg)^T (M_W^2)^{-1} (bg) = \sum_{k=0}^{K} \frac{(\sum_{l=0}^{k} b_l)^2}{f_{k+1}^2}. \tag{A.1}$$

The first step is to notice that, if the g_i factors are brought into the matrix to be inverted, *i.e.* $g(M^2)^{-1}g = (\frac{1}{g}M^2\frac{1}{g})^{-1}$, all the gauge couplings in the mass matrix are cancelled out. One is therefore left with the following matrix to invert:

$$\left(\frac{1}{g} \cdot M_W^2 \cdot \frac{1}{g}\right) = \begin{pmatrix} f_1^2 & -f_1^2 & & & \\ -f_1^2 & f_1^2 + f_2^2 & -f_2^2 & & \\ & -f_2^2 & f_2^2 + f_3^2 & \ddots & \\ & & \ddots & \ddots & -f_K^2 \\ & & & -f_K^2 & f_K^2 + f_{K+1}^2 \end{pmatrix}. \tag{A.2}$$

The easiest way to construct the inverse of this matrix is to build it starting from the bottom right. Trying to multiply the inverse from both the left and the right, one notices that all elements of the last row and last column need to be identical and equal to f_{K+1}^{-2}:

$$\left(\frac{1}{g} \cdot M_W^2 \cdot \frac{1}{g}\right)^{-1} = \left(\begin{array}{ccc|c} & & & f_{K+1}^{-2} \\ & & & \vdots \\ & & & f_{K+1}^{-2} \\ \hline f_{K+1}^{-2} & \cdots & f_{K+1}^{-2} & f_{K+1}^{-2} \end{array}\right). \tag{A.3}$$

It follows that the whole matrix has this nested structure, and one can recursively solve for the value of the entries at each level: the elements of the second-to-last row and column are $f_K^{-2} + f_{K+1}^{-2}$, and so forth; the last entry, at the top left, is $\sum_{k=1}^{K+1} f_k^{-2}$. Another way to write this matrix is

$$\left(\frac{1}{g} \cdot M_W^2 \cdot \frac{1}{g}\right)^{-1} = \frac{1}{f_{K+1}^2} \begin{pmatrix} 1 & 1 & \cdots & 1 \\ 1 & 1 & \cdots & 1 \\ \vdots & \vdots & \ddots & 1 \\ 1 & 1 & 1 & 1 \end{pmatrix} + \frac{1}{f_K^2} \begin{pmatrix} 1 & \cdots & 1 & 0 \\ \vdots & \ddots & 1 & 0 \\ 1 & 1 & 1 & 0 \\ 0 & 0 & 0 & 0 \end{pmatrix} + \dots . \tag{A.4}$$

This allows to see explicitly how the terms can be reorganised in the product with the b_k parameters. Each term in (A.4) gives

$$\frac{1}{f_{k+1}^2} \sum_{l,m=0}^{k} b_l \, b_m = \frac{1}{f_{k+1}^2} \left(\sum_{l=0}^{k} b_l\right)^2 , \tag{A.5}$$

and this concludes the proof.

A generalisation of this result to the different possible cases corresponding to having the first and last site in the moose gauged or not is given in [122].

Appendix B

4-Site expressions to order A

It is convenient to define γ_0, the 0th order term in the A expansion of γ, as it appears very often:

$$\gamma_0 \equiv \sqrt{1 - \frac{C_0\,\zeta}{1+\zeta}}. \tag{B.1}$$

B.1 $\triangle$ parameters

The Δ parameters, to $\mathcal{O}\left(A\right)$, are

$$\begin{aligned}
\Delta\rho &= \frac{2c_1 + \zeta(1+c_2)}{\sqrt{2}\sqrt{(1+\zeta)\left(2c_1^2 + \zeta(1+c_2^2)\right)}} + \frac{-\frac{1-2c_1+c_2}{1+\zeta} + \gamma_0(1+\zeta)(c_2-1)}{\sqrt{2}\sqrt{(1+\zeta)\left(2c_1^2 + \zeta(1+c_2^2)\right)}}\,A + \mathcal{O}\left(A^2\right), \\
\Delta k &= -1 + \frac{2}{1-\sqrt{1-s_{2\theta}^2}}\left(\frac{c_2(1-\gamma_0)(1+\zeta)}{2c_1+\zeta(1+c_2)}\right)\Bigg\{1+ \\
&\quad \frac{1}{2}\left(-\frac{1}{1+\zeta} + \frac{\zeta}{\gamma_0(1+\zeta)} + \frac{2+\gamma_0(1+\zeta)}{\gamma_0(1+\zeta)} + \frac{2(1+c_2+\gamma_0(1+\zeta)-c_2\gamma_0(1+\zeta))}{2c_1+\zeta(1+c_2)}\right)A\Bigg\} \\
&\quad + \mathcal{O}\left(A^2\right), \\
\Delta r_W &= \frac{1-s_{2\theta}^2-\gamma_0^2}{1-\gamma_0^2} + \frac{s_{2\theta}^2(2+\zeta)}{(1-\gamma_0)(1+\zeta)}\,A + \mathcal{O}\left(A^2\right).
\end{aligned} \tag{B.2}$$

B.2 Masses

The masses of the gauge bosons, to $\mathcal{O}(A)$, are

$$\begin{aligned}\frac{\left(m_Z^1\right)^2}{M_1^2} &= 1 + \left(1 + \frac{1}{\zeta}\right) A + \mathcal{O}\left(A^2\right), \\ \frac{\left(m_Z^2\right)^2}{M_1^2} &= (1+\zeta) + \frac{A}{\zeta} + \mathcal{O}\left(A^2\right)\end{aligned} \tag{B.3}$$

for the neutral gauge bosons, and

$$\begin{aligned}\frac{\left(m_W^0\right)^2}{M_1^2} &= \frac{1+\gamma_0}{2} A + \mathcal{O}\left(A^2\right), \\ \frac{\left(m_W^1\right)^2}{M_1^2} &= 1 + \frac{(1+\gamma_0)(1+\zeta)}{2\zeta} A + \mathcal{O}\left(A^2\right), \\ \frac{\left(m_W^2\right)^2}{M_1^2} &= (1+\zeta) + \frac{1+\gamma_0}{2\zeta} A + \mathcal{O}\left(A^2\right)\end{aligned} \tag{B.4}$$

for the charged ones.

References

[1] E. Accomando, D. Becciolini, L. Fedeli, D. Dominici, and S. De Curtis, "Improved analysis of the bounds from the electroweak precision tests on the 4-site model," *Phys.Rev.* **D83** (2011) 115021, `arXiv:1105.3896 [hep-ph]`.

[2] E. Accomando, D. Becciolini, S. De Curtis, D. Dominici, and L. Fedeli, "W' production at the LHC in the 4-site Higgsless model," *Phys.Rev.* **D84** (2011) 115014, `arXiv:1107.4087 [hep-ph]`.

[3] E. Accomando, D. Becciolini, S. De Curtis, D. Dominici, L. Fedeli, *et al.*, "Interference effects in heavy W'-boson searches at the LHC," *Phys.Rev.* **D85** (2012) 115017, `arXiv:1110.0713 [hep-ph]`.

[4] Wolfram Research, Inc., *Mathematica*. Version 7.0, Champaign, IL, 2008.

[5] **ATLAS** Collaboration, G. Aad *et al.*, "Observation of a new particle in the search for the Standard Model Higgs boson with the ATLAS detector at the LHC," *Phys.Lett.* **B716** (2012) 1–29, `arXiv:1207.7214 [hep-ex]`.

[6] **CMS** Collaboration, S. Chatrchyan *et al.*, "Observation of a new boson at a mass of 125 GeV with the CMS experiment at the LHC," *Phys.Lett.* **B716** (2012) 30–61, `arXiv:1207.7235 [hep-ex]`.

[7] B. W. Lee, C. Quigg, and H. Thacker, "The Strength of Weak Interactions at Very High-Energies and the Higgs Boson Mass," *Phys.Rev.Lett.* **38** (1977) 883–885.

[8] E. Accomando, L. Fedeli, S. Moretti, S. De Curtis, and D. Dominici, "Charged di-boson production at the LHC in a 4-site model with a composite Higgs boson," `arXiv:1208.0268 [hep-ph]`.

[9] S. Weinberg, "Phenomenological Lagrangians," *Physica* **A96** (1979) 327.

[10] N. Arkani-Hamed, S. Dimopoulos, and G. Dvali, "The Hierarchy problem and new dimensions at a millimeter," *Phys.Lett.* **B429** (1998) 263–272, `arXiv:hep-ph/9803315 [hep-ph]`.

[11] L. Randall and R. Sundrum, "A Large mass hierarchy from a small extra dimension," *Phys.Rev.Lett.* **83** (1999) 3370–3373, `arXiv:hep-ph/9905221 [hep-ph]`.

[12] S. R. Coleman and J. Mandula, "All Possible Symmetries of the S Matrix," *Phys.Rev.* **159** (1967) 1251–1256.

[13] R. Haag, J. T. Lopuszanski, and M. Sohnius, "All Possible Generators of Supersymmetries of the s Matrix," *Nucl.Phys.* **B88** (1975) 257.

[14] F. Englert and R. Brout, "Broken Symmetry and the Mass of Gauge Vector Mesons," *Phys.Rev.Lett.* **13** (1964) 321–323.

[15] P. W. Higgs, "Broken Symmetries and the Masses of Gauge Bosons," *Phys.Rev.Lett.* **13** (1964) 508–509.

[16] R. Casalbuoni, S. De Curtis, D. Dominici, and R. Gatto, "Effective Weak Interaction Theory with Possible New Vector Resonance from a Strong Higgs Sector," *Phys.Lett.* **B155** (1985) 95.

[17] J. Gasser and H. Leutwyler, "Chiral Perturbation Theory: Expansions in the Mass of the Strange Quark," *Nucl.Phys.* **B250** (1985) 465.

[18] M. Bando, T. Kugo, S. Uehara, K. Yamawaki, and T. Yanagida, "Is rho Meson a Dynamical Gauge Boson of Hidden Local Symmetry?," *Phys.Rev.Lett.* **54** (1985) 1215.

[19] H. Georgi, "A Tool Kit For Builders Of Composite Models," *Nucl.Phys.* **B266** (1986) 274.

[20] R. S. Chivukula and H.-J. He, "Unitarity of deconstructed five-dimensional Yang-Mills theory," *Phys.Lett.* **B532** (2002) 121–128, `arXiv:hep-ph/0201164 [hep-ph]`.

[21] N. Arkani-Hamed, A. G. Cohen, and H. Georgi, "(De)constructing dimensions," *Phys.Rev.Lett.* **86** (2001) 4757–4761, `arXiv:hep-th/0104005 [hep-th]`.

[22] R. S. Chivukula, D. A. Dicus, and H.-J. He, "Unitarity of compactified five-dimensional Yang-Mills theory," *Phys.Lett.* **B525** (2002) 175–182, `arXiv:hep-ph/0111016 [hep-ph]`.

[23] D. Becciolini, M. Redi, and A. Wulzer, "AdS/QCD: The Relevance of the Geometry," *JHEP* **1001** (2010) 074, `arXiv:0906.4562 [hep-ph]`.

[24] J. M. Maldacena, "The Large N limit of superconformal field theories and supergravity," *Adv.Theor.Math.Phys.* **2** (1998) 231–252, `arXiv:hep-th/9711200 [hep-th]`.

[25] R. Casalbuoni, S. De Curtis, D. Dolce, and D. Dominici, "Playing with fermion couplings in Higgsless models," *Phys.Rev.* **D71** (2005) 075015, `arXiv:hep-ph/0502209 [hep-ph]`.

[26] P. Langacker, "The Physics of Heavy Z' Gauge Bosons," *Rev.Mod.Phys.* **81** (2009) 1199–1228, `arXiv:0801.1345 [hep-ph]`.

[27] E. Accomando, A. Belyaev, L. Fedeli, S. F. King, and C. Shepherd-Themistocleous, "Z' physics with early LHC data," *Phys.Rev.* **D83** (2011) 075012, `arXiv:1010.6058 [hep-ph]`.

[28] R. S. Chivukula, E. H. Simmons, H.-J. He, M. Kurachi, and M. Tanabashi, "Ideal fermion delocalization in Higgsless models," *Phys.Rev.* **D72** (2005) 015008, `arXiv:hep-ph/0504114 [hep-ph]`.

[29] M. E. Peskin and D. V. Schroeder, *An Introduction to Quantum Field Theory*. Westview Press, 1995, ISBN 978-0201503975.

[30] T. Sakai and S. Sugimoto, "Low energy hadron physics in holographic QCD," *Prog.Theor.Phys.* **113** (2005) 843–882, `arXiv:hep-th/0412141 [hep-th]`.

[31] R. S. Chivukula, B. Coleppa, S. Di Chiara, E. H. Simmons, H.-J. He, *et al.*, "A Three Site Higgsless Model," *Phys.Rev.* **D74** (2006) 075011, `arXiv:hep-ph/0607124 [hep-ph]`.

[32] E. Accomando, S. De Curtis, D. Dominici, and L. Fedeli, "Drell-Yan production at the LHC in a four site Higgsless model," *Phys.Rev.* **D79** (2009) 055020, `arXiv:0807.5051 [hep-ph]`.

[33] G. Altarelli, R. Barbieri, and S. Jadach, "Toward a model independent analysis of electroweak data," *Nucl.Phys.* **B369** (1992) 3–32.

[34] M. E. Peskin and T. Takeuchi, "A New constraint on a strongly interacting Higgs sector," *Phys.Rev.Lett.* **65** (1990) 964–967.

[35] M. E. Peskin and T. Takeuchi, "Estimation of oblique electroweak corrections," *Phys.Rev.* **D46** (1992) 381–409.

[36] G. Altarelli and R. Barbieri, "Vacuum polarization effects of new physics on electroweak processes," *Phys.Lett.* **B253** (1991) 161–167.

[37] G. Altarelli, R. Barbieri, and F. Caravaglios, "Electroweak precision tests: A Concise review," *Int.J.Mod.Phys.* **A13** (1998) 1031–1058, `arXiv:hep-ph/9712368 [hep-ph]`.

[38] G. Altarelli, R. Barbieri, and F. Caravaglios, "Nonstandard analysis of electroweak precision data," *Nucl.Phys.* **B405** (1993) 3–23.

[39] R. Barbieri, A. Pomarol, R. Rattazzi, and A. Strumia, "Electroweak symmetry breaking after LEP-1 and LEP-2," *Nucl.Phys.* **B703** (2004) 127–146, `arXiv:hep-ph/0405040 [hep-ph]`.

[40] K. Agashe and R. Contino, "The Minimal composite Higgs model and electroweak precision tests," *Nucl.Phys.* **B742** (2006) 59–85, `arXiv:hep-ph/0510164 [hep-ph]`.

[41] **ALEPH, DELPHI, L3, OPAL, SLD, LEP Electroweak Working Group, SLD Electroweak Group, SLD Heavy Flavour Group** Collaboration, "Precision electroweak measurements on the Z resonance," *Phys.Rept.* **427** (2006) 257–454, arXiv:hep-ex/0509008 [hep-ex].

[42] **CDF, D0** Collaboration, T. E. W. Group, "2012 Update of the Combination of CDF and D0 Results for the Mass of the W Boson," arXiv:1204.0042 [hep-ex].

[43] W. H. Press, S. A. Teukolsky, W. T. Vetterling, and B. P. Flannery, *Numerical Recipes 3rd Edition: The Art of Scientific Computing*. Cambridge University Press, 2007, ISBN 978-0521880688.

[44] R. S. Chivukula, E. H. Simmons, S. Matsuzaki, and M. Tanabashi, "The Three Site Model at One-Loop," *Phys.Rev.* **D75** (2007) 075012, arXiv:hep-ph/0702218 [HEP-PH].

[45] T. Abe, S. Matsuzaki, and M. Tanabashi, "Does the three site Higgsless model survive the electroweak precision tests at loop?," *Phys.Rev.* **D78** (2008) 055020, arXiv:0807.2298 [hep-ph].

[46] B. Lee and J. Zinn-Justin, "Spontaneously broken gauge symmetries. 3. Equivalence," *Phys.Rev.* **D5** (1972) 3155–3160.

[47] R. Contino, C. Grojean, M. Moretti, F. Piccinini, and R. Rattazzi, "Strong Double Higgs Production at the LHC," *JHEP* **1005** (2010) 089, arXiv:1002.1011 [hep-ph].

[48] A. Carcamo Hernandez and R. Torre, "A 'Composite' scalar-vector system at the LHC," *Nucl.Phys.* **B841** (2010) 188–204, arXiv:1005.3809 [hep-ph].

[49] B. Bellazzini, C. Csaki, J. Hubisz, J. Serra, and J. Terning, "Composite Higgs Sketch," *JHEP* **1211** (2012) 003, arXiv:1205.4032 [hep-ph].

[50] T. Abe, N. Chen, and H.-J. He, "LHC Higgs Signatures from Extended Electroweak Gauge Symmetry," *JHEP* **1301** (2013) 082, arXiv:1207.4103 [hep-ph].

[51] M. Gintner and J. Juran, "A 125 GeV scalar improves the low-energy data support for the top-BESS model," arXiv:1301.2124 [hep-ph].

[52] H.-J. He, Y.-P. Kuang, Y.-H. Qi, B. Zhang, A. Belyaev, *et al.*, "CERN LHC Signatures of New Gauge Bosons in Minimal Higgsless Model," *Phys.Rev.* **D78** (2008) 031701, arXiv:0708.2588 [hep-ph].

[53] T. Ohl and C. Speckner, "Production of Almost Fermiophobic Gauge Bosons in the Minimal Higgsless Model at the LHC," *Phys.Rev.* **D78** (2008) 095008, arXiv:0809.0023 [hep-ph].

[54] T. G. Rizzo, "The Determination of the Helicity of W' Boson Couplings at the LHC," *JHEP* **0705** (2007) 037, arXiv:0704.0235 [hep-ph].

[55] S. Drell and T.-M. Yan, "Massive Lepton Pair Production in Hadron-Hadron Collisions at High-Energies," *Phys.Rev.Lett.* **25** (1970) 316–320.

[56] **UA1** Collaboration, G. Arnison *et al.*, "Experimental Observation of Isolated Large Transverse Energy Electrons with Associated Missing Energy at $\sqrt{s} = 540$ GeV," *Phys.Lett.* **B122** (1983) 103–116.

[57] **UA2** Collaboration, M. Banner *et al.*, "Observation of Single Isolated Electrons of High Transverse Momentum in Events with Missing Transverse Energy at the CERN $\bar{p}p$ Collider," *Phys.Lett.* **B122** (1983) 476–485.

[58] **UA1** Collaboration, G. Arnison *et al.*, "Experimental Observation of Lepton Pairs of Invariant Mass Around 95 GeV/c^2 at the CERN SPS Collider," *Phys.Lett.* **B126** (1983) 398–410.

[59] **UA2** Collaboration, P. Bagnaia *et al.*, "Evidence for $Z^0 \to e^+ e^-$ at the CERN $\bar{p}p$ Collider," *Phys.Lett.* **B129** (1983) 130–140.

[60] **Gargamelle Neutrino** Collaboration, F. Hasert *et al.*, "Observation of Neutrino Like Interactions Without Muon Or Electron in the Gargamelle Neutrino Experiment," *Phys.Lett.* **B46** (1973) 138–140.

[61] C. Prescott, W. Atwood, R. L. Cottrell, H. DeStaebler, E. L. Garwin, *et al.*, "Parity Nonconservation in Inelastic Electron Scattering," *Phys.Lett.* **B77** (1978) 347–352.

[62] M. Dittmar, "Neutral current interference in the TeV region: The Experimental sensitivity at the LHC," *Phys.Rev.* **D55** (1997) 161–166, `arXiv:hep-ex/9606002 [hep-ex]`.

[63] T. G. Rizzo, "Indirect Searches for Z-prime-like Resonances at the LHC," *JHEP* **0908** (2009) 082, `arXiv:0904.2534 [hep-ph]`.

[64] F. Petriello and S. Quackenbush, "Measuring Z' couplings at the CERN LHC," *Phys.Rev.* **D77** (2008) 115004, `arXiv:0801.4389 [hep-ph]`.

[65] C.-W. Chiang, N. D. Christensen, G.-J. Ding, and T. Han, "Discovery in Drell-Yan Processes at the LHC," *Phys.Rev.* **D85** (2012) 015023, `arXiv:1107.5830 [hep-ph]`.

[66] G. Bella, E. Etzion, N. Hod, Y. Oz, Y. Silver, *et al.*, "A Search for heavy Kaluza-Klein electroweak gauge bosons at the LHC," *JHEP* **1009** (2010) 025, `arXiv:1004.2432 [hep-ex]`.

[67] A. Papaefstathiou and O. Latunde-Dada, "NLO production of W ' bosons at hadron colliders using the MC@NLO and POWHEG methods," *JHEP* **0907** (2009) 044, `arXiv:0901.3685 [hep-ph]`.

[68] E. Boos, V. Bunichev, L. Dudko, and M. Perfilov, "Interference between W' and W in single-top quark production processes," *Phys.Lett.* **B655** (2007) 245–250, `arXiv:hep-ph/0610080 [hep-ph]`.

[69] **CDF** Collaboration, T. Aaltonen *et al.*, "Search for a New Heavy Gauge Boson W' with Electron + missing ET Event Signature in $p\bar{p}$ collisions at $\sqrt{s} = 1.96$ TeV," *Phys.Rev.* **D83** (2011) 031102, `arXiv:1012.5145 [hep-ex]`.

[70] **CDF** Collaboration, T. Aaltonen *et al.*, "A Search for high-mass resonances decaying to dimuons at CDF," *Phys.Rev.Lett.* **102** (2009) 091805, `arXiv:0811.0053 [hep-ex]`.

[71] **D0** Collaboration, V. Abazov *et al.*, "Search for W' bosons decaying to an electron and a neutrino with the D0 detector," *Phys.Rev.Lett.* **100** (2008) 031804, `arXiv:0710.2966 [hep-ex]`.

[72] **D0** Collaboration, V. M. Abazov *et al.*, "Search for a heavy neutral gauge boson in the dielectron channel with 5.4 fb-1 of $p\bar{p}$ collisions at $\sqrt{s} = 1.96$ TeV," *Phys.Lett.* **B695** (2011) 88–94, `arXiv:1008.2023 [hep-ex]`.

[73] **ATLAS** Collaboration, G. Aad *et al.*, "ATLAS search for a heavy gauge boson decaying to a charged lepton and a neutrino in pp collisions at $\sqrt{s} = 7$ TeV," `arXiv:1209.4446 [hep-ex]`.

[74] **ATLAS** Collaboration, "Search for high-mass dilepton resonances in 20 fb^{-1} of pp collisions at $\sqrt{s} = 8$ TeV with the ATLAS experiment," Tech. Rep. ATLAS-CONF-2013-017, Mar, 2013.

[75] **CMS** Collaboration, V. Khachatryan *et al.*, "Search for a heavy gauge boson W' in the final state with an electron and large missing transverse energy in pp collisions at $\sqrt{s} = 7$ TeV," *Phys.Lett.* **B698** (2011) 21–39, `arXiv:1012.5945 [hep-ex]`.

[76] **CMS** Collaboration, S. Chatrchyan *et al.*, "Search for a W' boson decaying to a muon and a neutrino in pp collisions at $\sqrt{s} = 7$ TeV," *Phys.Lett.* **B701** (2011) 160–179, `arXiv:1103.0030 [hep-ex]`.

[77] **CMS** Collaboration, "Search for Resonances in the Dilepton Mass Distribution in pp Collisions at $\sqrt{s} = 8$ TeV," Tech. Rep. CMS-PAS-EXO-12-061, 2013.

[78] **CMS** Collaboration, S. Chatrchyan *et al.*, "Search for leptonic decays of W' bosons in pp collisions at $\sqrt{s} = 7$ TeV," *JHEP* **1208** (2012) 023, `arXiv:1204.4764 [hep-ex]`.

[79] **CMS** Collaboration, "Search for leptonic decays of W' bosons in pp collisions at $\sqrt{s} = 8$ TeV," Tech. Rep. CMS-PAS-EXO-12-060, 2013.

[80] **ATLAS** Collaboration, G. Aad *et al.*, "Search for high-mass resonances decaying to dilepton final states in pp collisions at a center-of-mass energy of 7 TeV with the ATLAS detector," `arXiv:1209.2535 [hep-ex]`.

[81] **D0** Collaboration, V. Abazov *et al.*, "Search for W' Boson Resonances Decaying to a Top Quark and a Bottom Quark," *Phys.Rev.Lett.* **100** (2008) 211803, `arXiv:0803.3256 [hep-ex]`.

[82] **CMS** Collaboration, S. Chatrchyan *et al.*, "Search for a W' boson decaying to a bottom quark and a top quark in pp collisions at $\sqrt{s} = 7$ TeV," `arXiv:1208.0956 [hep-ex]`.

[83] J. Pumplin, D. Stump, J. Huston, H. Lai, P. M. Nadolsky, *et al.*, "New generation of parton distributions with uncertainties from global QCD analysis," *JHEP* **0207** (2002) 012, `arXiv:hep-ph/0201195 [hep-ph]`.

[84] J. Smith, W. van Neerven, and J. Vermaseren, "The Transverse Mass and Width of the W Boson," *Phys.Rev.Lett.* **50** (1983) 1738.

[85] J. C. Pati and A. Salam, "Lepton Number as the Fourth Color," *Phys.Rev.* **D10** (1974) 275–289.

[86] R. Mohapatra, J. C. Pati, and L. Wolfenstein, "The Superweak Model of CP-Violation in Unified Gauge Theories," *Phys.Rev.* **D11** (1975) 3319.

[87] G. Senjanovic and R. N. Mohapatra, "Exact Left-Right Symmetry and Spontaneous Violation of Parity," *Phys.Rev.* **D12** (1975) 1502.

[88] S. Gopalakrishna, T. Han, I. Lewis, Z.-g. Si, and Y.-F. Zhou, "Chiral Couplings of W' and Top Quark Polarization at the LHC," *Phys.Rev.* **D82** (2010) 115020, `arXiv:1008.3508 [hep-ph]`.

[89] M. Frank, A. Hayreter, and I. Turan, "Production and Decays of W_R bosons at the LHC," *Phys.Rev.* **D83** (2011) 035001, `arXiv:1010.5809 [hep-ph]`.

[90] A. Maiezza, M. Nemevsek, F. Nesti, and G. Senjanovic, "Left-Right Symmetry at LHC," *Phys.Rev.* **D82** (2010) 055022, `arXiv:1005.5160 [hep-ph]`.

[91] M. Nemevsek, F. Nesti, G. Senjanovic, and Y. Zhang, "First Limits on Left-Right Symmetry Scale from LHC Data," *Phys.Rev.* **D83** (2011) 115014, `arXiv:1103.1627 [hep-ph]`.

[92] I. Antoniadis, N. Arkani-Hamed, S. Dimopoulos, and G. Dvali, "New dimensions at a millimeter to a Fermi and superstrings at a TeV," *Phys.Lett.* **B436** (1998) 257–263, `arXiv:hep-ph/9804398 [hep-ph]`.

[93] E. Accomando, I. Antoniadis, and K. Benakli, "Looking for TeV scale strings and extra dimensions," *Nucl.Phys.* **B579** (2000) 3–16, `arXiv:hep-ph/9912287 [hep-ph]`.

[94] E. Boos, I. Volobuev, M. Perfilov, and M. Smolyakov, "Searches for W' and Z' in models with large extra dimensions," *Theor.Math.Phys.* **170** (2012) 90–96, `arXiv:1106.2400 [hep-ph]`.

[95] K. Agashe, H. Davoudiasl, S. Gopalakrishna, T. Han, G.-Y. Huang, *et al.*, "LHC Signals for Warped Electroweak Neutral Gauge Bosons," *Phys.Rev.* **D76** (2007) 115015, `arXiv:0709.0007 [hep-ph]`.

[96] K. Agashe, S. Gopalakrishna, T. Han, G.-Y. Huang, and A. Soni, "LHC Signals for Warped Electroweak Charged Gauge Bosons," *Phys.Rev.* **D80** (2009) 075007, `arXiv:0810.1497 [hep-ph]`.

[97] N. Arkani-Hamed, A. G. Cohen, and H. Georgi, "Electroweak symmetry breaking from dimensional deconstruction," *Phys.Lett.* **B513** (2001) 232–240, `arXiv:hep-ph/0105239 [hep-ph]`.

[98] C. T. Hill, S. Pokorski, and J. Wang, "Gauge invariant effective Lagrangian for Kaluza-Klein modes," *Phys.Rev.* **D64** (2001) 105005, `arXiv:hep-th/0104035 [hep-th]`.

[99] H.-C. Cheng, C. T. Hill, S. Pokorski, and J. Wang, "The Standard model in the latticized bulk," *Phys.Rev.* **D64** (2001) 065007, `arXiv:hep-th/0104179 [hep-th]`.

[100] H. Abe, T. Kobayashi, N. Maru, and K. Yoshioka, "Field localization in warped gauge theories," *Phys.Rev.* **D67** (2003) 045019, `arXiv:hep-ph/0205344 [hep-ph]`.

[101] A. Falkowski and H. D. Kim, "Running of gauge couplings in AdS(5) via deconstruction," *JHEP* **0208** (2002) 052, `arXiv:hep-ph/0208058 [hep-ph]`.

[102] L. Randall, Y. Shadmi, and N. Weiner, "Deconstruction and gauge theories in AdS(5)," *JHEP* **0301** (2003) 055, `arXiv:hep-th/0208120 [hep-th]`.

[103] D. Son and M. Stephanov, "QCD and dimensional deconstruction," *Phys.Rev.* **D69** (2004) 065020, `arXiv:hep-ph/0304182 [hep-ph]`.

[104] J. de Blas, A. Falkowski, M. Perez-Victoria, and S. Pokorski, "Tools for deconstructing gauge theories in AdS(5)," *JHEP* **0608** (2006) 061, `arXiv:hep-th/0605150 [hep-th]`.

[105] R. Casalbuoni, S. De Curtis, D. Dominici, and R. Gatto, "Physical Implications of Possible J=1 Bound States from Strong Higgs," *Nucl.Phys.* **B282** (1987) 235.

[106] R. S. Chivukula, E. H. Simmons, H.-J. He, M. Kurachi, and M. Tanabashi, "Multi-gauge-boson vertices and chiral Lagrangian parameters in Higgsless models with ideal fermion delocalization," *Phys.Rev.* **D72** (2005) 075012, `arXiv:hep-ph/0508147 [hep-ph]`.

[107] R. S. Chivukula, E. H. Simmons, H.-J. He, M. Kurachi, and M. Tanabashi, "Ideal fermion delocalization in five dimensional gauge theories," *Phys.Rev.* **D72** (2005) 095013, `arXiv:hep-ph/0509110 [hep-ph]`.

[108] J. Bechi, R. Casalbuoni, S. De Curtis, and D. Dominici, "Effective fermion couplings in warped 5D Higgsless theories," *Phys.Rev.* **D74** (2006) 095002, arXiv:hep-ph/0607314 [hep-ph].

[109] R. Casalbuoni, S. De Curtis, D. Dominici, and D. Dolce, "Holographic approach to a minimal Higgsless model," *JHEP* **0708** (2007) 053, arXiv:0705.2510 [hep-ph].

[110] E. Accomando, S. De Curtis, D. Dominici, and L. Fedeli, "The Four site Higgsless model at the LHC," *Nuovo Cim.* **B123** (2008) 809–811, arXiv:0807.2951 [hep-ph].

[111] E. Accomando, S. De Curtis, D. Dominici, and L. Fedeli, "Z' production at the LHC in the four-site Higgsless model," *Phys.Rev.* **D83** (2011) 015012, arXiv:1010.0171 [hep-ph].

[112] J. Andersen, O. Antipin, G. Azuelos, L. Del Debbio, E. Del Nobile, *et al.*, "Discovering Technicolor," *Eur.Phys.J.Plus* **126** (2011) 81, arXiv:1104.1255 [hep-ph].

[113] A. Belyaev, R. Foadi, M. T. Frandsen, M. Jarvinen, F. Sannino, *et al.*, "Technicolor Walks at the LHC," *Phys.Rev.* **D79** (2009) 035006, arXiv:0809.0793 [hep-ph].

[114] J. R. Andersen, T. Hapola, and F. Sannino, "W' and Z' limits for Minimal Walking Technicolor," *Phys.Rev.* **D85** (2012) 055017, arXiv:1105.1433 [hep-ph].

[115] G. Altarelli, B. Mele, and M. Ruiz-Altaba, "Searching for new heavy vector bosons in $p\bar{p}$ colliders," *Z.Phys.* **C45** (1989) 109.

[116] H. Georgi, E. E. Jenkins, and E. H. Simmons, "The Ununified Standard Model," *Nucl.Phys.* **B331** (1990) 541.

[117] T. Sjostrand, S. Mrenna, and P. Z. Skands, "PYTHIA 6.4 Physics and Manual," *JHEP* **0605** (2006) 026, arXiv:hep-ph/0603175 [hep-ph].

[118] **CMS** Collaboration, "Search for W' in the leptonic channels in pp Collisions at $\sqrt{s} = 7$ TeV," Tech. Rep. CMS-PAS-EXO-11-024, 2011.

[119] D. London and J. L. Rosner, "Extra Gauge Bosons in E(6)," *Phys.Rev.* **D34** (1986) 1530.

[120] S. King, S. Moretti, and R. Nevzorov, "Exceptional supersymmetric standard model," *Phys.Lett.* **B634** (2006) 278–284, arXiv:hep-ph/0511256 [hep-ph].

[121] D. Berdine, N. Kauer, and D. Rainwater, "Breakdown of the Narrow Width Approximation for New Physics," *Phys.Rev.Lett.* **99** (2007) 111601, arXiv:hep-ph/0703058 [hep-ph].

[122] R. S. Chivukula, E. H. Simmons, H.-J. He, M. Kurachi, and M. Tanabashi, "Electroweak corrections and unitarity in linear moose models," *Phys.Rev.* **D71** (2005) 035007, arXiv:hep-ph/0410154 [hep-ph].